Invasions with Fat-Tailed and Long-Distance Dispersal

Benjamin R. Liu

A dissertation
submitted in partial fulfillment of the
requirements for the degree of

Doctor of Philosophy

University of Washington

2021

Reading Committee:

Mark Kot, Chair

Bernard Deconinck

Mark Lewis

Program Authorized to Offer Degree:
Applied Mathematics

University of Washington

Abstract

Invasions with Fat-Tailed and Long-Distance Dispersal

Benjamin R. Liu

Chair of the Supervisory Committee:
Professor Mark Kot
Applied Mathematics

Ecologists have recognized fat-tailed and long-distance dispersal (LDD) as critical to our understanding of population spread and invasions; heavy- and fat-tailed kernels fit empirical dispersal data better than classical thin-tailed kernels, and long-distance dispersal has driven some of the most rapid invasions. Despite their importance, researchers have struggled to incorporate fat-tailed and long-distance dispersal into mathematical models of spread. Analytical techniques for fat-tailed dispersal and for LDD in spatially explicit models of spread have seen little development.

In this dissertation, I develop new analyses and techniques to study invasions with fat-tailed and long-distance dispersal. I study invasions with two types of dispersal kernels associated with long-distance dispersal: fat-tailed (power-law decay) kernels, which have a propensity for generating extreme events, and thin-tailed mixed-dispersal kernels, which combine multiple dispersal kernels that disperse over different scales.

I first characterize the asymptotic rate of spread for invasions with fat-tailed dispersal. I use the tail additivity properties of regularly varying probability densities to analyze invasions with point- and front-release initial conditions, as well as for populations with weak Allee effects. I show the rate of spread to be geometric, with base determined by the net reproductive rate and the degree of fatness of the dispersal kernel tails. I show that the dynamics of fat-tailed invasions have several key qualitative differences from those of thin-

tailed invasions. I next turn to the transient, or short-to-intermediate timescale dynamics of invasions with long-distance dispersal. I show that LDD, whether implemented by fat-tailed or mixed-dispersal kernels, can lead to biphasic range expansion, where the invasion has two distinct phases and rates of spread; the initial phase of spread is governed by short-distance dispersal, while long-distance dispersal accelerates the invasion in the ultimate phase of spread. Biphasic linear–linear spread is possible under mixed thin-tailed kernels, while biphasic linear–accelerating spread can occur under fat-tailed kernels. I show that for some families of mixed dispersal, the effects of LDD are persistent even when the probability of long-distance dispersal approaches zero; while reducing the probability delays the onset of the second phase of spread, the ultimate speed of spread remains elevated. For fat-tailed kernels, I show how speed rarefaction curves can be used to delineate between the peak and tail of the dispersal kernel, and to define a "shoulder" of the dispersal kernel separating short- and long-distance dispersal.

TABLE OF CONTENTS

LIST OF FIGURES

ACKNOWLEDGMENTS

I would like to express my heartfelt gratitude to my advisor, Mark Kot. Thank you for your guidance and mentorship, and for introducing me to integrodifference equations. Through many stimulating conversations, we worked to reconcile the oddities of fat-tailed spread with classical results and paradigms. Thank you for your commitment to excellence in publishing, for your careful proofreading, and for making my references shine.

I would also like to thank each member of my dissertation committee. Dr. Bernard Deconinck, from who I first learned of the beauty of complex analysis, and who always maintained high standards and was for me a pillar of mathematical rigor at the University of Washington. Mark Lewis for his expertise in mathematical ecology; I have referred to his excellent textbook often, and am grateful to have had such a trusted and respected authority to oversee my work. From Patrick Tobin, I gained a more thorough appreciation for ecology and invasions; I thank him for expanding my perspective, and for introducing me to Himalayan blackberry.

Thank you to my parents, for fostering my creativity and cultivating the environment in which I was shaped. Thank you to Lily for being the best girl, and to Max for being 75% cat, 10% owl, 10% surveillance camera, and 5% cactus. Thank you Jonathan Beaumariage for your constant friendship.

Thank you to the great professors at the University of Washington. Thank you to Chris Bretherton, from whom I gained new perspectives in complex analysis. Thank you to Randy Leveque, for your overflowing wealth of knowledge in finite difference schemes and overall outstanding service and commitment to your community. Thank you to Craig Gin, for our conversations, collaborations, and for giving me wide latitudes to explore and generate ideas in our teaching.

I would also like to thank many of my fellow students at the University of Washington. From my cohort, thank you Kelsey Maass, Yu-Chen Cheng, and Sean Santos, Brian Krouse, and Kenan Li for your friendship and collaborations. Thank you Matthew Farrell, for undertaking day-three problems and for striving for excellence. Thank you to Kelsey Marcinko for your support and friendship, for being a partner in many projects and undertakings, and for knowing that I do enjoy MATLAB questions. Thank you Weston Barger, for totally serious conversations and for your support in difficult times when I needed a spotter. Thank you to Nora Gilbertson, for your friendship and support, and for conversations both silly and serious. Thank you to Katherine Owens, for a shared facet of humor and for your friendship. Thank you to Diya Sashidhar, for data, data, and data. Thank you to Megan Morrison for your constant kindness. From my first year, thank you to friends Riley Molloy and Ali Brauer. Thank you to Natalie Wellen for your friendship and for expanding my perspectives. Thank you to Ryan Creedon, Brian De Silva, Jeremy Upsal, and Kathleen Champion for your friendship.

I would like to thank Elizabeth Cherry for her mentorship throughout my time at RIT and beyond. Thank you for transforming me into a researcher, and for teaching me so many valuable skills. Thank you for your commitment to excellence in many domains, including teaching, research, and mentorship.

I would like to thank the many excellent teachers who have taught and shaped me. Matthew Hoffman, who taught me about Bezier splines, and for undertaking several extracurricular projects with me. David Ross, an excellent teacher who I regard as an archetypal applied mathematician. Thank you to Likin Simon Romero, the topologist who taught me analysis, forever changing the way I think; thank you also for your good humor and steadfast commitment to excellent and engaging teaching. Patricia Clark, for teaching me in Calculus and encouraging me in research. Thank you to Anurag Agarwal, from whom I learned a valuable lesson in personal responsibility; your expectations for excellence pushed me to new

heights, and your encouragement meant so much to me. Nathan Cahill, who gave me perspectives on convolutions that I carried for years and sprinkled throughout my work. Akhtar Khan, for your kind thoughtfulness, excellent instruction, and for teaching me that norms are for measuring differences.

I would like to thank Amy Johnson for teaching me in physics, catalyzing my drive for achievement, and for enabling my precocious tendencies; thank you also for storing my chairs and allowing me to balance stools and scales that I was never around to hear fall down. Thank you to Rachel Stavely-Hale, for teaching and encouraging me in mathematics, in the classroom and beyond, and for your commitment to excellence in education. Thank you to Dan Ogrydziak, for sharing unique perspectives in math and life.

In this dissertation, chapter two is adapted from a manuscript authored by myself and Dr. Mark Kot that was previously published in *Journal of Theoretical Biology* (Liu and Kot, 2019). Chapter three is adapted from a manuscript published in *Theoretical Ecology* (Liu, 2021).

DEDICATION

For those who came before me, and those who will follow.

The truth is that the limitation of human faculties often imposes upon us, as a condition of advance, temporary departure from the standard of strict method. The work of the discoverer may thus precede that of the systematizer; and the division of labour will have its advantage here as well as in other fields.

— Lord Rayleigh, *Nature*, Vol. 43 (1890), p. 26.

Chapter 1

INTRODUCTION

The spatial spread of a population is a complex process involving many factors and mechanisms. One feature shared by all spreading populations is dispersal. Whether through passive means, such as the transport of seeds by wind or animals, or by active means, such as flight, the offspring of each generation disperse or move relative to their progenitors. The study of dispersal and its connection to invasions has developed over many years as researchers have more carefully observed and tracked invasions, developed and refined techniques for gathering and analyzing dispersal data, and discovered new processes and mechanisms underlying dispersal and spread (Bullock et al., 2002; Austerlitz et al., 2004).

Ecologists have recognized fat-tailed and long-distance dispersal as critical to our understanding of population spread and invasions (Higgins and Richardson, 1999; Trakhtenbrot et al., 2005; Nathan, 2006; Schurr et al., 2009). Scientists studying dispersal have found that heavy- and fat-tailed dispersal kernels fit empirical data better than classical thin-tailed dispersal forms (Clark et al., 1999; Bullock and Clarke, 2000; Paradis et al., 2002; Nathan et al., 2012; Bullock et al., 2017). In studies of invasions, researchers have found evidence of long-distance dispersal for many species (Cain et al., 2000) and in some cases have determined it to be the driving force behind some of the most rapid examples of spread (Clark, 1998).

Despite the importance of fat-tailed and long-distance dispersal, researchers have struggled to incorporate these factors into models of spread. This difficulty has its origins in both the history and in the paradigms that developed around models of invasions. Early study was based on reaction-diffusion models (Nathan et al., 2012), and included techniques from partial differential equations and dynamical systems; ideas such as traveling waves, convergence, and long-term asymptotics were central. Mathematical ecologists extended these ideas and developed analytic techniques to obtain similar results for integrodifference equa-

tions and general models of spread (Kot et al., 1996; Weinberger, 1982). These techniques and characterizations almost always required that dispersal be thin-tailed. The inability to extend these methods to heavy- and fat-tailed dispersal, and the accelerating invasions they produce, stalled further analytic development.

In this dissertation, I develop new analyses and techniques to study invasions with fat-tailed and long-distance dispersal. I introduce regular variation and tail additivity as tools for analyzing fat-tailed kernels (Liu and Kot, 2019). I study mixed-dispersal and fat-tailed kernels, two approaches for modeling long-distance dispersal that can be incorporated into integrodifference equation (IDE) models. I show that invasions with long-distance dispersal have rich transient dynamics, where the rate of invasion can switch after long times, yielding biphasic range expansions (Liu, 2021).

In the remainder of this chapter, I outline the development of models of spread and the phenomena and ideas that have motivated the modern development of the field. I then discuss relevant work that researchers have conducted to understand long-distance dispersal and heavy- and fat-tailed kernels. In Chapter 2, I characterize the asymptotics of fat-tailed dispersal. I also outline some of the ways that accelerating invasions defy classical paradigms. In Chapter 3, I broaden my focus to include mixed-dispersal kernels, and I turn my attention to the transient, or intermediate-to-long-term dynamics of invasions with mixed-dispersal and fat-tailed kernels. In Chapter 4, I discuss results and impacts.

1.1 Background

The earliest models of population spread in ecology were reaction-diffusion equations. Skellam (1951) popularized these models with his famous study of the invasive spread of the common muskrat (*Ondatra zibethicus*) in central Europe, where he found that the square-root of invaded territory grew linearly with time. These models, based on partial differential equations, have a long history of study in the fields of mathematics and physics, and are well characterized. Reaction-diffusion equations give rise to invasions that quickly establish a boundary or invasion front that advances at a constant speed.

Diffusion models are widely popular in ecology, but are unsuitable for the study of some instances of spread. Perhaps the most famous example, now known as Reid's paradox (Clark et al., 1998), centers around the recolonization of Europe by oak trees following the last ice age. Reid (1899) observed that the spread of the oak was inexplicably fast when compared to the average dispersal distance of scattered seeds and the time required for their growth. Skellam (1951) formalized this problem in terms of diffusion models, and demonstrated that diffusion alone was an implausible mechanism for spread.

In addition to under-predicting the speed of some invasions, the assumption of Gaussian dispersal also conflicts with empirical observation. Reaction-diffusion models implicitly assume Gaussian dispersal, or that dispersal is driven by a diffusive process. Equivalently, diffusion models assert that the displacement between the source and settling location of an offspring or propagule is distributed according to a normal distribution (Lewis, 1997).

Researchers have collected dispersal data for many species, both plant and animal, giving rise to the study of the dispersal kernel, or the statistical distribution of distances that offspring settle relative to their source (Nathan et al., 2012). Contrary to diffusion-based models of spread, empirical studies that have measured dispersal kernels have found them to be non-normal. Although there is great variety to dispersal in ecology, the overwhelming trend is that dispersal is leptokurtic, or having higher excess kurtosis than that of a normal distribution (Bateman, 1950).

Leptokurtic is a term from probability and statistics indicating that propagules disperse both closer and farther more often than typical of a normal distribution (Lewis et al., 2016); to compensate, mid-range dispersal occurs less often. These comparisons are made against a normal distribution of equal variance. Normal distributions can disperse more widely or narrowly for different variances, but all normal distributions have zero excess kurtosis and so are not leptokurtic. Instances of measured dispersal that are leptokurtic therefore cannot be the result of a purely diffusive process.

Invasions may spread faster than predicted by diffusion if dispersal is leptokurtic (Kot et al., 1996). Although reaction-diffusion models of invasions can be made to spread faster

by increasing the variance of dispersal, doing so disagrees with dispersal data and does not make dispersal leptokurtic. For invasive species with leptokurtic dispersal, reaction-diffusion models will always either fail to match observed dispersal patterns, or underestimate the speed of spread of the invasion.

Beyond the variance and kurtosis, mathematical ecologists have shown that the entire dispersal kernel affects the rate of an invasion (Kot et al., 1996). Modern studies of dispersal and spread focus on the tails of the dispersal kernel (Bullock and Clarke, 2000), which dictate the probability of dispersing over long distances. In ecology, the tails of a dispersal kernel are called "fat," "heavy," "long," or "exponentially unbounded" under a variety of circumstances. Some authors use these terms synonymously with leptokurticity (Clark et al., 1998; Gilbert et al., 2004; Kesler et al., 2010; Liebhold and Tobin, 2010). More specific criteria include when the dispersal kernel decays more slowly than any decaying exponential function (Hastings et al., 2005; Gharouni et al., 2015) or asymptotically to a power law (Katul et al., 2005; Van Houtan et al., 2007). In other cases, these terms are applied when dispersal data follows a concave-upward rather than concave-downward trend when plotted on a logarithmic scale (Clark et al., 1999; Devaux et al., 2005).

In probability and statistics, the terms heavy tailed and fat tailed have more precise meanings. Heavy-tailed kernels form the complement of thin-tailed kernels; a symmetric kernel is either thin-tailed or heavy-tailed. Within the heavy-tailed class, fat-tailed kernels are those kernels whose tails asymptotically decay according to power laws. Kernels within the heavy- and fat-tailed categories are used in finance and risk analysis (Embrechts et al., 1997), generally have properties that make them more likely to generate extreme events, and are characterized more precisely in mathematical terms (Bingham et al., 1987; Borovkov, 2008; Foss et al., 2011). In a recent study, Bullock et al. (2017) compared the fits of several common dispersal kernels to seed dispersal data from 144 plant species, and found that heavy- and fat-tailed kernels were among the best, and thin-tailed kernels among the worst, at fitting dispersal data.

Integrodifference equations (IDE) are one way of incorporating many types of dispersal,

including leptokurtic and fat-tailed dispersal, into models of spread. Integrodifference equations are discrete-time analogues of reaction-diffusion models that use dispersal kernels to capture movement (Kot and Schaffer, 1986). When the dispersal kernel is Gaussian, IDE models behave qualitatively similarly to reaction-diffusion models; indeed, the speed of spread of an invasion in a reaction-diffusion equation matches that of an IDE model with a Gaussian dispersal kernel of matching variance. Other thin-tailed kernels produce qualitatively similar invasions with different rates of spread. Leptokurtic dispersal kernels produce invasions that spread faster than diffusively.

With the popularization of IDE models, mathematical ecologists also demonstrated that heavy- and fat-tailed kernels could give rise to invasions that accelerate without bound (Kot et al., 1996). This behavior is in stark contrast to that of thin-tailed kernels, where the invasion speed is bounded and generally asymptotically approaches a finite limit: the spreading speed. While there have been some attempts to reconcile heavy-tailed dispersal with constant-speed invasions (Clark et al., 2001), researchers have avoided heavy-tailed kernels in invasion models. Heavy-tailed kernels pose problems for analysis; techniques for analyzing thin-tailed kernels, often based on moment generating functions or the assumption of a finite spreading speed, cannot be adapted to these kernels (Kot et al., 1996; Lewis et al., 2016; Lutscher, 2019).

A subject related to the dispersal kernel and fat tails is long-distance dispersal (LDD). Researchers first recognized long-distance dispersal for its role in the colonization of islands and the initiation of invasions (Darwin, 1859). More recently, researchers have recognized LDD as an ongoing factor that continuously contributes to population spread (Clark et al., 1998; Cain et al., 2000; Trakhtenbrot et al., 2005; Schurr et al., 2009). Long-distance dispersal differs from leptokurticity and heavy tails, although the differences are not always made clear in the literature. Leptokurticity, heavy- and fat-tails are terms from probability that describe the dispersal kernel or dispersal data. Long-distance dispersal is, on the other hand, an ecological term describing dispersal events that are "extreme" or "outliers." Precise general criteria defining long-distance dispersal are rarely given and there is no universal

consensus (Nathan, 2005; Nathan et al., 2012; Jordano, 2017). While there are obvious parallels between the two, the precise ecological mechanisms and modeling approaches that connect long-distance dispersal and the tails of the dispersal kernel are still unclear.

Despite being a critical aspect of dispersal, there is much we do not know about how long-distance dispersal occurs. Under one hypothesis, long-distance dispersal occurs for a small proportion of propagules that disperse using distinct, long-distance dispersal vectors. These vectors may not be morphologically adapted, but they may, nevertheless, carry propagules further than standard vectors (Higgins et al., 2003). Wind-dispersed seeds may also be carried by birds or other animals; such transport may occur only rarely, but with great potential impact. Alternatively, long-distance dispersal may occur through extreme events, when common dispersal vectors have an intrinsic capacity to sometimes disperse long distances. Wind-blown seeds, which typically fall a short distance from their source, may occasionally move long distances in extreme weather (Horn et al., 2001; Nathan et al., 2002).

Long-distance dispersal can be implemented in a number of ways in models of spread (Shigesada et al., 1995; Clark et al., 2001; Shigesada and Kawasaki, 2002; Kawasaki et al., 2006). Two approaches that are compatible with the dispersal kernel are mixed-dispersal kernels and heavy-tailed dispersal kernels. Mixed-dispersal kernels align well with the paradigm of long-distance dispersal by nonstandard vectors; these kernels are composed of distinct component kernels, each of which acts on a fixed proportion of all propagules. Heavy-tailed kernels pair well with the model of extreme events intrinsic to standard modes of dispersal.

1.2 Prior work

Many researchers have studied long-distance dispersal, heavy- and fat-tailed kernels, and range expansions. Here, I briefly review several studies that are particularly relevant or related to my work.

Weinberger (1982) conducted important analyses to generalize the behavior of Fisher's reaction-diffusion equation to a broader class of models. Weinberger considered a class of models with discrete time and non-overlapping generations, and gave conditions under which the spreading speed and minimum traveling wave speed existed and were equal. To achieve this, Weinberger made assumptions on the reproduction function and form of dispersal; in particular, several key results required that dispersal be exponentially bounded, or thin tailed.

With their stratified diffusion models, Shigesada, Kawasaki, and Takeda (1995) made one of the earliest efforts to extend models of spread to incorporate long-distance dispersal. Supporting their work with now-classical examples of invasions, Shigesada et al. defined three classes of range expansion, Types 1, 2, and 3, corresponding to linear spread, biphasic linear–linear spread, and continuously accelerating, respectively. These models aimed to produce non-linear range expansions, and were inspired by the hypothesized stratified dispersal processes, whereby dispersal occurs at two scales. Local spread mainly advances the contiguous invasion front similarly to diffusion, while long-distance dispersal produces new, spatially separate colonies. The classification of range expansions by Type 1,2, and 3 is still in use today.

Shigesada et al. (1995) developed two models for stratified diffusion: the scattered colony and coalescing colony models. In the models, a central bulk of the population grows according to diffusion, and long-distance dispersers emanating from this source establish isolated colonies, which may or may not be absorbed depending on the assumptions of the models. These models were important for demonstrating that long-distance dispersal could not only boost the speed of spread, but qualitatively alter the course of range expansion of the invasion.

Both models are spatially implicit, which makes them incompatible with integrodifference equations; it is currently an open area of inquiry as to how deterministic, spatially explicit models might produce Type 2 and Type 3 range expansions (Ramanantoanina et al., 2014).

The work of Kot, Lewis, and van den Driessche (1996) firmly established integrodifference equations as models of spread. With IDE models, dispersal could be generalized beyond Gaussian diffusion, opening the door for the study of new dispersal forms in mathematical ecology. Prior to this work, the most prevalent dispersal forms used in mathematical models were the Gaussian and Laplace (negative exponential) kernels. The authors built on the work of Weinberger (1982) to generalize and find the asymptotic spreading speed for any thin-tailed kernel in terms of its moment generating function. This work also demonstrated that heavy- and fat-tailed kernels could produce accelerating invasions.

Researchers have used mixed dispersal to model dispersal data (Streiff et al., 1999; Bullock and Clarke, 2000; Horn et al., 2001; Hovestadt et al., 2011) as well as in some spatially explicit models of spread (Higgins and Richardson, 1999; Buckley et al., 2005; Kawasaki et al., 2006; Goto et al., 2006; Slavov et al., 2009). In studies of spread, the focus is almost universally on the asymptotic spreading speed. Shigesada and Kawasaki (2002) and Lutscher (2019), for example, analyzed Laplace–Laplace mixed kernels, but focused exclusively on how the addition of long-distance dispersers boosts the spreading speed. A notable exception is the work of Ramanantoanina et al. (2014), who sought a mechanistic explanation for Type 2 range-expansions in the IDE framework. The authors used a structured population model with two classes of dispersal ability, and found that long-distance dispersers inevitably dominated the invasion front, leading to a biphasic range-expansion.

Klein et al. (2006) interpreted a probabilistic property of many heavy-tailed distributions in ecological terms, touching on a critical difference between thin- and heavy-tailed kernels. The authors sought to understand how the "propagule pool" far from two sources would differ in the cases of thin- and fat-tailed dispersal. For thin-tailed dispersal, the closer of the two sources dominates the propagule pool because of the decay of the tails of the kernel. This is not the case with many heavy-tailed kernels, where the change in relative magnitude

in the tail is much slower at great distances from the source. This is in fact the defining characteristic of the *long-tailed* or *asymptotically locally constant* class of distributions (Borovkov, 2008). The authors conclude that this difference could have profound implications for metapopulation structure and dynamics.

Lutscher (2019) recently investigated spread in populations with mixed dispersal abilities. This work is a continuation and broadening of previous unpublished work by Cook (Murray, 2002) and others (Lewis and Schmitz, 1996; Lutscher, 2008) on populations with sedentary and dispersing individuals. The main result is that in a population with mainly sedentary individuals, even an infinitesimal proportion (in the limit) of dispersers can result in the entire population having a positive spreading speed. The more recent work of Lutscher (2019) broadened this result so that in a population with mixed dispersal abilities, even an infinitesimal proportion of long-distance dispersers can boost the spreading speed above that of a population of only short-distance dispersers. Analytically, this phenomenon hinges on whether the moment generating function of the long-distance dispersal kernel has compact support.

Researchers also study heavy- and fat-tailed dispersal in integrodifferential equations. Integrodifferential equations are a continuous-time analogue of discrete-time integrodifference equations that allow for dispersal to be specified with a dispersal kernel, including ones with heavy and fat tails. Garnier (2011) showed how heavy-tailed kernels produced accelerating fronts; his results are phrased in terms of level sets and the inverse image of the dispersal kernel. Alfaro and Coville (2017) conducted similar analyses with fat-tailed dispersal in the presence of degenerate weak Allee effects. By relating the degree of degeneracy of the Allee effect to the fatness of the kernel, they found conditions where the weak Allee effect would suppress acceleration.

Heavy and fat tails are also studied in reaction-diffusion equations, but not as models of dispersal. Hamel and Roques (2010) analyzed spread in Fisher's equation with front-like initial conditions that slowly decay, and found that in these cases the invasion accelerated without bound. Alfaro (2017) conducted analyses combining degenerate weak Allee effects

and slowly decaying initial conditions similar to his work on integrodifferential equations (Alfaro and Coville, 2017). Although reaction-diffusion equations are not useful from the perspective of generalizing dispersal, these studies are important for furthering the characterization of accelerating waves. In these studies, dispersal is thin-tailed, and time is continuous, but the slow decay of specially chosen initial condition leads to effects similar to those of heavy-tailed dispersal in discrete-time integrodifference equations. In a sense, integrodifference equations allow for slowly decaying initial conditions to be transferred to the dispersal kernel.

Researchers have used fractional derivatives to generalize reaction-diffusion equations. In a standard reaction-diffusion equation, dispersal is modeled with the Laplace operator, or a second-order derivative; by replacing this operator with a fractional derivative, dispersal becomes super-diffusive. Baeumer et al. (2007) showed a correspondence between fractional reaction-diffusion equations and integrodifference equations with infinitely divisible dispersal kernels; as the time-step shrinks to zero, the solutions of the integrodifference equation converge to that of a fractional reaction-diffusion equation. In this dissertation, I do not touch on the infinitely divisible class of dispersal kernels, but they include kernels with fat tails; an important class of infinitely divisible kernel is the family of stable distributions, which generalize the Gaussian and Cauchy distributions. Baeumer et al. (2007) showed that fractional reaction-diffusion equations can produce invasions that accelerate at exponential rates.

Chapter 2

ACCELERATING INVASIONS AND THE ASYMPTOTICS OF FAT-TAILED DISPERSAL

Classical models for biological invasions, such as Fisher's (1937) reaction-diffusion model, implicitly assume Gaussian dispersal (Lewis, 1997; Lewis et al., 2016). Many recent researchers have, in contrast, focused on leptokurtic, heavy-tailed, and long-distance dispersal (Bullock and Clarke, 2000; Cain et al., 2000; Nathan et al., 2003; Nathan, 2005; Klein et al., 2006; Nathan et al., 2008; Mundt et al., 2009). Leptokurtic and heavy-tailed dispersal assign a much larger probability to traveling long distances than does Gaussian dispersal.

Integrodifference equations (IDEs) provide one way of accounting for long-distance dispersal. IDEs are discrete-time, continuous-space population models that assume discrete, non-overlapping generations and distinct growth and dispersal stages (Kot et al., 2012). IDEs are more flexible than reaction-diffusion models in that they specify dispersal using a dispersal kernel, a probability density function for the displacement of the propagules (Kot et al., 1996; Nathan et al., 2012).

One of the key properties of a dispersal kernel is whether it is thin- or heavy-tailed. Thin-tailed kernels possess moment generating functions, while heavy-tailed kernels do not. With thin-tailed kernels, IDEs behave like reaction-diffusion equations: they quickly produce traveling waves that advance with constant invasion speeds (Weinberger, 1982; Kot, 1992; but see Sullivan et al., 2017 for an important counterexample). Gaussian kernels generate invasion speeds that exactly match those of reaction-diffusion systems, while leptokurtic distributions produce invasions that move faster but with finite speeds. Existing work (Lewis et al., 2006; Kot and Neubert, 2008) has characterized the invasion speed of thin-tailed invasions in terms of moment generating functions.

Invasion with heavy-tailed dispersal is more poorly understood. Methods based on mo-

ment generating functions cannot be extended to heavy-tailed kernels since these kernels lack moment generating functions. Kot et al. (1996) performed heuristic analyses and conducted simulations for heavy-tailed kernels with moments all finite. They argued that invading populations have spatial distributions with tails that mirror those of the underlying dispersal kernel itself. They concluded that heavy-tailed invasions accelerate without bound, achieving infinite invasion speeds; however, their arguments were limited to point-release invasions and could not be extended with generality to kernels with heavier tails.

Accelerating invasions are qualitatively different than those that progress at a constant speed. Beyond simply needing new analytic techniques for finding the rate of invasion, underlying assumptions about the nature of these invasions such as how we measure and define spatial extent and the rate of change of that extent need to be modified when dealing with accelerating invasions.

In this chapter, we use *regularly varying densities* to model fat-tailed invasions in one dimension. Regular variation can be thought of as a generalization of the behavior of power-law functions. We adapt the *tail additivity* properties of regularly varying probability densities to model invasions from newly-established and well-established populations. Tail additivity is an asymptotic property that allows the tails of convolved functions to be approximated in terms of the tails of the original functions. We show how these properties enable powerful analyses. We find the rate of spread for invasions for linear and nonlinear models, for populations with and without (weak) Allee effects.

This chapter has 9 sections. In *Model*, we introduce the nonlinear, one-dimensional integrodifference equation that we study, along with its linearization. We discuss the two components of the model, the dispersal kernel $k(x)$ and the growth function $f(n)$. We review the concepts of weak and strong Allee effects and summarize how these effects alter invasions. We also introduce the two types of initial conditions, point-release and front-release, that we will analyze. The section *Dispersal kernels and tails* covers classifications of tail heaviness, relevant definitions from probability, and introduces regularly varying densities and the tail additivity properties that are central to our analyses.

In *Point-release initial conditions*, we focus on invasions beginning with small, localized source populations. We use tail additivity to analyze linear and nonlinear models and to derive invasion rates for fat-tailed kernels. Our analyses apply to populations that grow with no Allee effect or weak Allee effects, and, in *Weak Allee effects*, we demonstrate this with numerical simulations and show how fat-tailed invasions change as the strength of the Allee effect changes. In contrast to newly emerging populations, we also have populations that already occupy large territories. We analyze invasions by well-established populations in the section *Front-release initial conditions*.

Our analyses of point- and front-release invasions lead us to conclude that they invade at different rates. We discuss this and show examples in *Invasion rates and initial conditions*. We also perform simulations with a type of initial condition that is intermediate between point- and front-release invasions. In *Accelerating waves*, we discuss the differences between constant-speed and accelerating invasions and how these differences require us to adapt our strategies for measurement and analysis. In *Discussion*, we interpret and discuss the implications of our results and talk about some directions for future work.

2.1 Model

Consider a population with discrete non-overlapping generations and distinct growth and dispersal stages. Let $n_t(x)$ be the (one-dimensional) density of this population at time t. We will model the density of this population in the next generation with the integrodifference equation (IDE)

$$n_{t+1}(x) = \int_{-\infty}^{\infty} k(x,y) f\left(n_t(y)\right) \mathrm{d}y. \tag{2.1.1}$$

Like the population, this model can be understood in terms of distinct stages. The *growth function* $f(n)$ describes the recruitment of the next generation, during the sedentary stage, as a function of the distribution of the current population. The *dispersal kernel* $k(x,y)$ is a probability density function that gives the probability that offspring from location y settle

in location x. The integral sums up dispersal from all possible sources.

If the dispersal kernel $k(x, y)$ only depends on the difference $x - y$, dispersal is homogeneous and the IDE reduces to a convolution,

$$\begin{aligned} n_{t+1}(x) &= \int_{-\infty}^{\infty} k(x-y) f\left(n_t(y)\right) \mathrm{d}y \\ &= \left[k * f(n_t)\right](x). \end{aligned} \tag{2.1.2}$$

We will focus on convolution-type IDEs throughout this dissertation.

In addition to *nonlinear* IDE (2.1.2), we also concern ourselves with its *linearization*,

$$\begin{aligned} n_{t+1}(x) &= R_0 \int_{-\infty}^{\infty} k(x-y) n_t(y) \mathrm{d}y \\ &= R_0 \cdot (k * n_t)(x). \end{aligned} \tag{2.1.3}$$

This IDE is obtained by linearizing the growth function $f(n)$ about zero, replacing $f(n)$ with $R_0 n$, since

$$f(n) \sim f'(0) n = R_0 n \quad \text{as} \quad n \to 0. \tag{2.1.4}$$

We linearize to study invasions where unoccupied territory is colonized. At these low densities where $n \approx 0$, the linear model has dynamics very similar to those of the nonlinear model. The linear model is, however, easier to analyze.

As we will see, there are three main components that affect how a population governed by these models will spread: the growth function, the dispersal kernel, and the initial distribution of the population.

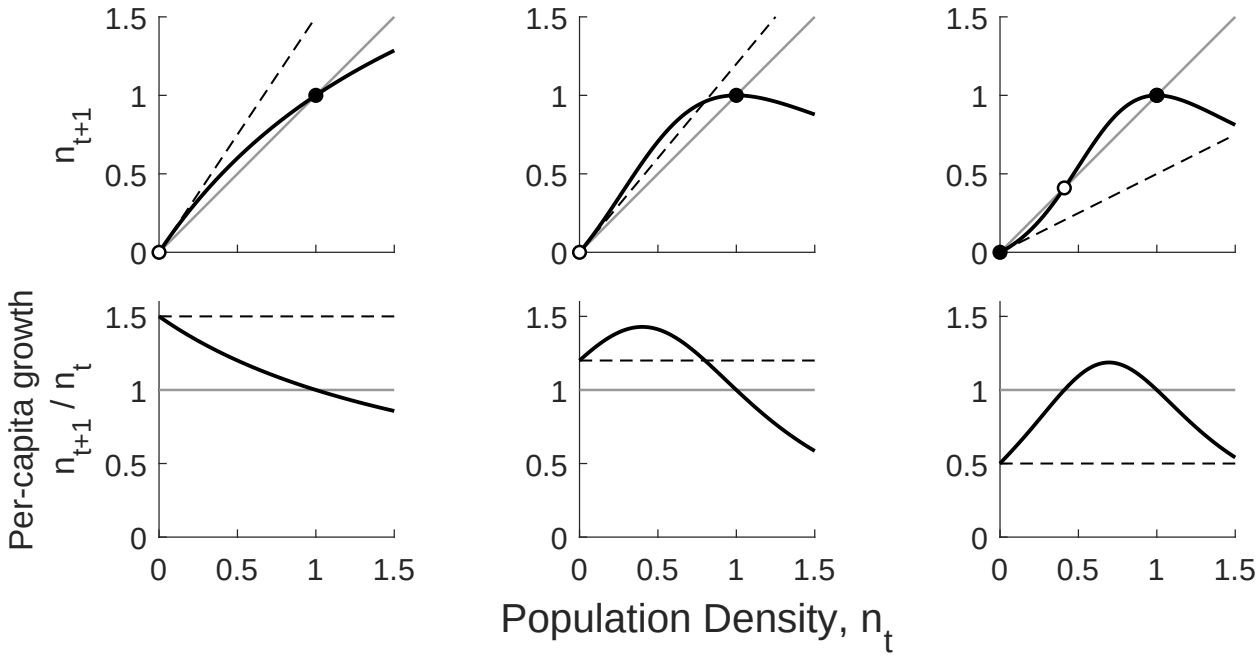

Figure 2.1: Example growth functions. Top plots show the growth function $n_{t+1} = f(n_t)$ (black curves) with the identity line $n_{t+1} = n_t$ (solid gray) and the line $n_{t+1} = R_0 n_t$ (dashed black). Circles indicate equilibria: filled circles are stable, and empty circles are unstable. Bottom plots show the per capita recruitment, n_{t+1}/n_t, which more clearly show Allee effects. **(Left)** Growth with no Allee effect. Such growth functions have no depensatory effects. The function has maximum slope R_0 at $n_t = 0$ and the per-capita recruitment never exceeds R_0. **(Center)** Growth function with a weak Allee effect. Such growth is characterized by a net reproductive rate $R_0 > 1$ and the per-capita recruitment exceeding R_0 at some point $n^* > 0$. In other words, the graph of $n_{t+1} = f(n_t)$ rises above $n_{t+1} = R_0 n_t$. **(Right)** Growth function with a strong Allee effect. The growth function lies below the line $n_{t+1} = n_t$ for small values of n_t. This means $R_0 < 1$.

2.1.1 Nonlinear growth and Allee effects

The growth function $f(n)$ describes the survival and reproduction, or recruitment, during the sedentary stage. Without dispersal, the population density at time $t + 1$ is given by

$$n_{t+1} = f(n_t). \tag{2.1.5}$$

Typically both zero and the carrying capacity are fixed points of the growth function.

Fixed points are points where $n_{t+1} = n_t = n^*$ or $f(n^*) = n^*$ and are also known as equilibria. If we rescale the carrying capacity to be one, this means that $f(0) = 0$ and $f(1) = 1$. Other fixed points can also occur, as in the case of bistability where an unstable equilibrium lies between (asymptotically) stable equilibria at zero and one. We will, however, focus exclusively on monostable growth functions, where $n^* = 1$ is a stable and $n^* = 0$ is an unstable equilibrium. Examples of growth functions and their equilibria can be seen in Figure 2.1. In this figure, equilibria are indicated by filled (stable) and hollow (unstable) circles.

In practice, the growth function is typically smooth or at least continuous. Discontinuous growth functions are sometimes used, especially in mathematical studies where simple forms are required to make analysis tractable (Kot et al., 1996; Wang et al., 2002; Lewis et al., 2016) or when the effect of changing specific aspects of the growth function need to be measured in isolation. We always assume that the derivative exists at $n = 0$, and we call $R_0 = f'(0)$ the net reproductive rate. The value R_0 determines how a population grows at low densities and is important in determining its rate of invasion.

When the growth function satisfies $f(n) \leq R_0 n$, it is said to have *no Allee effect*, and the rate of invasion is completely determined by the form of dispersal $k(x)$ and the value R_0. When this condition is violated, an Allee effect is present, meaning that the per capita recruitment $f(n_t)/n_t$ decreases, for decreasing n_t, near the origin. Allee effects can be weak or strong (Wang et al., 2002) and they are distinguished by whether $f(n)$ is greater than or less than n near the origin or, equivalently, whether $R_0 > 1$ or $R_0 < 1$. If $R_0 > 1$, then an arbitrarily small population persists and grows. If, in contrast, $R_0 < 1$, too few offspring replace their parents and the population perishes. Figure 2.1 shows examples of growth functions with no Allee effect as well as with weak and strong Allee effects.

Allee effects are especially important when considering and extrapolating from the behavior of a linear model such as (2.1.3). It has long been conjectured that the invasion speed of a nonlinear model will match that of its linearization under two conditions (van den Bosch et al., 1990):

(i) The average rate of reproduction of an individual experiencing throughout its life an environment 'occupied' by a certain (possibly varying) population is always smaller than the rate of reproduction in a 'virgin' environment (i.e. in particular there are no Allee-like effects), and that

(ii) The influence of an individual on the environment very far from its (present) position is negligible.

Mollison (1991) clarifies that (ii) relates not to long-distance dispersal, but rather to nonlocalities in the growth of the population: there should be no long-distance density dependence. This is not an issue in our model formulation, where the population growth $f(n(x))$ depends only on the density at that same point.

2.1.2 Initial conditions

The population density $n_0(x)$ at the starting time $t = 0$ is called the *initial condition*. Any initial population density can be considered, but we will focus on two types of conditions.

Point-release initial conditions specify that the initial population is released in a small area, approximated by a point. In practice this is handled in a number of ways. If N_0 is the initial total population, then one can choose a width L on which to set the population density at a constant level, which approximates the initial distribution as a patch of concentrated population,

$$n_0(x) = \begin{cases} \dfrac{N_0}{L} & -L/2 \leq x \leq L/2 \\ 0 & \text{otherwise.} \end{cases} \tag{2.1.6}$$

Decreasing the width L narrows the patch and concentrates the population.

Another common approach is to specify the initial condition as a scaled Gaussian distri-

bution,

$$n_0(x) = \frac{N_0}{\sqrt{2\pi\sigma^2}} e^{-x^2/(2\sigma^2)}. \tag{2.1.7}$$

As in the case of the finite patch, the standard deviation σ of the Gaussian can be made small to reduce its width and concentrate the population. For analysis based on the linear model, where one can mathematically switch the order of growth and integration, the Dirac delta function is commonly used, and can be thought of as the limiting case of the Gaussian where $\sigma \to 0$; for more information, see the derivation of a formal solution under the linear model in section *Point-release initial conditions*.

Front-release initial conditions are those where a front or boundary exists, to one side of which is populated territory and to the other uncolonized territory. In contrast with a newly emerging or developing point-release invasion, a front-like invasion has a well-established population behind the front.

We would like to make precise the notion of a well-established population that is invading new territory. We define a one-dimensional spatial population density $n(x)$ to be *front-like* if: (1) $n(x)$ is non-decreasing, (2) $n(x)$ goes to zero as x approaches $-\infty$, and (3) $n(x)$ goes to the population carrying capacity as x approaches $+\infty$.

Alternative definitions of front-like population density profiles are possible. Alfaro and Coville (2017) define "front like initial data" $u_0(x)$ as having (i) $0 \leq u_0(x) < 1$, (ii) $\liminf_{x\to-\infty} u_0(x) > 0$, and (iii) $u_0 \equiv 0$ for some $a \leq x < \infty$. This condition imposes a stricter condition on the virgin territory (that the population density truly vanishes rather than decays to zero) and a weaker condition on the colonized territory (that the population density stays above a nonzero value, rather than approaching the carrying capacity). Our definition suits our analyses where we cast population densities as cumulative distribution functions.

2.2 Dispersal kernels and tails

In this section we discuss aspects of probability theory relevant to dispersal in ecology. We begin with a review of terminology from the probability literature. This builds to a discussion of tail heaviness, including some terms that are often treated differently in ecology and probability. We introduce regularly varying densities and the tail additivity properties of their convolutions that form the basis for our analyses. We conclude with examples of fat-tailed kernels that we use in numerical simulations throughout the chapter.

2.2.1 Probability review

Dispersal can be thought of as as a random process, with X the random displacement (in one dimension) and $k(x)$ the probability density function for this displacement. In ecology, this probability density function is often called the dispersal kernel.

In addition to the probability density function, every distribution can be characterized by a *cumulative distribution function* or cdf that encodes the probability of X being any value up to a specified value x,

$$K(x) = \Pr\{X \leq x\}. \tag{2.2.1}$$

A cdf is related to its pdf by the derivative: $K'(x) = k(x)$.

The term "dispersal kernel" is somewhat vague, because some use it to describe the probability distribution of dispersal distances. Nathan proposes calling this the *dispersal distance kernel* (Nathan et al., 2012). Under Nathan's conventions, we will be working exclusively with *dispersal location kernels* in one dimension, and we will denote these kernels as $k(x)$ for the pdf and $K(x)$ for the cdf.

In this dissertation we focus on distributions that are *symmetric*, so $k(x) = k(-x)$ for all real x. This simplifies things a great deal and allows us to be relaxed about subtleties such as heavy *left* or *right* tails with differing rates of invasion to the left or right; our dispersal

kernels are simply heavy-tailed, meaning both tails are heavy. Asymmetric kernels can lead to unequal rates of leftward and rightward spread and are sometimes introduced by advective forces such as the current in a river or by the movement of a habitat in climate-change models (Lutscher and Seo, 2011; Vasilyeva and Lutscher, 2012; Phillips and Kot, 2015).

The expected value $E[X]$ of X is its mean value, also called the *first raw moment*, and is calculated as

$$E[X] = \int_{-\infty}^{\infty} xk(x)\mathrm{d}x. \tag{2.2.2}$$

This integral does not converge for some kernels with very heavy tails, such as the Cauchy distribution; this is not a fault of the definition of the mean, but rather a statement about the extraordinarily heavy tails of these distributions.

Other expectations of functions of X can also be computed. For instance, the n-th raw moment of X is given by

$$\mu_n' = E[X^n] = \int_{-\infty}^{\infty} x^n k(x)\mathrm{d}x. \tag{2.2.3}$$

The raw moments may all be finite values, or some may *diverge* or fail to exist when the expectation integral does not converge, as in the case of the mean of the Cauchy distribution.

The moment generating function (mgf) of a distribution is defined as the expectation

$$M(s) = E\left[e^{sX}\right] = \int_{-\infty}^{\infty} e^{sx}k(x)\mathrm{d}x. \tag{2.2.4}$$

The mgf may be defined on the whole real line or only part of it. The value $M(0) = 1$ is always defined, but $M(s)$ may be undefined for all nonzero values of s. When this is the case, we say that the mgf does not exist or that the distribution lacks a mgf. The moment

generating function is so-named because if the mgf exists, then its Taylor series,

$$M(s) = 1 + \mu_1' s + \frac{\mu_2'}{2!} s^2 + \frac{\mu_3'}{3!} s^3 + \cdots , \tag{2.2.5}$$

encodes the raw moments of the distribution.

2.2.2 Degrees of heaviness and types of tails

Various descriptions of kernel shape and tail heaviness are used in probability and ecology. Classical approaches such as reaction-diffusion equations model dispersal by diffusion, which implicitly assumes Gaussian dispersal. Excess kurtosis, a measure of broadness of dispersal in relation to the Gaussian distribution, was a natural metric for studies that departed from Gaussian dispersal. Today it is more common to speak of "heavy-tailed" or "fat-tailed" distributions. Long-distance dispersal events are said to occur due to heavy-tailed dispersal, and the dispersal kernel may have high excess kurtosis.

The kurtosis of a random variable X is defined as the expectation

$$\kappa = E\left[\left(\frac{X - \mu}{\sigma}\right)^4\right], \tag{2.2.6}$$

where $\mu = E[X]$ is the mean and $\sigma^2 = E[(X - \mu)^2]$ the variance. The kurtosis of the standard normal (Gaussian) distribution is 3, and so the kurtosis of other distributions when compared to the Gaussian is reported as the *excess kurtosis*, $\kappa - 3$. Distributions with zero excess kurtosis are called mesokurtic, those with negative excess kurtosis are platykurtic, and positive excess kurtosis are termed leptokurtic. Kurtosis is sometimes used in descriptions of tail heaviness. Leptokurtic distributions are those whose extreme values are "more probable than normal" (Cooke et al., 2014). In ecology, dispersal is most commonly leptokurtic (Bateman, 1950; Nathan et al., 2012).

Thin-tailed or *light-tailed* distributions possess moment generating functions. For continuous random variables, this means that there exists some $s > 0$ such that

$$E\left[e^{sX}\right] = \int_{-\infty}^{\infty} e^{sx} k(x) \mathrm{d}x < \infty. \tag{2.2.7}$$

Thin-tailed distributions are sometimes called *exponentially-bounded* in ecology. This means that there exists some $c > 0$ and x^* such that $k(x) < \exp(-cx)$ for all $x > x^*$. When a distribution is exponentially bounded, integral (2.2.7) must converge for some nontrivial s, and so the moment generating function must exist, although the converse is not true: there exist some exotic probability densities that are not exponentially-bounded, yet which do possess moment generating functions.

Two common thin-tailed distributions are the Gaussian or normal distribution,

$$k(x) = \frac{1}{\sqrt{2\pi\sigma^2}} e^{-x^2/(2\sigma^2)}, \tag{2.2.8}$$

and the Laplace (double-exponential) distribution,

$$k(x) = \frac{1}{2b} e^{-|x|/b}, \tag{2.2.9}$$

both written here with zero mean. These density functions are shown in Figure 2.2, plotted in a variety of scales. The thin tails of these distributions can be visually identified by the fact that they decay as rapidly or faster than a diagonal line in a linear-log plot, which means they are exponentially-bounded.

Heavy-tailed distributions lack moment generating functions. The set of heavy-tailed distributions is therefore the complement (for symmetric kernels) of thin-tailed distributions. Using Taylor series (2.2.5), we see that a moment generating function can fail to exist if some of its moments are divergent (infinite). Another possibility is that all of the moments exist and are finite but taken together the infinite series fails to converge. Distributions may be

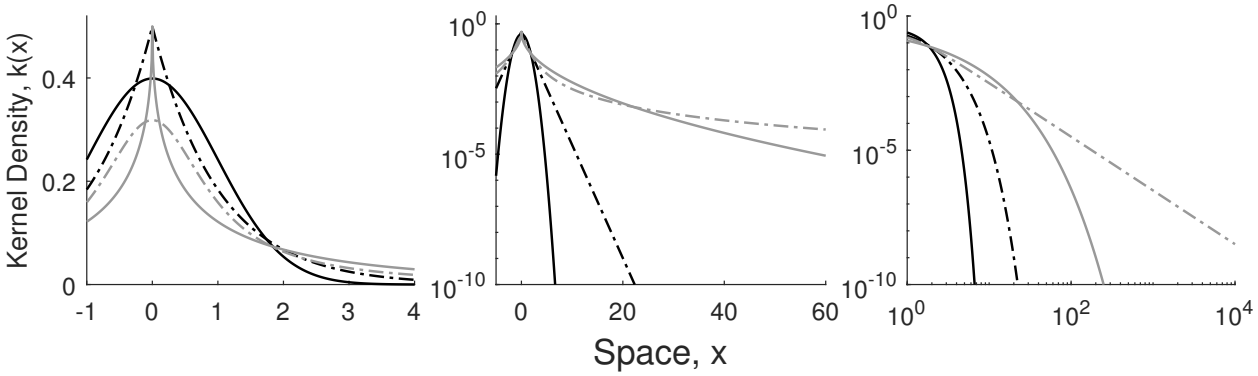

Figure 2.2: Tails of various probability density functions. Gaussian (solid black), Laplace (dashed black), Cauchy (dashed gray), and exponential square-root (solid gray) distributions, equations (2.2.8), (2.2.9), (2.2.10), and (2.2.12), at a variety of scales. The first two distributions are thin-tailed, the third distribution is fat-tailed, and the fourth distribution is heavy-tailed but not fat-tailed. **(Left)** The kernels plotted on a linear-linear scale, showing the shape of the kernels near the origin. **(Center)** A linear-log scale plot, where the relative magnitudes of the tails are more clearly visible. The tails of the Laplace density decay exponentially, and so appear as straight lines. The heavier-tailed exponential square-root and Cauchy kernels flatten in linear-log scale. **(Right)** The kernels on a log-log scale. Here the fat-tailed Cauchy kernel has tails that tend toward straight lines.

heavy-tailed for either of these reasons.

Heavy-tailed distributions do not have exponentially-bounded tails. In fact, most commonly used heavy-tailed distributions (with monotonically decreasing tails) will eventually dominate any decaying exponential. That is, for any decaying exponential function, e^{-sx} for any value of $s > 0$, then at some point x^*, $k(x) > e^{-sx}$ for all $x > x^*$. This means that no matter how slowly the exponential decays, eventually $k(x)$ will exceed it.

A classic example of a heavy-tailed kernel is the Cauchy distribution,

$$k(x) = \frac{b}{\pi(b^2 + x^2)}. \tag{2.2.10}$$

Its heavy-tailedness can be seen by examining the limit of $k(x)/\exp(-sx)$,

$$\lim_{x\to\infty} \frac{be^{sx}}{\pi(b^2+x^2)} = \infty, \tag{2.2.11}$$

which follows from the fact that any growing exponential function grows faster than any polynomial. Since the limit $k(x)/\exp(-sx)$ is infinite, the magnitude of $k(x)$ eventually dominates the decaying exponential (for any value of s). Another heavy-tailed kernel is the exponential square-root,

$$k(x) = \frac{1}{b} e^{-2\sqrt{|x|/b}}. \tag{2.2.12}$$

Again examining the limit of $k(x)/\exp(-sx)$, we find

$$\lim_{x\to\infty} \frac{1}{b} e^{sx-2\sqrt{x/b}} = \infty, \tag{2.2.13}$$

which can be seen by observing that any linear function will grow faster than any square-root function, again showing that $k(x)$ eventually dominates any decaying exponential. These distributions are presented in Figure 2.2 alongside two thin-tailed ones. Their heavy tails can be seen clearly on a linear-log plot where their tails flatten and eventually dominate any decreasing diagonal line.

Fat-tailed distributions are among the heaviest of heavy-tailed kernels. They decay asymptotically as power laws, so that there exists some $\alpha > 1$ and $c > 0$ such that

$$k(x) \sim cx^{-\alpha}, \qquad x \to \infty. \tag{2.2.14}$$

Here α is the *degree* or *order* of tail fatness that specifies the order of power-law decay of the tail and c is a normalization constant that causes $k(x)$ to integrate to one. The notation

$k(x) \sim g(x)$ reads as $k(x)$ *is asymptotically equivalent to* $g(x)$, and means that

$$\lim_{x\to\infty} \frac{k(x)}{g(x)} = 1. \tag{2.2.15}$$

An example of a fat-tailed kernel is Cauchy kernel (2.2.10), which can be verified as fat-tailed since it is a rational function,

$$k(x) = \frac{b}{\pi(b^2 + x^2)} \sim \frac{b}{\pi} x^{-2}. \tag{2.2.16}$$

This kernel appears in Figure 2.2 alongside thin- and a heavy-, but not fat-tailed, kernel. On a log-log plot fat-tailed kernels appear as straight lines, which is a result of their asymptotic convergence to power laws.

It is worth noting that when a fat-tailed kernel is rescaled, for example by setting $\widehat{k}(x) = 2k(2x)$, we obtain the same degree of tail fatness:

$$\widehat{k}(x) = \frac{2b}{\pi\left[b^2 + (2x)^2\right]} \sim \frac{2b}{\pi}(2x)^{-2} = \frac{b}{2\pi} x^{-2}. \tag{2.2.17}$$

Although fat-tailed kernels can be rescaled, which can affect their shape, their tails are always proportional to a standard decaying power law.

Fat-tailed distributions are always heavy-tailed, but not all heavy-tailed distributions are fat. An example of a heavy-tailed kernel that is not fat-tailed is exponential square-root (2.2.12). This kernel decays slower than any exponential and so lacks a moment generating function, but faster than any power law.

In the ecological literature, kernels are often distinguished as either thin-tailed or fat-tailed. In truth, the opposite of a thin-tailed kernel is a heavy-tailed kernel: thin-tailed distributions possess moment generating functions, whereas heavy-tailed do not, and these two categories account for all (symmetric) kernels. The use of thin- and fat- to describe these complementary sets is presumably because "fat" is linguistically the opposite of "thin." Fat-tailed kernels have a much more specific form: their tails asymptotically decay like power

laws.

2.2.3 Regularly varying densities

Fat-tailed distributions have a specific form but are still general enough to capture a wide variety of distributions. A yet more general form is that of regularly varying densities. These densities are built around the concepts of *slow* and *regular variation*.

A positive, measurable function $g(x)$ is *slowly varying* (at infinity) if for all $t > 0$,

$$\lim_{x\to\infty} \frac{g(tx)}{g(x)} = 1. \tag{2.2.18}$$

Slowly varying functions include positive constants and functions whose limits are positive constants, but also functions that grow sufficiently slowly, such as the logarithm (Bingham et al., 1987).

Power-law growth and decay form the basis for extension of slow variation to regular variation. A function $g(x)$ is *regularly varying with index* p if, for all $t > 0$,

$$\lim_{x\to\infty} \frac{g(tx)}{g(x)} = t^p. \tag{2.2.19}$$

Slowly varying functions are therefore technically regularly varying functions with index $p = 0$. An equivalent formulation of regular variation is that if $g(x)$ is a regularly varying function then

$$g(x) = x^p L(x) \tag{2.2.20}$$

for some slowly varying function $L(x)$. Regular variation can therefore be thought of as a power law multiplying a slowly varying function – a form more general than asymptotic equivalence to a power law.

Regularly varying functions permit greater variety in functional forms than asymptotic equivalence. An example of a regularly varying function that is not asymptotically equivalent

to a power law is $g(x) = x^{-2} \log x$. $g(x)$ is regularly varying with index $p = -2$ since $\log x$ is slowly varying. For asymptotic equivalence to x^{-2}, the limit $g(x)/x^{-2}$ must tend to one, but

$$\lim_{x\to\infty} \frac{g(x)}{x^{-2}} = \lim_{x\to\infty} \frac{x^{-2}\log x}{x^{-2}} = \infty. \tag{2.2.21}$$

On the other hand, suppose that $g(x)$ is asymptotically equivalent to a power-law function, $g(x) \sim x^p$. This means that

$$\lim_{x\to\infty} \frac{g(x)}{x^p} = 1 \qquad \text{and} \qquad \lim_{x\to\infty} \frac{g(tx)}{(tx)^p} = 1, \quad t > 0. \tag{2.2.22}$$

By applying limit laws, we have

$$\lim_{x\to\infty} \frac{g(tx)}{g(x)} = \lim_{x\to\infty} \left[\frac{g(tx)}{(tx)^p}\right] \left[\frac{x^p}{g(x)}\right] t^p = t^p, \tag{2.2.23}$$

from which we conclude that $g(x)$ is regularly varying with index p. We now see that the class of regularly varying functions encapsulates the class of power-law functions.

So far we have discussed regularly varying *functions*, but we now narrow our view to regularly varying *densities* – those probability distributions with pdfs that are regularly varying. We can now take advantage of results for regularly varying densities to study fat-tailed dispersal kernels – those kernels that follow power-law decay. For our purposes, the most useful results are due to Bingham et al. (2006), who studied the convolutions of regularly varying densities. If $g(x)$ and $h(x)$ are probability densities on the real line that are regularly varying at ∞, then the convolution $(g * h)(x)$ satisfies (Bingham et al., 2006),

$$(g * h)(x) \to g(x) + h(x), \qquad x \to \infty, \tag{2.2.24}$$

and thus is also regularly varying. This implies that the convolution of a regularly varying

density $g(x)$ with itself has the simple asymptotic approximation

$$(g * g)(x) \to 2g(x), \qquad x \to \infty. \tag{2.2.25}$$

Furthermore, since $(g * g)(x)$ is also regularly varying, we can conclude by induction that the n-fold convolution or *convolution-power* (Feller, 1971) of $g(x)$ satisfies

$$\begin{aligned}(g^{n*})(x) &= \big(\overbrace{g * g * \cdots * g}^{n\text{-many}}\big)(x) \\ &\sim ng(x), \qquad x \to \infty.\end{aligned} \tag{2.2.26}$$

Further, if $g(x)$ and $h(x)$ are probability densities on the real line with $g(x)$ regularly varying and $h(x) = o(g(x))$ as $x \to \infty$, then their convolution has the property (Bingham et al., 2006)

$$(g * h)(x) \to g(x), \qquad x \to \infty. \tag{2.2.27}$$

The notation $h(x) = o(g(x))$ means that $g(x)$ *dominates* $h(x)$ such that

$$\lim_{x\to\infty} \frac{h(x)}{g(x)} = 0. \tag{2.2.28}$$

The density function $g(x)$ has, in effect, a heavier tail than $h(x)$ if it dominates $h(x)$. Property (2.2.27) is useful because $h(x)$ need not be regularly varying and can, for example, be thin-tailed.

Although we have stressed that regularly varying densities form a broader set than fat-tailed ones, throughout the remainder of this chapter we will focus exclusively on fat-tailed kernels. From a modeling perspective, fat-tailed kernels are common and come in sufficient variety that this is not unduly restrictive. Our purpose for introducing regularly varying densities is to take advantage of their useful tail additivity properties when dealing with the more restrictive fat-tailed case. Nevertheless, extension of our work to regularly varying

densities would be a useful endeavor and a potential area for future work.

2.2.4 Example fat-tailed kernels

To perform numerical experiments, we must select particular or example fat-tailed kernels. We chose kernels based on two well-known thin-tailed kernels: the Gaussian and Laplace distributions. These kernels have qualitatively different shapes at the origin: the Gaussian has a smooth, round shape and the Laplace kernel is peaked. The fat-tailed Gaussian has a round profile similar to the Gaussian, and the fat-tailed Laplace kernel has a peak like the Laplace kernel. These kernels are shown in Figure 2.3 alongside their thin-tailed counterparts.

The fat-tailed Gaussian is Student's (1908) t-distribution. The t-distribution is a well-known fat-tailed density that is commonly used in statistical tests. A two-dimensional variant, the 2Dt distribution, has been developed and used in ecological modeling (Clark et al., 1999; Bullock et al., 2017). We retain the standard parameterization,

$$k(x) = \frac{\Gamma\left(\frac{\nu+1}{2}\right)}{\Gamma\left(\frac{\nu}{2}\right)\sqrt{\nu\pi}}\left(1+\frac{x^2}{\nu}\right)^{-\left(\frac{\nu+1}{2}\right)}, \tag{2.2.29}$$

with $\nu \geq 1$ measuring the "degrees of freedom"; the order of tail fatness is $\alpha = \nu + 1$. As $\nu \to \infty$, the t-distribution converges to the standard normal distribution, but it retains its fat tails for all finite ν. For $\nu = 1$, the t-distribution reduces to Cauchy distribution (2.2.10).

The fat-tailed Laplace kernel,

$$k(x) = \frac{\alpha - 1}{2\alpha\left(1 + |x|/\alpha\right)^{\alpha}}. \tag{2.2.30}$$

is based on the two-dimensional "geometric" or "power-law" kernel (Nathan et al., 2012). Kernel (2.2.30) is a well-defined probability density for $\alpha > 1$, but it may have infinite variance. For $\alpha > 3$, the fat-tailed Laplace kernel has finite variance. As $\alpha \to \infty$, the fat-tailed Laplace kernel converges to the Laplace kernel, but for all finite values of α, the kernel has fat tails whereas the Laplace kernel is thin-tailed.

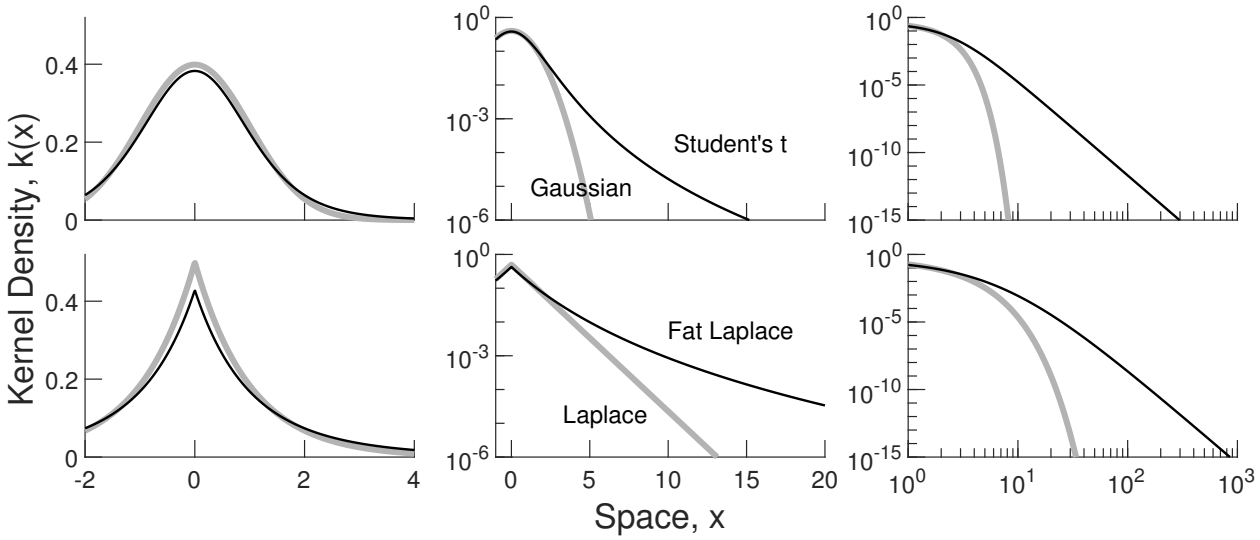

Figure 2.3: Fat-tailed kernels used in numerical simulations. **(Top)** The fat-tailed Gaussian kernel (Student's t-distribution) alongside its thin-tailed counterpart, the Gaussian distribution. The kernels appear quite similar in linear scales, with similar rounded shapes. In linear-log scale, the difference in the tails is more evident, as the Gaussian decays rapidly while the t-distribution decays at a slowing rate. In log-log scale, the tails of the t-distribution tend to straight lines because they converge to power laws. **(Bottom)** The fat-tailed Laplace kernel and the (thin-tailed) Laplace kernel. Both have a peaked shape at the origin, but differ in the tails similarly to the Gaussian and t-distribution.

We remark that these kernels are members of larger classes of kernels. The Gaussian and Laplace kernels are both special cases of the *exponential power* (Kotz et al., 2001) or *generalized normal* distribution,

$$k(x) = \frac{\beta}{2\alpha\Gamma(1/\beta)} e^{-(|x|/\alpha)^\beta}. \tag{2.2.31}$$

The exponential power distribution has been used in ecological modeling of pollen dispersal (Nathan et al., 2012). The fat-tailed Laplace kernel and t-distribution are themselves special cases of the *generalized Cauchy distribution* (Miller and Thomas, 1972), which is a fat-tailed analogue of the exponential power family in the same manner that the t-distribution is the fat-tailed analogue of the Gaussian. The generalized Cauchy distribution has a parameter ν

for controlling tail fatness as well as a parameter c, analogous to β in equation (2.2.31), that controls the tail heaviness of the limiting distribution.

Using these as our example kernels has several benefits. Primarily, we can compare against the known behavior of the Gaussian and Laplace kernels. The Gaussian and Laplace kernels are both thin-tailed kernels whose invasion speeds have been well-characterized. They are known to have different invasion speeds, with the Laplace kernel outstripping a Gaussian kernel of equal variance for the same net reproductive rate R_0. As we will see, the invasion speeds of the thin-tailed kernels do affect their fat-tailed counterparts.

2.3 Point-release initial conditions

A point-release invasion begins with a small population initially confined to a small area, approximated by a point. A point-release invasion describes a newly emerging population, sometimes starting from transplanted individuals or from a long-distance dispersal event that has carried a propagule a far distance from its source.

In this section, we derive a formal solution to linear integrodifference equation (2.1.3) in terms of convolutions of the kernel, and we use tail additivity to obtain a tail approximation. We assume general power-law decay of the kernel (fat tails) to find the rate of invasion. We then develop a more sophisticated analysis based on scaling arguments and analogies to probability densities that allows us to draw the same conclusions for the nonlinear model, including when the growth function has a weak Allee effect.

2.3.1 Linear model

When the initial condition is a point release, we can approximate it as a *delta function*, $\delta(x)$. The delta function is defined as a *generalized function* that integrates to one,

$$\int_{-\infty}^{\infty} \delta(x)\mathrm{d}x = 1, \tag{2.3.1}$$

and that is zero everywhere except at the origin,

$$\delta(x) = 0 \quad \text{for all } x \neq 0. \tag{2.3.2}$$

The delta function is not a true function, since it has no well-defined value at the origin. It can be thought of as the limit of increasingly narrow Gaussian distributions, concentrating total probability at the origin.

A key property of the delta function is the *sifting property* (Bracewell, 1986),

$$\int_{-\infty}^{\infty} f(x-y)\delta(y)\mathrm{d}y = f(x). \tag{2.3.3}$$

This property essentially states that the delta function is the function that preserves any other function under convolution. This is immediately useful to us: if the initial population density is localized at a point and N_0 is the number of individuals or *source strength*, then the initial condition can be modeled with a delta function, $n_0(x) = N_0\delta(x)$, and we can easily find the first generation $n_1(x)$ under linear model (2.1.3),

$$\begin{aligned} n_1(x) &= N_0 R_0 \int_{-\infty}^{\infty} k(x-y)\delta(y)\mathrm{d}y \\ &= N_0 R_0 k(x). \end{aligned} \tag{2.3.4}$$

We remark that the use of the delta function as an initial condition is not always valid. In the nonlinear model, where we must compute $f(n_0(x))$, a delta function initial condition poses a problem because $\delta(0)$ has no defined value, and so $f(\delta(0))$ likewise has no defined value (Greenberg, 2015). In the present case, using a delta function is permissible because of the simplified form of the linear model that reduces to a convolution. Indeed, the action of the delta function is defined in terms of a convolution-type integral (Greenberg, 2015).

The simple form of $n_1(x)$ in terms of the kernel allows us to find an exact formal solution

of the linear model in terms of self-convolutions of the kernel,

$$\begin{aligned} n_t(x) &= N_0 R_0^t \big(\overbrace{k * k * \cdots * k}^{t\text{-many}} \big)(x) \\ &= N_0 R_0^t k^{t*}(x). \end{aligned} \tag{2.3.5}$$

Even given the form of $k(x)$, the convolution $(k * k)(x)$ may be difficult or impossible to find in closed form, and further convolutions are yet more difficult to obtain.

Assuming that $k(x)$ is regularly varying, we can make much progress. By tail additivity property (2.2.26), we have $k^{t*}(x) \sim tk(x)$, and so we obtain the asymptotic equivalence

$$n_t(x) \sim N_0 R_0^t t k(x), \qquad x \to \infty. \tag{2.3.6}$$

This tells us that the tail of $n_t(x)$ is the same as that of the dispersal kernel $k(x)$, but scaled by a factor of $N_0 R_0^t t$. Given the form of the kernel $k(x)$ we can in principle invert the kernel to recover the position of the invasion front.

Figure 2.4 shows the true and approximate solutions, equations (2.3.5) and (2.3.6), for a point-release invasion under the linear model. We see that at standard linear scales, the approximation is not particularly convincing. Shifting to log scale, the approximation clearly coincides with the true solution for large x in the tails. We also see that successive generations have tails of increasing magnitudes: this is the factor $R_0^t t$ in equation (2.3.6).

2.3.2 Rate of invasion for fat-tailed kernels

Without knowing the specific kernel form, we can make much headway by assuming general power-law decay. Let $\overline{N}$ denote a threshold value, and let x_t be the position of the positive invasion front at time t, so that the invasion front and threshold value are related by

$$n_t(x_t) = \overline{N}. \tag{2.3.7}$$

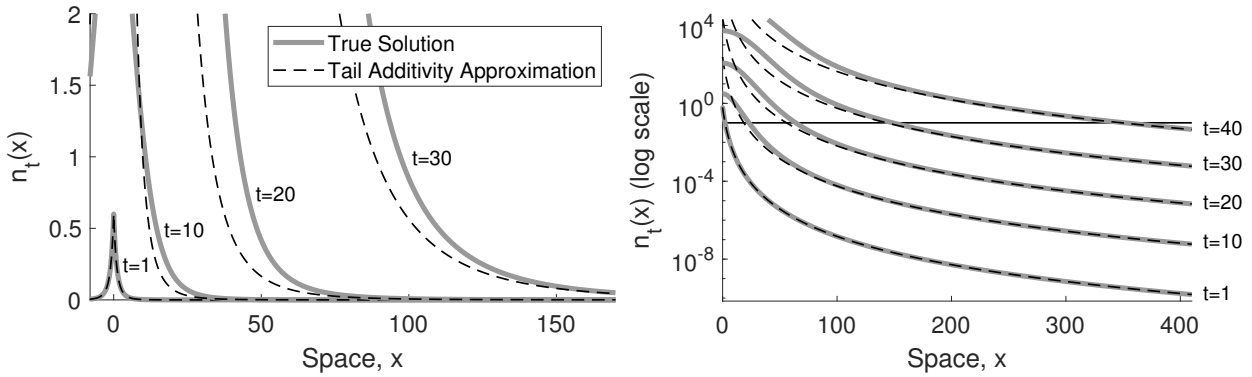

Figure 2.4: True solution and tail additivity approximation for the linear model. **(Left)** The true solution (gray lines) and approximation (2.3.6) due to tail additivity (black dashed lines) at times $t = 1, 10, 20, 30$. Dispersal is according to fat-tailed Laplace kernel (2.2.30) with tail fatness $\alpha = 5$ and $R_0 = 1.5$. **(Right)** In logarithmic scale, the tail addivitity approximation is seen to be accurate in the tails. The solid black line corresponds to the fixed detection threshold $\overline{N} = 0.1$, a typical value used to measure the extent of the invasion.

That is, the population density at the invasion front is the threshold value. Then at successive front positions, we have

$$n_{t+1}(x_{t+1}) = n_t(x_t) = \overline{N}. \tag{2.3.8}$$

Applying approximation (2.3.6), we have

$$N_0 R_0^{t+1}(t+1)k(x_{t+1}) \approx N_0 R_0^t t\, k(x_t) \tag{2.3.9}$$

so that

$$R_0 \left(\frac{t+1}{t}\right) k(x_{t+1}) \approx k(x_t). \tag{2.3.10}$$

Now assume that $k(x) \sim cx^{-\alpha}$ is a fat-tailed probability density function. We then obtain

$$x_{t+1}^{\alpha} \approx R_0 \left(\frac{t+1}{t}\right) x_t^{\alpha}. \tag{2.3.11}$$

For large t the factor $(t+1)/t$ becomes negligible and we observe geometric growth of the invasion front:

$$x_{t+1} \approx R_0^{1/\alpha}\, x_t, \qquad t \to \infty. \tag{2.3.12}$$

We say that such an invasion has a *geometric rate of spread*, with *base* $R_0^{1/\alpha}$. For an in-depth discussion of this approach for finding the invasion rate, please see the discussion in *Accelerating waves*.

It is important to note that the tail additivity property that we rely on in these arguments is an asymptotic relation, meaning that it holds as x becomes large. What this precisely means in terms of rates of convergence or when the relation can be said to hold 'well' depends on the distribution and parameters. A general rule is that as R_0 is made larger, the spatial extent grows more rapidly, moving the front position further into the tail of the distribution faster, where the asymptotics hold best.

We remark that although we have taken x_t to be the positive (rightward) invasion front position, we could also track the negative (leftward) front. Since the dispersal kernel $k(x)$ and initial condition are both symmetric and centered about the origin, spread will occur symmetrically in both directions.

2.3.3 Numerical examples

Numerical simulations are a natural complement to traditional analysis, especially in our case where our main results are asymptotic and deal with large time. Numerical examples enlighten us as to the early-time or transient dynamics that dominate spread rates in the early stages of invasion before the asymptotic, dynamics take effect.

In our simulations, the domain is a large interval, with half-width H, centered about the origin, and represented by a grid of points with uniform spacing Δx. The population densities $n_t(x)$ and the dispersal kernel $k(x)$ are represented on this domain, effectively truncating any infinite tails. Edge effects from the boundaries of the domain can affect the progress of an

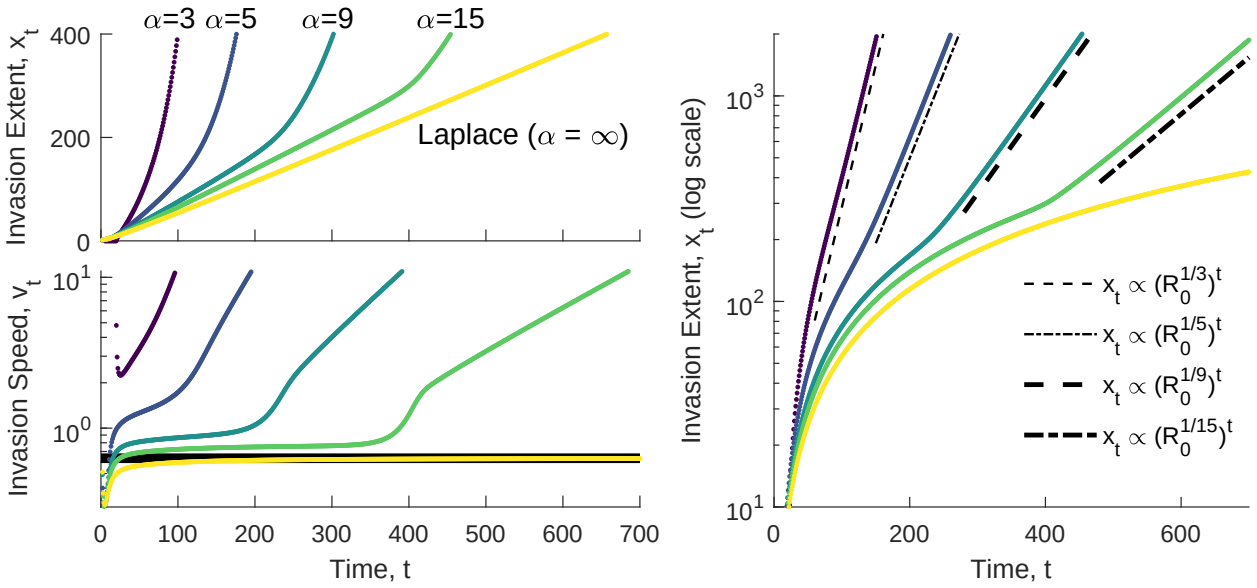

Figure 2.5: Rates of spread for fat-tailed invasions. Plots show the invasion extent x_t in both linear and logarithmic scales, as well as the invasion speed v_t for invasions with fat-tailed Laplace-kernel dispersal with $\alpha = 3, 5, 9, 15$. Also shown is invasion according to Laplace-kernel dispersal ($\alpha = \infty$). **(Left)** Fat-tailed invasions exhibit a transient phase of constant invasion speed during which the invasion progresses at a linear rate of spread. Plotting the per-step invasion speed $v_t = x_t - x_{t-1}$ shows that the invasion speed during the constant speed transient is closely related to the spreading speed of the Laplace kernel (black line). **(Right)** Plotting the invasion extent in log space reveals straight line trends, indicating geometric growth. The long-term or asymptotic rate of spread for fat-tailed point-release invasions is geometric with base $R_0^{1/\alpha}$.

invasion front, so a buffer is included when selecting the width of the domain, and simulations are re-run if the invasion front tends too close to either boundary. For the nonlinear model, we use the Beverton–Holt growth function (Beverton and Holt, 1957), except in the section *Weak Allee effects* where we use specialized growth functions with weak Allee effects. Point-release initial conditions for the nonlinear model were specified by setting $n_t(x) = N_0$, the source strength, for all gridpoints x_j satisfying $-1/2 < x_j < 1/2$ and $N_0/2$ for $|x_j| = 1/2$.

Our simulations are implemented in MATLAB. We use a midpoint-rule integration scheme for computing convolutions. This rule is implemented by the numerical convolution command `conv` with the `'same'` option, which computes a numerical convolution of two vectors

truncated to the same length as the starting vector. To measure population extent by a threshold value $\overline{N}$, we used the `find` command to select the last grid point x_j satisfying $n_t(x_j) > \overline{N}$. We then used interpolation with the `interp1` command with the `'spline'` method (cubic spline interpolation) on the surrounding points $x_{j-1}, \ldots, x_{j+2}$ to compute an accurate approximation of the invasion extent x_t such that $n_t(x_t) = \overline{N}$.

Figure 2.5 shows invasion extent x_t over time for five point-release invasions. In each invasion, the net reproductive rate is $R_0 = 1.1$, and the dispersal kernel is fat-tailed Laplace kernel (2.2.29) with $\alpha = 3, 5, 9, 15$. Also plotted is the invasion with Laplace-kernel (thin-tailed) dispersal for comparison. The plots reveal several key facts. First, the invasions have initial or transient periods where they progress at near-linear rates of spread or constant speeds. Second, as α increased, the invasions coincide more closely with the invasion with Laplace-kernel dispersal, at least in the short term. Third, asymptotically or in the long term, the invasions spread at geometric rates. We now address each of these points.

The *constant-speed transient* period is perhaps the most noticeable feature of fat-tailed invasions. When x_t is plotted versus time in linear scale, the trend is initially linear, similar to thin-tailed or constant speed invasions. We see that as α is increased, the duration of the constant speed transient is increased. This is related to the second observation: that the invasions begin to coincide with the thin-tailed invasion. We have already remarked that as $\alpha \to \infty$, the fat-tailed Laplace kernel converges to the Laplace kernel; this means that, in a way, their invasions also converge. The invasion speed during the constant speed transient is finite and for our families of fat-tailed kernels can be related to their thin-tailed limiting distributions: the Gaussian for the t-distribution and the Laplace kernel for the fat-tailed Laplace kernel.

2.3.4 Nonlinear model

The previous point-release analysis is limited in that it is based on the linear model, and so by conventional reasoning does not apply to invasions with weak Allee effects where the linear conjecture does not hold. In this section, we carry out an alternative analysis, now

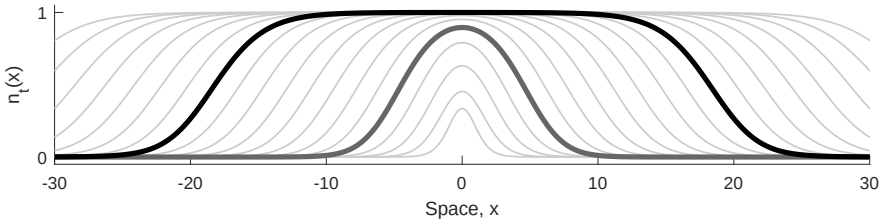

Figure 2.6: Population densities viewed as probability densities. Point-release invasions have population density profiles $n_t(x)$ that are scaled probability density functions (pdfs). By rescaling the generations $n_t(x)$ we obtain pdfs, to which we can apply asymptotic tail additivity laws.

with the nonlinear model. The general approach is to make mild assumptions on the initial condition and growth function such that each generation of the nonlinear model resembles a probability density function (pdf). By scaling each generation $n_t(x)$ by its total area, we obtain probability densities (Figure 2.6) and can use the tail additivity properties of regularly varying densities. We find that the tails of $n_t(x)$ again mirror those of the dispersal kernel, and we obtain the same asymptotic invasion rate of geometric growth as in the linear model.

We consider nonlinear model (2.1.2) with a point-release initial condition. We assume that $R_0 = f'(0) > 1$, so that there is at most a weak Allee effect, and that $f(n)$ has fixed points $n^* = 0$, unstable, and $n^* = 1$, a stable equilibrium. We assume that the initial condition has compact support, so that $n_0(x) = 0$ outside of a bounded interval. Therefore, each generation $n_t(x)$ will tend to zero for $|x|$ large, be bounded above by the carrying capacity, and integrate to a finite number. Thus, each generation will resemble a scaled probability density. Further, since $f(n) \to R_0 n$ as $n \to 0$ and $n_t(x) \to 0$ as $x \to \infty$,

$$f(n_t(x)) \to R_0 n_t(x) \quad \text{as} \quad x \to \infty. \tag{2.3.13}$$

By equation (2.3.13), if $n_t(x)$ is fat-tailed, then $f(n_t(x))$ will be fat-tailed as well, but scaled in magnitude by a factor of R_0.

Since a delta-function initial condition is not compatible with the nonlinear model, we

must make alternative assumptions about the initial condition. Define the total number of offspring at each generation, A_t, as

$$A_t = \int_{-\infty}^{\infty} f\left(n_t(x)\right) \mathrm{d}x. \tag{2.3.14}$$

We will assume that the initial condition $n_0(x)$ is such that $A_0 > 0$ is a well-defined real number and that the sequence $A_0, A_1, A_2, \ldots$ does not decrease. From the assumption that $n_0(x)$ has compact support, $f(n_0(x))/A_0$ is technically a thin-tailed probability density function. We therefore have

$$\begin{aligned} n_1(x) &= \left[k * f(n_0)\right](x) \\ &= A_0 \left[k * \frac{f(n_0)}{A_0}\right](x) \\ &\sim A_0 k(x). \end{aligned} \tag{2.3.15}$$

Here, the second equality comes from the linearity of the convolution operator, and the asymptotic equivalence from theorem (2.2.27).

With these facts we can find asymptotic tail approximations for the first few iterates. We first obtain $n_2(x)$,

$$\begin{aligned} n_2(x) &= \left[k * f(n_1)\right](x) \\ &= A_1 \left[k * \frac{f(n_1)}{A_1}\right](x) \\ &\sim A_1 \left[k(x) + \frac{f\left(n_1(x)\right)}{A_1}\right], \end{aligned} \tag{2.3.16}$$

where the second equality comes from the linearity of the convolution operator, and the

asymptotic equivalence follows from theorem (2.2.24). Next, using (2.3.13), we have

$$\begin{aligned} n_2(x) &\sim A_1 k(x) + R_0 n_1(x) \\ &\sim A_1 k(x) + R_0 A_0 k(x). \end{aligned} \tag{2.3.17}$$

Similarly,

$$\begin{aligned} n_3(x) &= \left[k * f(n_2)\right](x) \\ &\sim A_2 \left[k(x) + \frac{f\left(n_2(x)\right)}{A_2}\right] \\ &\sim A_2 k(x) + R_0 n_2(x) \\ &\sim A_2 k(x) + R_0 A_1 k(x) + R_0^2 A_0 k(x). \end{aligned} \tag{2.3.18}$$

We see that the t-th generation has the asymptotic form

$$n_t(x) \sim s_t k(x) \tag{2.3.19}$$

with

$$\begin{aligned} s_t &= A_{t-1} + R_0 A_{t-2} + \cdots + R_0^{t-1} A_0 \\ &= \sum_{k=0}^{t-1} R_0^k A_{t-1-k}. \end{aligned} \tag{2.3.20}$$

If we knew A_t, we could exactly predict the tail scale s_t of each generation of the population $n_t(x)$. Unfortunately, it is not easy to compute the total number of offspring at each generation. By relating the total population size N_t to the number of offspring, and by bounding the total population size by the rate of spread of the invasion, we can bound the rate of invasion from below and above, ultimately finding that the nonlinear model has the same geometric rate of spread as the linear model. Details of this argument are in *Nonlinear*

point release.

2.4 Weak Allee effects

A weak Allee effect is intermediate between compensation (no Allee effect) and critical depensation (a strong Allee effect). Although a growth function either does or does not have a weak Allee effect, the invasion rate often transitions smoothly rather than sharply as an Allee effect is introduced. As an example, consider the Nagumo equation (Britton, 1986),

$$\frac{\partial u}{\partial t} = u(u-\beta)(1-u) + D\frac{\partial^2 u}{\partial x^2}. \tag{2.4.1}$$

The growth in (2.4.1) has three parameter regimes: no Allee effect for $\beta < -1$, a weak Allee effect for $-1 < \beta < 0$, and a strong Allee effect for $0 < \beta < 1$. Separate analyses find the speed of invasion for the cases of no Allee effect and strong Allee effect, and it is observed that these analyses each correctly predict the invasion speed within part of the weak-Allee regime (Lewis et al., 2016).

In this section, we use simulations to analyze the rates of invasion for two families of growth functions that sit at the extremes of the weak Allee effect. The first extreme lies at the transition between a weak Allee effect and no Allee effect, and the second lies between a weak and a strong Allee effect. We find that the asymptotic results derived in the previous section do hold, but the degree of Allee effect can greatly affect the initial invasion rate and the duration of initial transient invasion speeds that precede the ultimate rate of invasion.

2.4.1 Transition to depensation

We first examine the transition to depensation; that is, how the rate of spread changes as a weak Allee effect is introduced. We construct a family of growth functions with a parameter

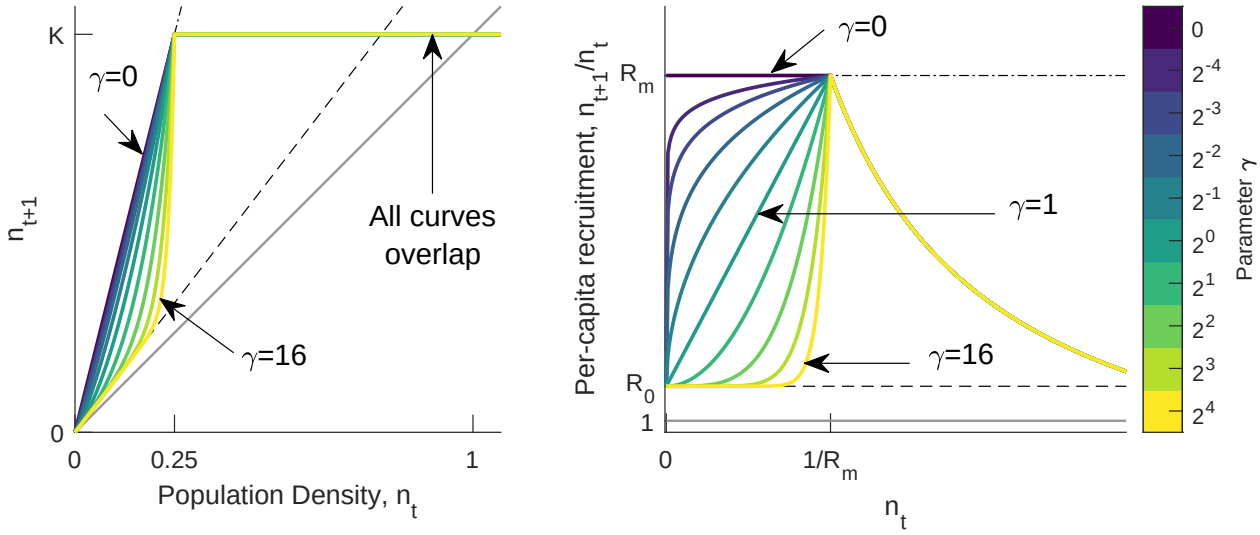

Figure 2.7: Weakening a weak Allee effect. **(Left)** The family of growth functions (2.4.2) smoothly encompasses the cases of no Allee and weak Allee effect. Curves shown are the function with parameter values $\gamma = 0, 2^{-4}, 2^{-3}, \ldots, 2^4$. For $\gamma = 0$, the growth function has no Allee effect and the net reproductive rate is R_m. For $\gamma > 0$, the net reproductive rate is R_0. **(Right)** The per-capita recruitment n_{t+1}/n_t.

γ that controls how prominent the weak Allee effect is,

$$f(n) = \begin{cases} n\left[R_0 + (R_m - R_0)(R_m n)^\gamma\right] & n < 1/R_m \\ 1 & n \geq 1/R_m. \end{cases} \tag{2.4.2}$$

We have plotted this growth function in Figure 2.7 with $R_0 = 1.1, R_m = 4$, and values of $\gamma = 0, 2^{-4}, 2^{-3}, \ldots, 2^4$.

There are two extreme cases: when $\gamma = 0$, the growth function reduces to a piecewise linear function,

$$f(n) = \begin{cases} R_m n & n < 1/R_m \\ 1 & n \geq 1/R_m. \end{cases} \tag{2.4.3}$$

This growth function has net reproductive rate R_m and no Allee effect. On the other hand,

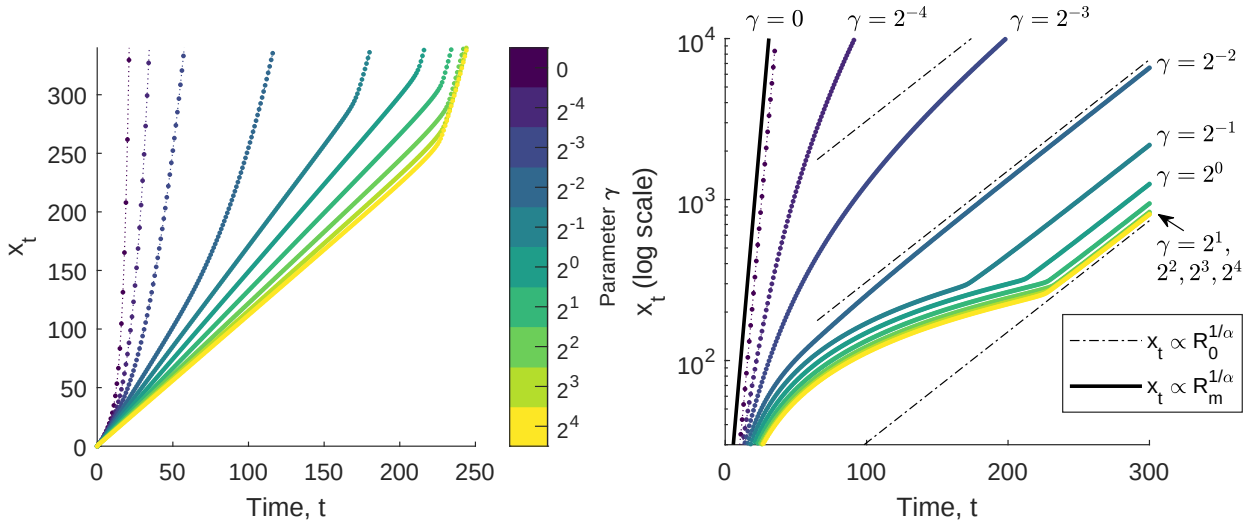

Figure 2.8: Rates of invasion as a weak Allee effect is introduced. Colors correspond to those in Figure 2.7. **(Left)** The invasion extent over time of ten simulations with the growth functions shown in Figure 2.7 with $R_0 = 1.1$ and $R_m = 4$. In all simulations the dispersal kernel is the t-distribution with $\nu = 5$. As γ is increased, the strength of the Allee effect is increased and the constant speed transient becomes pronounced. As γ is reduced, the Allee effect is weakened and the invasion has a faster initial rate of spread. **(Right)** Viewed in a logarithmic scale, the asymptotic rate of spread can be more clearly seen. For larger values of γ we see geometric growth with base $R_0^{1/\alpha}$.

as $\gamma \to \infty$, the function converges to a different piecewise linear function,

$$f(n) = \begin{cases} R_0 n & n < 1/R_m \\ 1 & n \geq 1/R_m. \end{cases} \tag{2.4.4}$$

This growth function has net reproductive rate R_0, but has maximum per capita recruitment R_m, attained at $n = 1/R_m$.

For values of $0 < \gamma < \infty$, growth function (2.4.2) has behavior between these cases. The function has the value $f(1/R_m) = 1$ and therefore has maximum per capita recruitment R_m attained at the point $n = 1/R_m$; however, $f'(0) = R_0$, and so an Allee effect is always present.

Populations that grow under these growth functions invade very differently depending on the degree of the weak Allee effect, as can be seen in Figure 2.8. For $\gamma = 0$, the population invades rapidly at a geometric rate with base $R_m^{1/\alpha}$, which is expected, since in this case the growth function has no Allee effect and has net reproductive rate R_m. On the other hand, for $\gamma = 1/2, 1, 2, 4, 8, 16$, the populations exhibit constant speed transients for over one hundred iterations before transitioning to invasion at a geometric rate with base $R_0^{1/\alpha}$. For $0 < \gamma < 1/2$ the invasions initially invade rapidly and faster than geometrically with base $R_0^{1/\alpha}$, but the trends indicate a slowing rate of invasion that converges to geometric with base $R_0^{1/\alpha}$. Thus our asymptotic result — that the invasions will converge to a geometric rate of spread with base $R_0^{1/\alpha}$ — holds, but the rate of convergence can be made very slow by careful choice of growth function.

2.4.2 Transition to critical depensation

We now address the case of weak Allee effects that border on the strong Allee case. In a strong Allee effect $R_0 < 1$, so this case can be thought of as strengthening a weak Allee effect such that $R_0 > 1$ approaches one. We construct a family of growth functions with an Allee effect where R_0 can be made close to one,

$$f(n) = \frac{R_0 n}{1 - (2 - R_0 - bR_0)n + (1 - bR_0)n^2}. \tag{2.4.5}$$

This growth function satisfies $f'(0) = R_0$ and $f'(1) = b$. For our simulations we set $b = .5$ and $R_0 = 1.1, 1.01, 1.001$. As we will soon see, the invasions that result from near-strong weak Allee effects have extremely long transient dynamics, so this growth function was selected to ensure that each generation $n_t(x)$ was smooth to allow for simulations and numerical integration on a coarse numerical grid.

Figure 2.9 shows plots of invasion extent for the three invasions with $R_0 = 1.1, 1.01, 1.001$. For all three simulations, we observe an initial constant speed transient that gives way to geometric growth. As we decrease R_0 to one, the duration of the constant speed transient

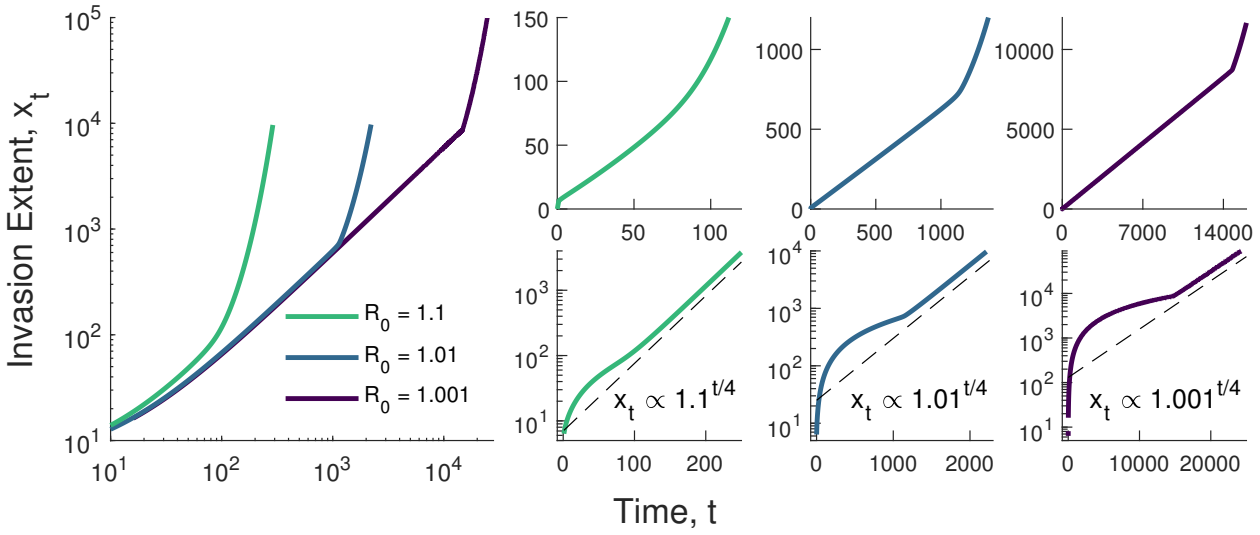

Figure 2.9: Acceleration of invasions is delayed as a weak Allee effect is strengthened. Invasions with near-strong weak Allee effects have extremely long periods of nearly-constant invasion speeds. Plots show invasion extent over time for point-release invasions with weak Allee growth function (2.4.5) with $R_0 = 1.1, 1.01, 1.001$. Dispersal is according to the t-distribution with $\nu = 5$. The constant speed transient period lengthens as R_0 is reduced but the (eventual) asymptotic rate of spread is always geometric with base $R_0^{1/\alpha}$. For the case where $R_0 = 1.001$ the invasion progresses at a near-constant invasion speed for over 14 000 generations before transitioning to geometric growth. In all simulations the grid spacing is $\Delta x = 0.5$; the domain half-width is $H = 10\,000$ for $R_0 = 1.1, 1.01$ and $H = 100\,000$ for $R_0 = 1.001$.

lengthens, delaying the geometric phase; for $R_0 = 1.001$, the transient phase lasts for nearly 15 000 generations. In all cases the asymptotic rate of spread is geometric with base $R_0^{1/\alpha}$.

We remark that in the limit as $R_0 \to 1$, $R_0^{1/\alpha} \to 1$ as well, which marks a breakdown in both our analysis and in the analytic result: when the base of the exponent becomes one, there is no longer geometric growth. Thus the case where $R_0 = 1$ can be seen as a limiting case in two ways: first, the duration of the constant speed transient becomes infinite, and second, the geometric growth phase becomes degenerate.

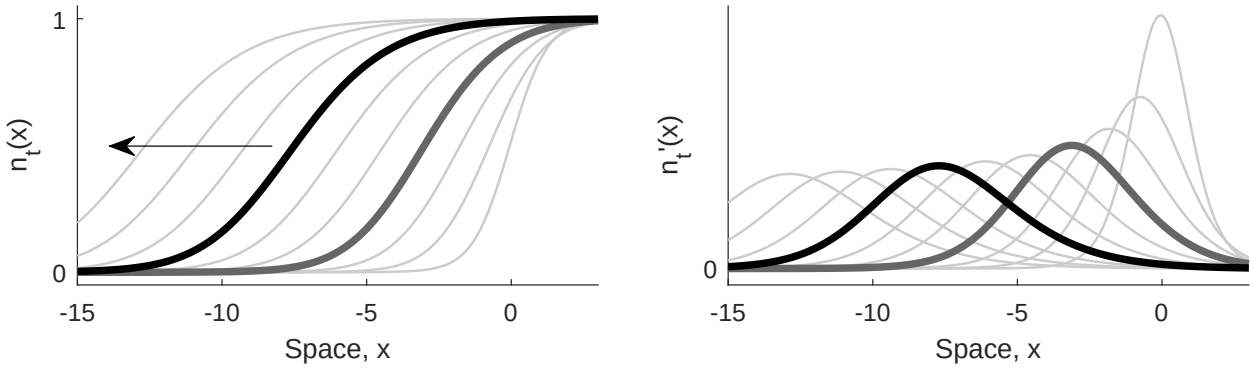

Figure 2.10: Population densities viewed as distribution functions. The generations $n_t(x)$ of a front-release invasion can be viewed as cumulative distribution functions (cdf). Their derivatives $n_t'(x)$ can then be viewed as probability density functions (pdf).

2.5 Front-release initial conditions

We now turn to invasion following front-release initial conditions, where well-established populations invade new territory. To simplify our arguments and analysis, we assume that the population carrying capacity has been re-scaled to one and restrict our attention to leftward-moving invasions. We derive a tail approximation for a front-release invasion under the nonlinear model, and then use it to find the rate of invasion.

The general approach is to make mild assumptions on the initial condition and growth function such that each generation of the nonlinear model resembles a cumulative distribution function. Figure 2.10 shows example front-release generations: $n_t(x)$ goes from zero at $-\infty$ to one (the rescaled carrying capacity) at $+\infty$, satisfying the conditions of a cumulative distribution function. This also means that the derivative, $n_t'(x)$, is a probability density function. Through transformations, we recast the nonlinear model as an iteration that moves between cumulative distributions and probability densities, and we track the shape and scale of the tails of these distributions.

To proceed, we must also make some assumptions about the growth function $f(n)$. In addition to $f(n)$ being monostable with $n = 0$ unstable and $n = 1$ stable, we assume that $f(n)$ has at most a weak Allee effect and is also *order-preserving*; this means that if $n \leq m$,

then $f(n) \leq f(m)$. From these assumptions, we can conclude that if $n_t(x)$ is a cdf, then $f(n_t(x))$ is also a cdf.

2.5.1 Tail approximation

Consider again the nonlinear model,

$$n_{t+1}(x) = [k * f(n_t)](x). \tag{2.5.1}$$

The process to obtain $n_{t+1}(x)$ from $n_t(x)$ can be succinctly expressed in terms of *operators*. Let $\mathbf{f}$ represent application of the growth function $f(n)$ to every point in the domain,

$$(\mathbf{f}n_t)(x) = f(n_t(x)), \tag{2.5.2}$$

and let $\mathbf{k}$ represent convolution with the dispersal kernel $k(x)$,

$$(\mathbf{kf}n_t)(x) = (k * \mathbf{f}n_t)(x) = [k * f(n_t)](x). \tag{2.5.3}$$

The *operators* $\mathbf{f}$ and $\mathbf{k}$ act on functions of x to produce new functions of x. The function $n_{t+1}(x)$ can be expressed by applying $\mathbf{f}$ to $n_t(x)$ and by then applying $\mathbf{k}$ to get

$$n_{t+1}(x) = \mathbf{kf}n_t(x). \tag{2.5.4}$$

Operator notation is convenient for expressing more complicated operations. Consider differentiation and integration: both act on functions of x and return functions of x, and so are operators. Let $\mathbf{D}_x$ denote differentiation with respect to space,

$$(\mathbf{D}_x n_t)(x) = \frac{\mathrm{d}}{\mathrm{d}x} n_t(x), \tag{2.5.5}$$

and let $\mathbf{D}_x^{-1}$ denote definite integration from $-\infty$ to x,

$$(\mathbf{D}_x^{-1} n_t)(x) = \int_{-\infty}^{x} n_t(y)\mathrm{d}y. \tag{2.5.6}$$

If we assume that the original function $n_t(x)$ has the limit $n_t(x) \to 0$ as $x \to -\infty$, then these two operators act as inverses of one another,

$$\mathbf{D}_x^{-1}\mathbf{D}_x n_t = n_t. \tag{2.5.7}$$

That is, if we differentiate $n_t(x)$ and then integrate the result, we re-obtain $n_t(x)$. These operators can also be related to the kernel pdf and cdf: $k = \mathbf{D}_x K$ and $K = \mathbf{D}_x^{-1} k$.

With these operators in place, we can rewrite the nonlinear model as

$$\begin{aligned} n_{t+1} &= \mathbf{k}\mathbf{D}_x^{-1}\mathbf{D}_x\mathbf{f}n_t \\ &= \mathbf{D}_x^{-1}\mathbf{k}\mathbf{D}_x\mathbf{f}n_t, \end{aligned} \tag{2.5.8}$$

where the rearrangement of the integration $\mathbf{D}_x^{-1}$ and the convolution $\mathbf{k}$ in the second line is allowed by the fact that both are linear operators that commute with one another. The added steps of differentiation and integration can be viewed as transformations that move between a space of cumulative distribution functions (that correspond to population density profiles) and probability density functions. The advantage of breaking up the iteration in this way is that each of the operations, $\mathbf{f}, \mathbf{D}_x, \mathbf{k}, \mathbf{D}_x^{-1}$ can be understood separately in terms of their affect on the tail of the population density.

This decomposition will allow us to track how the tail of the population evolves, but first we must specify an initial condition. The simplest front-like initial condition is the *Heaviside*

function,

$$n_0(x) = H(x) = \begin{cases} 0 & x < 0 \\ 1 & x \geq 0. \end{cases} \tag{2.5.9}$$

When the initial population density is given by the Heaviside function, the population density of the first generation will be given by the cdf $K(x)$ of the dispersal kernel. This is because

$$\begin{aligned} n_1(x) &= \int_{-\infty}^{\infty} k(y)H(x-y)\mathrm{d}y \\ &= \int_{-\infty}^{x} k(y)\mathrm{d}y \\ &= K(x). \end{aligned} \tag{2.5.10}$$

Using iteration (2.5.8) and tracking the intermediate results, we first apply the growth function,

$$\begin{aligned} \left(\mathbf{f}n_1\right)(x) &= f\left(n_1(x)\right) \\ &\sim R_0 K(x), \qquad x \to -\infty, \end{aligned} \tag{2.5.11}$$

then differentiate with respect to x,

$$\begin{aligned} \left(\mathbf{D}_x\mathbf{f}n_1\right)(x) &\sim R_0\mathbf{D}_x n_1(x) \\ &\sim R_0 k(x), \end{aligned} \tag{2.5.12}$$

convolve by the dispersal kernel,

$$\begin{aligned}(\mathbf{k}\mathbf{D}_x\mathbf{f}n_1)(x) &= \mathbf{k}\left[R_0k(x)\right] \\ &\sim R_0k(x) + k(x) \\ &= (R_0+1)k(x),\end{aligned} \tag{2.5.13}$$

and finally integrate from $-\infty$,

$$\begin{aligned}\left(\mathbf{D}_x^{-1}\mathbf{k}\mathbf{D}_x\mathbf{f}n_1\right)(x) &= \mathbf{D}_x^{-1}(R_0+1)k(x) \\ n_2(x) &\sim (R_0+1)K(x).\end{aligned} \tag{2.5.14}$$

In the above, all asymptotic relations hold as $x \to -\infty$ because we are examining a leftward-moving wave. We see that the first iterate has tail decay matching the cdf $K(x)$ and that the second iterate has the same degree of tail decay but multiplied by a factor of (R_0+1).

Repeating this for the third iterate,

$$\begin{aligned}n_3(x) &\sim \left[R_0(R_0+1)+1\right]K(x) \\ &= \left(R_0^2+R_0+1\right)K(x),\end{aligned} \tag{2.5.15}$$

and fourth iterate,

$$\begin{aligned}n_4(x) &\sim \left[R_0(R_0^2+R_0+1)+1\right]K(x) \\ &= \left(R_0^3+R_0^2+R_0+1\right)K(x).\end{aligned} \tag{2.5.16}$$

we find an emerging pattern. After n iterates, the finite geometric series that is the coefficient of $K(x)$ can be written as

$$1 + R_0 + R_0^2 + \cdots + R_0^{n-1} = \frac{R_0^n - 1}{R_0 - 1}. \tag{2.5.17}$$

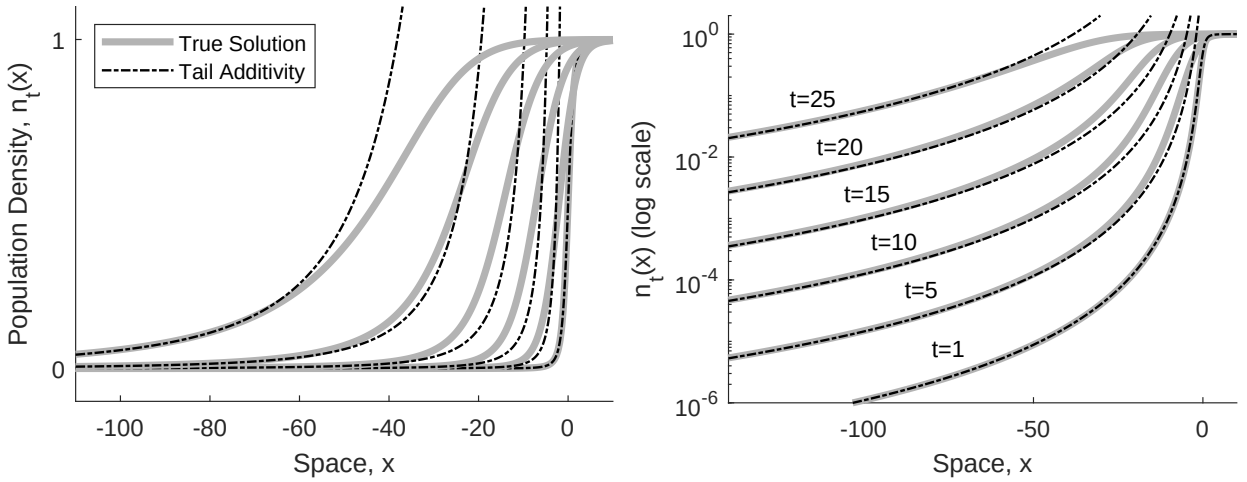

Figure 2.11: Comparison of true and approximate solution for a front-release invasion. **(Left)** The exact solution (gray lines) and approximation (2.5.18) due to tail additivity (black dashed lines) plotted at times $t = 1, 5, 10, 15, 20, 25$. The dispersal kernel is the t-distribution ($\nu = 9$) and the growth function is Beverton–Holt with $R_0 = 1.5$. **(Right)** The true solution and approximation in log space. The accuracy of the approximation can clearly be seen in the tails.

We ultimately find that

$$n_t(x) \sim \left(\frac{R_0^t - 1}{R_0 - 1}\right) K(x). \tag{2.5.18}$$

From this, we see, as for approximation (2.3.6) for point-release invasions, that the tail behavior of $n_t(x)$ again mirrors that of the kernel, but now, instead of it matching pdf $k(x)$, it matches cdf $K(x)$.

Figure 2.11 shows tail additivity approximation (2.5.18) for a front-release release invasion with nonlinear model (2.1.2) in linear- and log-scales. As for the point-release example, the approximation does not appear robust for small x and at linear scale but, when viewed in log-scale, the asymptotic convergence of the tails for large x is evident and can be seen to improve over time.

2.5.2 Rate of invasion for fat-tailed kernels

For a fat-tailed kernel with degree of tail fatness α, the pdf satisfies $k(x) \sim c(-x)^{-\alpha}$ as $x \to -\infty$, and the cdf will decay at a slower degree of $\alpha - 1$:

$$\begin{aligned} K(x) &= \int_{-\infty}^{x} k(y)\mathrm{d}y \\ &\sim \int_{-\infty}^{x} c(-y)^{-\alpha}\mathrm{d}y \\ &= \tilde{c}(-x)^{-(\alpha-1)}. \end{aligned} \tag{2.5.19}$$

Thus, the cdf has a fatter tail than the pdf.

To find the invasion rate under such a kernel, we proceed in the same way as for point-release invasions; since we are, however, tracking a leftward-moving invasion, we will let $-x_t$ denote the position of the invasion front so that $x_t > 0$. We next set

$$n_{t+1}(-x_{t+1}) = n_t(-x_t) = \overline{N} \tag{2.5.20}$$

and insert the front-release approximation (2.5.18) for $n_t(x)$. We obtain

$$(R_0^{t+1} - 1)K(-x_{t+1}) \approx (R_0^t - 1)K(-x_t). \tag{2.5.21}$$

Assuming that $K(x) \sim \tilde{c}(-x)^{-(\alpha-1)}$, then

$$x_{t+1}^{(\alpha-1)} \approx \left[\frac{R_0^{t+1} - 1}{R_0^t - 1}\right] x_t^{(\alpha-1)}. \tag{2.5.22}$$

As t increases, the bracketed quantity converges to R_0 (for $R_0 > 1$). As in the case of a point-release, we observe geometric growth of the wavefront,

$$x_{t+1} \approx R_0^{1/(\alpha-1)} x_t, \qquad t \to \infty. \tag{2.5.23}$$

We see, however, that the base of the geometric growth is $R_0^{1/(\alpha-1)}$ for front-release invasions rather than $R_0^{1/\alpha}$ for point-release invasions.

2.5.3 Other front-release initial conditions

The previous analysis was carried out assuming that the initial condition follows Heaviside function (2.5.9). This assumption can be relaxed considerably: the invasion rate will be the same if the initial condition is the cdf of any thin-tailed distribution, or even for any distribution that is less heavy-tailed than the dispersal kernel. This is because if $n_0'(x)$ is a probability density we can apply the additivity theorem (2.2.27), where one density dominates the other. Therefore

$$\begin{aligned} n_1'(x) &= \int_{-\infty}^{\infty} k(x-y) n_0'(y) \mathrm{d}y \\ &= \big(k * n_0'\big)(x) \\ &\sim k(x), \qquad x \to -\infty. \end{aligned} \tag{2.5.24}$$

Integrating to re-obtain $n_1(x)$, we have

$$n_1(x) \sim K(x), \tag{2.5.25}$$

which generalizes first-iterate (2.5.10). This means that the initial front-release condition can be, for example, a linear transition from zero to one occurring over any finite width or a smooth logistic curve.

2.6 Invasion rates and initial conditions

Our point- and front-release analyses show that the asymptotic invasion rate of a fat-tailed invasion depends on its initial condition. The tail decay of a point-release invasion mirrors that of the dispersal kernel pdf $k(x)$, whereas the tail decay of a front-release invasion is like that of its cdf $K(x)$. For fat-tailed kernels, the cdf has a slower rate of decay than the

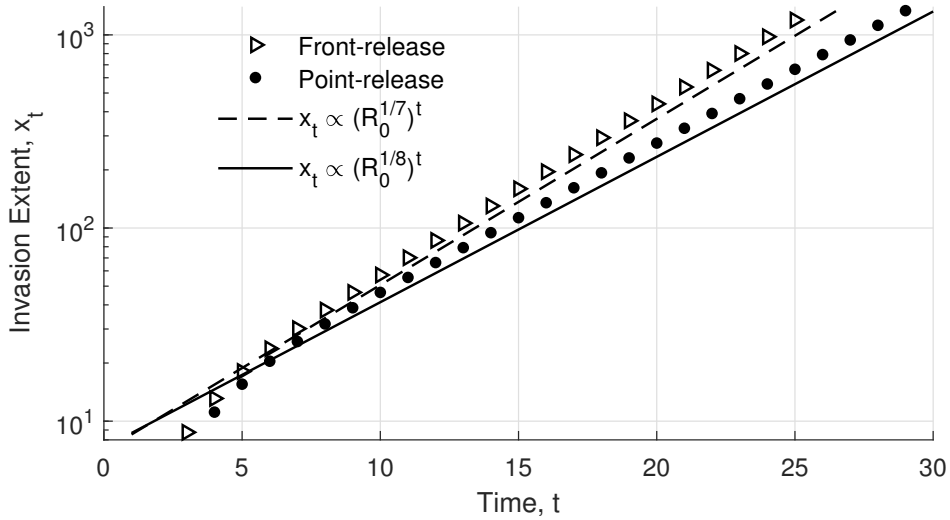

Figure 2.12: Front-release invasions spread at a faster geometric rate than point-release invasions. The plot show the invasion extent over time for point- and front-release invasions under the nonlinear model with Beverton–Holt growth ($R_0 = 4$) and fat-tailed Laplace-kernel dispersal. In log space, the invasion extents tend to straight line trends that indicate geometric growth. The fact that the two trends diverge shows that the rates of geometric growth differ between point- and front-release invasions. The two lines correspond to the rates predicted by our analyses. The numerical domain has half-width $H = 15\,000$ and grid-spacing $\Delta x = 0.1$.

pdf; if $k(x)$ has tail fatness of degree α, then $K(x)$ will have degree $\alpha - 1$. This in turn means that point-release invasions will invade geometrically with base $R_0^{1/\alpha}$ and that front-release invasions will spread geometrically with base $R_0^{1/(\alpha-1)}$.

This result shows that the initial condition of a fat-tailed invasion can have a lasting effect on the ultimate invasion rate of the population; the initial condition affects the ultimate rate of spread, and the effect is persistent for all time. Point- and front-release invasions will both asymptotically invade at geometric rates, but these rates differ. Figure 2.12 compares the invasion rates for point- and front-release invasions under the nonlinear model. We plot the invasion extent x_t on a logarithmic scale and see straight-line trends that indicate geometric growth. We see good agreement with the analytic predictions; both invasions spread at geometric rates: the point-release invasion with base $R_0^{1/\alpha}$ and the front-release with base

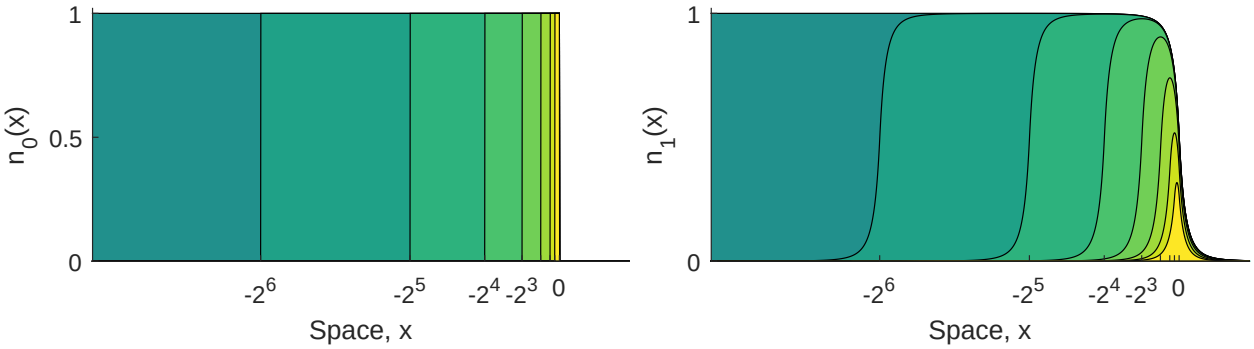

Figure 2.13: Plateau initial conditions. These conditions are intermediate between a point release and a front-release. **(Left)** Each shaded region shows an initial condition $n_0(x)$ that is a "plateau" of width $W = 2^k$ for $k = 0, 1, 2, \ldots, 7$. **(Right)** The first generation $n_1(x)$ following a plateau-release. The populations do not interact with one another. For narrow plateaus the generations look like a point release. The population densities line up at the right as the plateau width is increased, and converge to a front release.

$R_0^{1/(\alpha-1)}$. The difference is clearly visible on a logarithmic scale, where the diverging straight-line trends indicate different bases.

2.6.1 Plateau initial conditions

Our analyses have focused on point-release and front-release invasions, two extreme cases corresponding to invasions beginning with either a small and highly localized population or a large population spread over a semi-infinite area. A natural question is what occurs for intermediate cases, i.e., for those populations that are not so well-established as to have semi-infinite support but that also cannot be thought of as initially localized to a point.

To address this, we performed simulations with *plateau initial conditions*, where the initial population is one within an interval and zero outside. Precisely, we set $n_0(x) = 1$ for $-W < x \leq 0$ and $n_0(x) = 0$ elsewhere. We simulated plateaus on domains with half-width $H = 2^N$ and plateau widths $W = 2^0, 2^1, 2^2, \ldots, 2^N$ so as to range from the case of a near-point-release to a near-front-release. We show example plateau initial conditions and the population distributions that arise from them after one generation in Figure 2.13. Under our

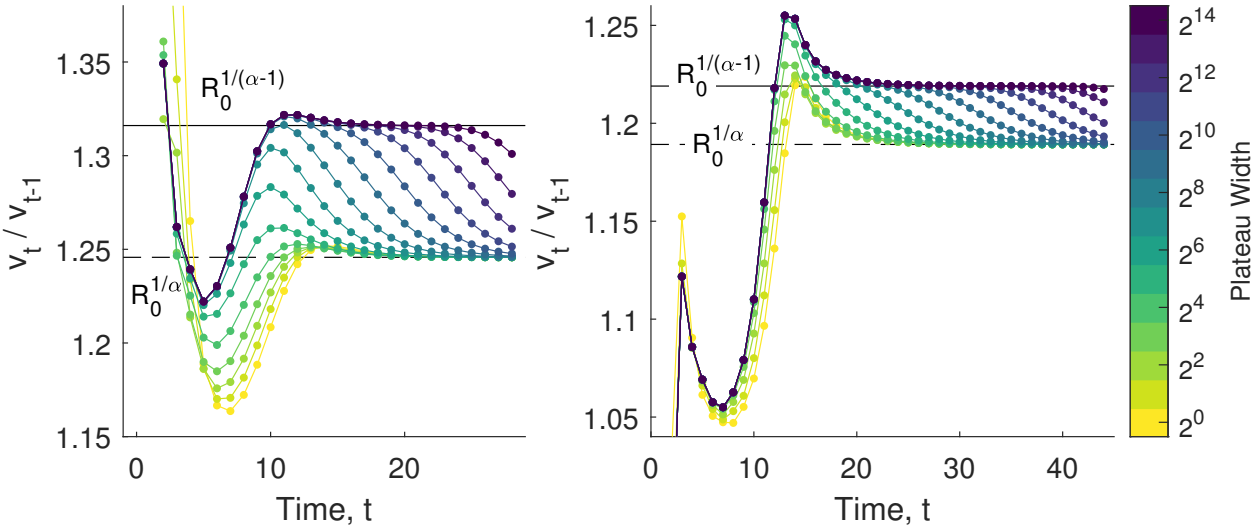

Figure 2.14: Invasion rates following plateau initial conditions. Plateau initial conditions produce invasions whose behavior shares qualities of both point- and front-release invasions. As the plateau width increases, the initial condition more closely resembles a front-release invasion, and so the invasion initially progresses geometrically with base $R_0^{1/(\alpha-1)}$ as is characteristic of a front-release invasion. After a delay related to the width of the plateau, the invasion slows to the rate associated with point-release invasions: geometric with base $R_0^{1/\alpha}$. **(Left)** Plateau invasions with fat-tailed Laplace-kernel dispersal ($\alpha = 5$) and $R_0 = 3$. The grid spacing is $\Delta x = 0.25$ and domain half-width $H = 2^{14}$. **(Right)** Plateau invasions with t-distribution dispersal ($\nu = 7$) and $R_0 = 4$. The grid spacing is $\Delta x = 0.5$ and domain half-width $H = 2^{14}$.

definitions, plateau initial conditions are not front-like (they are zero at both positive and negative infinity) but they become locally front-like as their width is increased. Extending the back of the plateau to larger negative values brings the local behavior of the plateaus near the origin into closer agreement with a front-release.

For a population invading at a geometric rate with $x_{t+1} = \rho x_t$, the invasion speed $v_t = x_t - x_{t-1}$ also obeys the relation $v_t = \rho v_{t-1}$. Computing v_t/v_{t-1} reveals the per-step rate of geometric growth. We expect $v_t/v_{t-1} \to R_0^{1/\alpha}$ for a point-release invasion and $v_t/v_{t-1} \to R_0^{1/(\alpha-1)}$ for a front-release. Figure 2.14 shows plots of the computed speed ratio for plateau initial conditions with t-distribution dispersal. We see that, for all plateau widths, the invasion experiences a transient period of around ten to twenty generations as the invasion

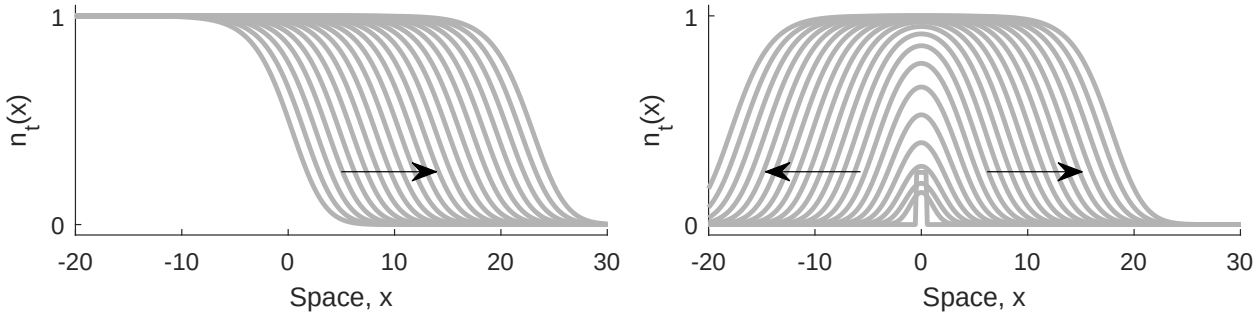

Figure 2.15: Thin-tailed invasions. Plots show twenty generations of **(Left)** a traveling wave solution and **(Right)** a point-release invasion. The invasion fronts of the point-release invasion quickly converge to match the shape of the constant-speed traveling waves. Solutions are computed numerically on a domain with half-width $H = 400$, $\Delta x = 1/16$ with Beverton–Holt growth with $R_0 = 2.0$, and Gaussian (standard normal) dispersal.

front is established and the rate of acceleration stabilizes. For narrow plateaus, the speed ratio approaches the predicted rate for point-release invasions, $R_0^{1/\alpha}$. For wide plateaus, the speed ratio instead approaches the predicted rate for front-release invasions, $R_0^{1/(\alpha-1)}$, but eventually declines and approaches $R_0^{1/\alpha}$. This makes intuitive sense because in the short-term a plateau initial condition looks and behaves like a front-release. On the other hand, in the long-term a spreading invasion will eventually dwarf any bounded initial condition, which will by that point more closely resemble a point-release. Only a genuine front-release with unbounded support will not resemble a point-release in the long-term, when compared against an ever-expanding invaded territory, and can maintain the greater rate of invasion for all time.

2.7 Accelerating waves

In this section, we outline the major qualitative differences between constant-speed and accelerating invasions and what these differences mean in terms of measurement and analysis.

2.7.1 Constant-speed invasions

Traveling waves are a cornerstone of thin-tailed invasions. A traveling wave solution has the form

$$n_t(x) = w(x - ct) = w(z), \tag{2.7.1}$$

where $z = x - ct$ is the *traveling wave coordinate*, a moving frame of reference that keeps pace with the movement of the wave. Figure 2.15 shows an example traveling wave generated by Gaussian dispersal with Beverton–Holt growth. The profile of the invasion front is preserved between generations and translates at a consistent rate or speed c so that

$$n_{t+1}(x) = n_t(x - c). \tag{2.7.2}$$

Any spatial position linked to features of the wave, such as the position of level sets or a point beyond which the wave integrates to a specific value, moves with the wave at the speed c. This means that many measures of invasion are equivalent.

Systems with thin-tailed dispersal often support traveling wave solutions of various speeds and have a minimum wave speed $c_{\min}$. When the initial condition is front-like, the solution will converge to a traveling wave. The wave speed is usually $c_{\min}$ when the initial condition is identically zero in the uninvaded territory or when the initial population density decays sufficiently rapidly. The traveling wave can be boosted to greater speeds, by specifying initial conditions that decay exponentially into the uninvaded territory, and can even be made to accelerate when heavy-tailed initial conditions are given (Alfaro, 2017).

The importance of the theory of traveling waves extends beyond front-release invasions. Even when the initial condition is compactly supported, the invasion front of a population that successfully invades will mirror that of a traveling wave (Lewis et al., 2016). An example of this can be seen in Figure 2.15, which shows thin-tailed traveling waves as well as point-release invasions.

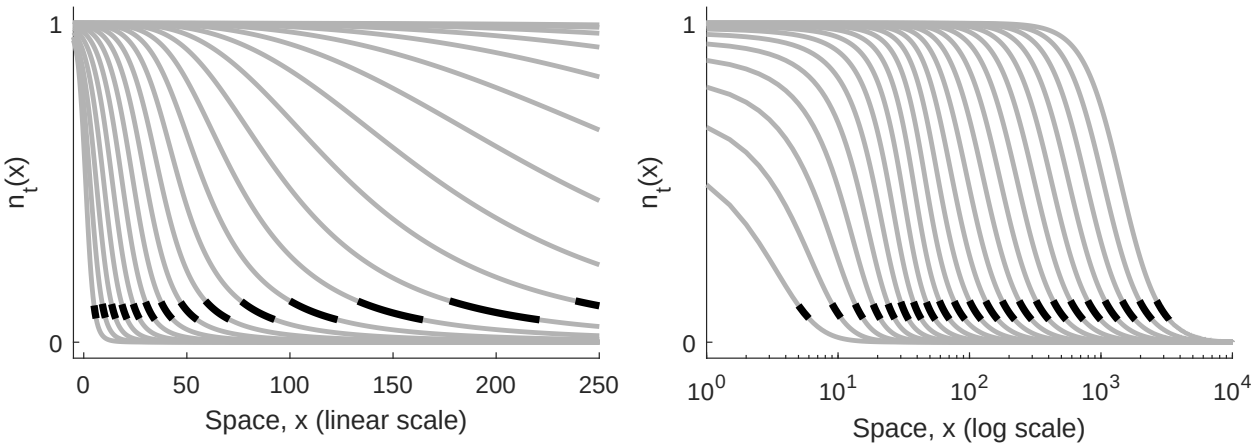

Figure 2.16: Invasion fronts of a geometrically accelerating invasion plotted using linear and logarithmic scales. Plots show $n_t(x)$ for $t = 5, 10, \ldots, 60$ for a front-release invasion with t-distribution ($\nu = 3$) dispersal. **(Left)** The fat-tailed invasion advances at an accelerating rate and the invasion front stretches and elongates as its speed increases. **(Right)** Plotting with x on a logarithmic scale the accelerating invasion front converges to a consistent profile akin to a traveling wave. The domain half-width is $H = 10\,000$, $\Delta x = 0.5$, and growth is Beverton–Holt with $R_0 = 1.2$.

The *spreading speed* c^* is defined as the unique speed that keeps pace with any invasion emanating from compact initial conditions. A significant result (Hsu and Zhao, 2008) states that the minimum wave speed matches the spreading speed: $c^* = c_{\min}$. This is a powerful result that is not immediately obvious. As a consequence, the question of the speed of thin-tailed invasions is greatly simplified: for virtually any initial condition used in practice, the invasion speed will be the same.

2.7.2 Accelerating invasions

The notion of an invasion front is fundamentally different in accelerating invasions from those with constant speed. In a traveling wave, the invasion front has a characteristic width such that the population level is negligible far ahead of the invasion. In an accelerating invasion, the front has no fixed width and actually grows without bound. This means that at successive generations a larger and larger patch surrounding the front has population density

comparable to that of the front position. An example of this can be seen in Figure 2.16, where the length of the domain captured between two level sets grows over time.

The traveling wave coordinate is not useful for analyzing accelerating waves since their shape and speed change with time. Since the invasion extent x_t grows geometrically, it is instead natural to apply a logarithmic transformation to the spatial variable. Figure 2.16 shows an accelerating invasion plotted in both normal space and log-transformed space. We see that on a linear-linear plot the invasion front elongates whereas in a log-linear plot the invasion front tends to a consistent shape, similar to that of a traveling wave.

The fact that point- and front-release invasions have differing rates of spread is another major indication that fat-tailed invasions are fundamentally different from thin-tailed ones and require careful attention. For thin-tailed invasions, the minimum wave speed is equivalent to the spreading speed; this means we need only find one invasion speed, regardless of the initial condition. Our results for point-, front-, and plateau-release invasions demonstrate that there is no equivalence of invasion rate between compact-release and front-release invasions when dispersal is fat-tailed. The rate of spread for fat-tailed invasions has fundamental dependence on the initial condition.

2.7.3 Rates of invasion

Thin-tailed invasions converge to constant-speed traveling waves, and we say that their rate of spread is linear. A large body of work is in place around this paradigm: approaches for finding the speed and even definitions for the speed are built around the assumption that the speed will approach a constant value. As an example, Kot and Neubert (2008) derived the invasion speed for thin-tailed kernels by taking the limit of distance divided by time,

$$c = \lim_{t\to\infty} \frac{x_t}{t}. \tag{2.7.3}$$

This and similar definitions take advantage of the fact that in the limit, x_t is proportional to the time t — the bulk of the magnitude of x_t is due to traveling at the speed c, and any

transient speedup or slowdown that occurs in finite time is negligible.

The invasion speed can also be calculated on a per-step basis by taking the difference of successive front positions,

$$v_t = x_t - x_{t-1}. \tag{2.7.4}$$

In the case of thin-tailed invasions, we observe that v_t converges to a finite value, the same speed c found by (2.7.3).

Accelerating invasions attain ever-greater speeds and so cannot be characterized by a single speed. We therefore draw the distinction that accelerating invasions have invasion *rates* rather than invasion *speeds*. An invasion may be generally described as having a spread rate, such as polynomial or geometric growth in time. A constant-speed invasion has a *arithmetic* rate of spread that is characterized by a single measurement, the invasion speed, but accelerating invasions necessarily have different rate types. In general each type of invasion rate requires a different characterization.

Geometric growth is characterized by multiplication by a constant growth factor: if the invasion front advances geometrically, then $x_{t+1} = \rho x_t$ for some factor $\rho > 1$. Taking the ratio of the position of the invasion front at successive times will yield the rate of growth between generations. Taking the limit as time becomes large, we recover the asymptotic rate of geometric invasion,

$$\lim_{t\to\infty} \frac{x_{t+1}}{x_t} = \rho. \tag{2.7.5}$$

The approach of measuring the limiting ratio x_{t+1}/x_t is, to our knowledge, a new way of measuring the rate of invasion. If misapplied, it can produce misleading or counter-intuitive results. Consider the case of applying limit (2.7.5) to a constant-speed invasion where $x_t = ct$.

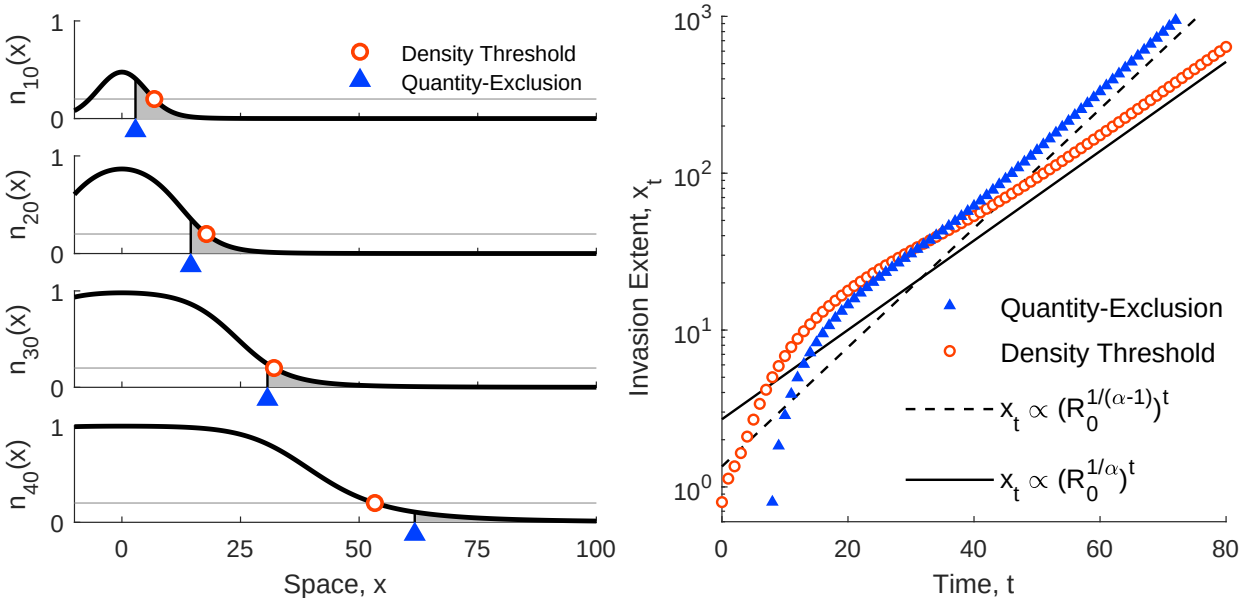

Figure 2.17: Two approaches for measuring invasion extent. To measure by density-threshold, we set a threshold value $\overline{N}$ and define x_t so that the population density at x_t is $\overline{N}$. To measure by quantity-exclusion we set a fixed quantity of individuals $\overline{Q}$ that lie beyond the invasion extent (area under the curve past x_t). The two measures of extent do not coincide for fat-tailed invasions, and predict different geometric rates of spread. **(Left)** A fat-tailed invasion measured by density–threshold and quantity-exclusion at four different times. **(Right)** The invasion extent x_t as predicted by the two measurement techniques. The trends diverge in log space, indicating different rates of geometric growth.

In this case the limiting ratio x_{t+1}/x_t becomes

$$\lim_{t\to\infty} \frac{x_{t+1}}{x_t} = \lim_{t\to\infty} \frac{c(t+1)}{ct} = 1. \tag{2.7.6}$$

This suggests that asymptotically, $x_{t+1} = x_t$, from which we are tempted to infer that the invasion front is stationary at large times. This faulty reasoning occurs because a perspective of geometric growth is unsuitable for an invasion progressing at a constant speed: compared to geometric growth, an invasion expanding at a slower rate stands still.

Another potential trap is when the rate of geometric growth ρ equals one. For any $\rho > 1$, an invasion extent $x_t = \rho^t$ will grow geometrically, even when ρ is very small. When $\rho = 1$,

a transition occurs where the behavior is qualitatively different, and there is no geometric growth. In our analyses, the net reproductive rate is assumed strictly greater than one, and the behavior in the case $R_0 = 1$ cannot be extrapolated. For this reason, we are careful to distinguish between weak and strong Allee effects as well as the degenerate case $R_0 = 1$ that lies between weak and strong Allee effects.

2.7.4 Measurements of invasion

The choice to measure the position of the invasion front by a threshold density is intuitive but not the only possibility. Ōkubo (1980) measured the extent of invasion by finding the boundary that separates the bulk of the population from a negligible number of individuals that "have escaped notice by a survey." We call this approach *quantity–exclusion* since the position of the invasion front depends on the exclusion of a fixed number of individuals rather than on population density. These approaches can yield different measures of invasion, as can be seen in Figure 2.17: in this case, measurement by quantity-exclusion is initially behind but eventually overtakes measurement by density-thresholding.

As an example, consider a point-release invasion with fat-tailed dispersal $k(x) \sim cx^{-\alpha}$ under the linear model. Then $n_t(x) \sim cR_0^t t x^{-\alpha}$ as $x \to \infty$ as we found in equation (2.3.6). Integrating the tail of the invasion, we find

$$\begin{aligned} \overline{Q} &= \int_{x_t}^{\infty} n_t(x)\mathrm{d}x \\ &\sim cR_0^t t \int_{x_t}^{\infty} x^{-\alpha}\mathrm{d}x \\ &= \frac{cR_0^t t}{\alpha - 1} x_t^{-(\alpha-1)}. \end{aligned} \tag{2.7.7}$$

Solving for x_t we find

$$x_t \sim \left[\frac{cR_0^t t}{\overline{Q}(\alpha - 1)}\right]^{1/(\alpha-1)}. \tag{2.7.8}$$

Proceeding in the same manner as when we derived the invasion speed for fat-tailed kernels from point-release invasions, we take the ratio x_{t+1}/x_t and obtain

$$\frac{x_{t+1}}{x_t} \approx \left[R_0 \left(\frac{t+1}{t}\right)\right]^{1/(\alpha-1)}. \tag{2.7.9}$$

So in the limit of large time, we see geometric growth at rate $R_0^{1/(\alpha-1)}$,

$$x_{t+1} \approx R_0^{1/(\alpha-1)} x_t, \qquad t \to \infty. \tag{2.7.10}$$

This result differs from our earlier predicted rate of spread, equation (2.3.12), based on the threshold measure of invasion, where the invasion front advanced with a geometric rate $R_0^{1/\alpha}$. The predicted invasion rate is still geometric, but with a different base. The same discrepancy in the base of the exponent is observed when analyzing front-release invasions: with density-thresholding we found the base to be $R_0^{1/(\alpha-1)}$, as in equation (2.5.23). With quantity-exclusion, however, it is $R_0^{1/(\alpha-2)}$.

2.8 Discussion

In this chapter, we have demonstrated a new tool for studying fat-tailed invasions. We analyzed linear and nonlinear integrodifference equations and two types of initial conditions using the properties of regular variation and regularly varying densities. Our analyses apply to populations with no Allee effect and weak Allee effects. We have shown that fat-tailed invasions advance asymptotically at geometric rates that depend on the net reproductive rate and the degree of fatness of the tails of the dispersal kernel.

Regular variation The theory of regular variation and of regularly varying densities and their associated tail additivity properties are powerful tools for analyzing fat-tailed invasions. These and related distributions are used in probability to obtain asymptotic approximations of probabilities of rare events and are also used in many other fields. IDE models are

especially well-suited to benefit from these tail approximations: the compounding effect of geometric growth over many generations raises the scale of the tails. The presence of Allee effects often complicates invasion analyses, but in our case both no-Allee and weak-Allee cases can be addressed at once.

Accelerating invasions There are significant qualitative differences between constant-speed and accelerating invasions. Many of the existing methods for analyzing constant-speed invasions, including definitions and ways of measuring invasion-front position and rates of growth of an invasion, need to be adapted or reworked to accommodate acceleration.

Allee effects We found that an invasion with a weak Allee effect behaves essentially the same as one with no Allee effect: the ultimate rate of invasion is governed entirely by the degree of tail fatness of the kernel and the net reproductive rate, $R_0 = f'(0)$. So long as $R_0 > 1$, the ultimate rate of invasion is geometric. Weak Allee effects that border the no-Allee or strong-Allee cases lead to invasions whose transient dynamics can last for long times.

At $R_0 = 1$, offspring exactly replace their parents. This is sometimes called a "degenerate" case (Alfaro and Coville, 2017); analyses for weak or strong Allee effects may hold when R_0 is close to one, but fail when $R_0 = 1$ exactly. In the related field of integro-differential equations, the difference between accelerating and constant-speed invasions has been connected to the critical transition at $R_0 = 1$, with fat-tailed dispersal kernels yielding accelerating invasions for R_0 strictly greater than one (Garnier, 2011). Our numerical simulations suggest the same for integrodifference equations: that as R_0 is lowered to one, the accelerating phase of a fat-tailed invasion is delayed for increasingly many generations, with the initial, constant-speed transient phase resembling a constant-speed invasion. At $R_0 = 1$, the accelerating phase is, in effect, delayed for infinitely many generations.

We have not addressed strong Allee effects where $R_0 < 1$. This is because fat-tailed invasions depend so heavily on individuals dispersed far into the tails. In the case of weak

Allee effects ($R_0 > 1$), pioneering individuals at low densities may not thrive like those at high densities, but they survive and manage to produce enough offspring to have a net positive increase in the local population that accumulates over time. In the strong Allee case, these individuals always die off. This means that there is no growing accumulation of individuals in the tails. Kot et al. (1996) performed a general analysis with a particular strong Allee effect and found that it limited invasion rates to finite speeds for all kernels, even fat-tailed ones. We conjecture that fat-tailed invasions will, in general, be tempered by strong Allee effects. They will not accelerate but will instead attain finite invasion speeds.

Constant-speed transients Fat-tailed invasions can exhibit long transients with near-constant invasion speeds. This phenomenon occurs for either weak or no Allee effect and is most pronounced when R_0 is barely greater than one. The cause of this phenomenon is complicated, but we believe it is due to an interplay between tail additivity property (2.2.25) and the central limit theorem. We hope to address this interplay in a future paper. Lag phase or lag time (Crooks, 2005) could be an ecological example of this phenomenon. Lag times are often observed in the initial establishment of invasion species, and can precede rapid expansion phases (Parker, 2004); we note, however, that constant-speed transients are not limited to point-release invasions and can also occur for well-established front-release invasions.

Effects of initial conditions The difference in invasion rates between newly established and well-established populations is to our knowledge a new result. We have shown that fat-tailed invasions for well-established populations (front-release) will invade at a greater geometric rate than new invasions from point releases, and that this effect is persistent for all time.

Thin-tailed invasions can be forced to invade at speeds greater than their natural spreading speed (Murray, 1989) and even at accelerating rates (Alfaro, 2017) by choice of initial condition, but these cases depend on the initial condition slowly decaying into the uncoloni-

zed territory; our point- and front-release initial conditions allow for the initial population to be exactly zero in the uninvaded territory.

In practice, populations never fit our idealized descriptions of point-like and front-like releases, but our analyses show that fat-tailed kernels have a capacity for differing rates of invasion not seen in thin-tailed invasions. With our numerical simulations we have also addressed intermediate cases, the plateau initial conditions that we introduced in section *Invasion rates and initial conditions*, that lie between the extremes of point- and front-release initial conditions. We found that these intermediate cases have behavior that blends the predicted behavior of point- and front-releases: they initially behave like a front-release but ultimately spread like a point-release after a (potentially long) time.

Generalizing linear spreading speed Thin-tailed invasions approach finite invasion speeds. The *spreading speed* c^* has the property that for any compactly-supported initial condition ($n_0(x) = 0$ outside of a bounded set) (Weinberger, 1982) and for all $\varepsilon > 0$,

$$\lim_{t\to\infty} \sup_{|x|>(c^*+\varepsilon)t} |n_t(x) - 0| = 0, \tag{2.8.1}$$

$$\lim_{t\to\infty} \sup_{|x|<(c^*-\varepsilon)t} |n_t(x) - 1| = 0. \tag{2.8.2}$$

These conditions have the physical interpretation that an observer moving at a speed $c^* + \varepsilon$ away from the origin in either direction will eventually completely overtake the invasion, whereas one moving at a speed $c^* - \varepsilon$ will eventually be totally engulfed within the invasion (Weinberger et al., 2002). Central to this definition is the assumption that the asymptotic rate of spread will be constant.

If the invasion accelerates, then there is no finite spreading speed c^*. For fat-tailed dispersal, our analyses show that this acceleration is at a geometric rate. This suggests a

modified *geometric spread rate* for these advancing wavefronts may have the properties

$$\lim_{t\to\infty} \sup_{|x|>(c^*+\varepsilon)^t} |n_t(x) - 0| = 0, \tag{2.8.3}$$

$$\lim_{t\to\infty} \sup_{|x|<(c^*-\varepsilon)^t} |n_t(x) - 1| = 0, \tag{2.8.4}$$

where the difference is that $(c^* \pm \varepsilon)t$ has been replaced with $(c^* \pm \varepsilon)^t$: the reference frame now moves at a geometric rate. Our point-release analysis indicate that for $n_0(x) = \delta(x)$, $c^* = R_0^{1/\alpha}$, where α is the degree of tail fatness. On the other hand, for front-release invasions we have found the ultimate rate of invasion is $R_0^{1/(\alpha-1)}$. We note, however, that this rate of spread corresponds to an initial condition with semi-infinite support. This suggests the condition that $n_0(x)$ be zero outside of a bounded set may carry over to this modified spreading-rate characterization. Indeed, when we explored plateau initial conditions in *Invasion rates and initial conditions*, we found that bounded but arbitrarily wide initial conditions all eventually tended to the rate of spread consistent with point-release invasions.

Invasion in two dimensions In this chapter, we have focused on invasions in one dimension. We did this to introduce regular variation, because the theory on regularly varying densities is most developed for one-dimensional densities. We also wanted to form a solid basis for studying heavy- and fat-tailed dispersal in more generality and in higher dimensions. Modern dispersal research focuses on dispersal in two dimensions, with the most commonly used kernel forms being two-dimensional (Nathan et al., 2012; Bullock et al., 2017).

Subexponential distributions Tail additivity property (2.2.25) is not limited to the class of regularly varying densities but is, in fact, part of a broader class of probability distributions. A distribution on the positive half-line with unbounded support is *subexponential* if

$$\overline{K * K}(x) \sim 2\overline{K}(x), \qquad x \to \infty, \tag{2.8.5}$$

where $\overline{F}(x) = \Pr\{X > x\}$ is the tail function or survivorship function.

Subexponential distributions have been studied with the goal of generalizing the useful tail additivity property to as large a class of distributions as possible. The definition, as well as much of the theory of subexponential distributions, is written in terms of tail functions, which are more general from the standpoint of probability theory, but less useful in applications that deal with probability densities. Beyond being simply written in terms of distribution functions, it has been shown that there exist subexponential distributions whose density functions lack the expected tail additivity property (Foss et al., 2011). This means that, despite what we may hope, the results cannot be simply 'translated' from distributions (cdfs) to densities (pdfs).

If a sufficiently well-behaved subclass of subexponential distributions can be isolated for which tail additivity of the pdf holds, then our results may easily generalize, potentially broadening the scope of these analyses from fat-tailed to more general heavy-tailed kernels. We also note that our analyses for front-release invasions may already generalize, if care is taken to keep all intermediate steps restricted to distribution functions or tail functions.

Appendix

2.A Nonlinear point release

In this appendix, we analyze point-release invasions under the nonlinear model. We show that the rate of invasion is geometric with base $R_0^{1/\alpha}$, which matches the linear model. Denoting this rate as ρ, we aim to prove that $\rho = R_0^{1/\alpha}$ by proving that $\rho \geq R_0^{1/\alpha}$ (the lower bound) and $\rho \leq R_0^{1/\alpha}$ (the upper bound). Throughout this appendix, we assume that the dispersal kernel density function has the form $k(x) \sim cx^{-\alpha}$, where $c > 0$ is some constant.

Lower bound on invasion rate: $\rho \geq R_0^{1/\alpha}$.

We assume that the total population size does not shrink below some fixed number A, so that $A_t \geq A$ for all time, including $t = 0$. Then, from (2.3.20), we have

$$\begin{aligned} s_t &\geq A + R_0 A + R_0^2 A + \cdots + R_0^{t-1} A \\ &= A\left(\frac{R_0^t - 1}{R_0 - 1}\right). \end{aligned} \tag{2.A.1}$$

Using inequality (2.A.1) a lower bound for s_t, we equate $\overline{N} = n_{t+1}(x_{t+1}) = n_t(x_t)$, replace $n_t(x)$ with $s_t k(x)$ from asymptotic approximation (2.3.19), and use $k(x) \sim cx^{-\alpha}$ to obtain

$$A\frac{R_0^{t+1} - 1}{R_0 - 1} c x_{t+1}^{-\alpha} \approx A\frac{R_0^t - 1}{R_0 - 1} c x_t^{-\alpha}. \tag{2.A.2}$$

So

$$\left(\frac{x_{t+1}}{x_t}\right)^{\alpha} \approx \frac{R_0^{t+1} - 1}{R_0^t - 1}, \tag{2.A.3}$$

and in the limit of large time,

$$x_{t+1} \approx R_0^{1/\alpha} x_t. \tag{2.A.4}$$

This gives the lower bound $\rho \geq R_0^{1/\alpha}$, since s_t was bounded from below by (2.A.1).

Upper bound on invasion rate: $\rho \leq R_0^{1/\alpha}$.

To bound the invasion rate from above, we will first establish two lemmas. These lemmas use the concept of Big-O and limit superior which we will now define.

A function $f(t)$ is called "Big-O $g(t)$" or order-of-$g(t)$ if there exists some constant $C > 0$

and $t_0 > 0$ such that

$$f(t) \leq Cg(t) \qquad \text{for all } t > t_0. \tag{2.A.5}$$

The Big-O relationship is notated as $f(t) = O(g(t))$.

The limit superior of a sequence $\{y_t\}$ is defined as the limit of the supremum (the maximum) of the tail of the sequence,

$$\limsup_{t\to\infty} y_t = \lim_{t^*\to\infty} \sup_{t\geq t^*} y_t. \tag{2.A.6}$$

We will use the limit superior to measure the limiting bound on the geometric rate of spread, x_{t+1}/x_t, which we measure as tending to the eventual value ρ.

Lemma 1. *If $A_t = O(\gamma^t)$ for some $\gamma > 1$, then*

$$s_t = O(b^t), \tag{2.A.7}$$

where $b = \max\{R_0, \gamma\}$. Additionally,

$$\limsup_{t\to\infty} \left(\frac{x_{t+1}}{x_t}\right) \leq b^{1/\alpha}. \tag{2.A.8}$$

Proof. Since $A_t = O(\gamma^t)$, there exists some constant $d > 0$ such that $A_t \leq d\gamma^t$ for all sufficiently large t. Using the full form (4.20) of s_t, we have

$$\begin{aligned} s_t &\leq R_0^0 d\gamma^{t-1} + R_0^1 d\gamma^{t-2} + \cdots + R_0^{t-1} d\gamma^0 \\ &= d\frac{R_0^t - \gamma^t}{R_0 - \gamma}. \end{aligned} \tag{2.A.9}$$

Here t is becoming large, so if $R_0 > \gamma$ then the right-hand side is $O(R_0^t)$. On the other hand, if $\gamma > R_0$ then the right-hand side is $O(\gamma^t)$. Hence, the first result holds.

For the second result, we set $\overline{N} = n_{t+1}(x_{t+1}) = n_t(x_t)$, insert $d(R_0^t - \gamma^t)/(R_0 - \gamma)$ in place

of s_t, and using the asymptotic relation $k(x) \sim cx^{-\alpha}$, we have

$$\frac{R_0^{t+1} - \gamma^{t+1}}{R_0 - \gamma} c d x_{t+1}^{-\alpha} \approx \frac{R_0^t - \gamma^t}{R_0 - \gamma} c d x_t^{-\alpha}. \tag{2.A.10}$$

Both constants c and d may be cancelled, and after re-arrangement, we obtain

$$\left(\frac{x_{t+1}}{x_t}\right)^{\alpha} \approx \frac{R_0^{t+1} - \gamma^{t+1}}{R_0^t - \gamma^t}. \tag{2.A.11}$$

If $R_0 > \gamma$, then as $t \to \infty$ the right-hand side tends to R_0; on the other hand, if $\gamma > R_0$, then it tends to γ. Since $d(R_0^t - \gamma^t)/(R_0 - \gamma)$ is an upper bound for s_t, this gives an upper bound on the limit of the ratio x_{t+1}/x_t,

$$\limsup_{t \to \infty} \left(\frac{x_{t+1}}{x_t}\right)^{\alpha} \leq \max\left\{R_0, \gamma\right\}, \tag{2.A.12}$$

from which the second result holds. □

Lemma 2. *If $s_t = O\left(b^t\right)$ for some $b > 1$, then*

$$N_t = O\left[(b^{1/\alpha})^t\right]. \tag{2.A.13}$$

Proof. Recall from equation (2.3.19) that $n_t(x) \sim s_t k(x)$. Using $k(x) \sim cx^{-\alpha}$, we have $n_t(x) \sim cs_t k(x)$. Denoting the position x_t at which the invasion front falls below a detection threshold $\overline{N}$ satisfies $n_t(x_t) = \overline{N}$, then

$$x_t \approx \left(\frac{cs_t}{\overline{N}}\right)^{1/\alpha}. \tag{2.A.14}$$

The total population N_{tail} in the tail beyond the invasion front x_t can be found by

integrating $n_t(x)$,

$$\begin{aligned} N_{\text{tail}} &= \int_{x_t}^{\infty} n_t(x)\mathrm{d}x \\ &\sim \int_{x_t}^{\infty} s_t x^{-\alpha}\mathrm{d}x \\ &= \frac{s_t}{\alpha-1}\left[x^{-(\alpha-1)}\right]_{\infty}^{x_t} \\ &= \frac{s_t}{\alpha-1}x_t^{-(\alpha-1)} \\ &\approx \left(\frac{s_t}{\alpha-1}\right)\left(\frac{cs_t}{\overline{N}}\right)^{-1+1/\alpha} \\ &= \frac{s_t^{1/\alpha}(\overline{N}/c)^{1-1/\alpha}}{\alpha-1}. \end{aligned} \tag{2.A.15}$$

The population behind the invasion front, N_{bulk}, can similarly be found by integrating, and bounded from above trivially,

$$N_{\text{bulk}} = \int_0^{x_t} n_t(x)\mathrm{d}x \leq \int_0^{x_t} \mathrm{d}x = x_t, \tag{2.A.16}$$

so $N_{\text{bulk}} \leq \left(\frac{cs_t}{\overline{N}}\right)^{1/\alpha}$.

Since $N_t = N_{\text{bulk}} + N_{\text{tail}}$, we obtain a bound on the total population,

$$N_t \leq s_t^{1/\alpha}\left[\frac{(\overline{N}/c)^{1-1/\alpha}}{\alpha-1} + (\overline{N}/c)^{-1/\alpha}\right]. \tag{2.A.17}$$

The bracketed quantity is positive and does not depend on t. Since $s_t = O(b^t)$, then $N_t = O\left[(b^{1/\alpha})^t\right]$. □

Define R_m as the maximal per capita recruitment,

$$R_m = \inf\left\{R : Rn \geq f(n), \forall n > 0\right\}. \tag{2.A.18}$$

This value corresponds to the least net reproductive rate among all linear growth functions

that are upper-bounds on $f(n)$. For a smooth growth function $f(n)$, the line $R_m n$ is the most shallow tangent line that lies above $f(n)$ for all $n \geq 0$.

The linear model with net reproductive rate R_m bounds the nonlinear model from above, in that the total population N_t at time t is bounded above by $N_t < cR_m^t$ for some constant c. Hence, $N_t = O(R_m^t)$.

Since $R_m > R_0$, we then have from Lemma 1 that $s_t = O(R_m^t)$. Lemma 2 then gives us that $N_t = O\left[(R_m^{1/\alpha})^t\right]$. Since $k(x)$ is a redistribution kernel, the total number of successfully-dispersed offspring of one generation are equal in number to the total population of the next generation, so $A_{t-1} = N_t$. Hence $A_t = O\left(R_m^{1/\alpha}\right)^t$.

If $R_m^{1/\alpha} < R_0$, then we may once more apply Lemma 1 to now obtain a tighter bound on s_t: this lemma allows us to conclude that $s_t = O(b^t)$ with $b = \max\{R_0, R_m^{1/\alpha}\} = R_0$, so $s_t = O(R_0^t)$. We then use the second result, equation (2.A.8), of Lemma 1 to obtain the final result,

$$\limsup_{t\to\infty}\left(\frac{x_{t+1}}{x_t}\right) \leq R_0. \tag{2.A.19}$$

If on the other hand, $R_m^{1/\alpha} > R_0$, we repeat the argument from the preceding paragraph. We have that $A_t = O(\gamma^t)$ with $\gamma = R_m^{1/\alpha}$. Using Lemma 1, we obtain that $s_t = O(b^t)$ with $b = \max\left\{R_0, R_m^{1/\alpha}\right\} = R_m^{1/\alpha}$. Then, we may apply Lemma 2 to obtain

$$N_t = O\left[\left(b^{1/\alpha}\right)^t\right] = O\left[\left(R_m^{1/\alpha^2}\right)^t\right]. \tag{2.A.20}$$

In this way, we show

$$N_t = O\left[\left(R_m^{1/\alpha^n}\right)^t\right], \tag{2.A.21}$$

for successive values of n, until $R_m^{1/\alpha^n} < R_0$. Ultimately, we obtain

$$\limsup_{t\to\infty}\left(\frac{x_{t+1}}{x_t}\right) \leq R_0. \tag{2.A.22}$$

Finally, we have that in the limit as $t \to \infty$,

$$\frac{x_{t+1}}{x_t} \leq R_0^{1/\alpha}, \tag{2.A.23}$$

and so

$$\rho \leq R_0^{1/\alpha}. \tag{2.A.24}$$

Chapter 3

BIPHASIC RANGE EXPANSIONS WITH SHORT- AND LONG-DISTANCE DISPERSAL

Although long-distance dispersal (LDD) has been recognized as a key factor in the spread of populations, many aspects of LDD are still poorly understood (Cain et al., 2000). Long-distance dispersal can surely hasten invasions (Shigesada and Kawasaki, 2002), but how else does it affect invasions? The mechanisms underlying LDD are also poorly understood (Higgins et al., 2003). Long-distance dispersal events are often attributed to multiple dispersal vectors, with infrequent but extreme vectors facilitating far-flung dispersal, but can LDD occur without so-called mixed dispersal? The terms "fat-tailed" and "heavy-tailed" dispersal are often associated with long-distance dispersal, but it is unclear exactly how these terms from probability relate to long-distance dispersal or range expansion.

Much of classical ecological theory has focused on asymptotic dynamics, yet transient dynamics have increasingly been recognized as important, especially over ecologically relevant time scales (Hastings et al., 2018). Mathematical analyses of long-distance dispersal have typically focused on the spreading speed, or asymptotic, long-time average speed of spread (Higgins and Richardson, 1999; Shigesada and Kawasaki, 2002; Kawasaki et al., 2006; Lutscher, 2019). This focus on asymptotics leaves unaddressed many practical questions about how LDD affects invasions. How rare can LDD be while still meaningfully affecting invasions, and what possible impacts can it have? How is the range expansion, or full course of an invasion, rather than just its speed, affected?

The scattered- and coalescing-colony models of stratified diffusion by Shigesada et al. (1995) are an important exception to the focus on asymptotics in the study of LDD. Their work showed that diffusion paired with long-distance dispersal could generate range expansions of three types: linear, biphasic linear–linear, and accelerating (Shigesada et al., 1995);

however, their models were spatially implicit and assumed that all short-distance dispersal occurred by diffusion. In this chapter, I study a spatially explicit integrodifference equation model of spread with generalizable dispersal, and demonstrate its capacity to produce two types of biphasic range expansion.

Long-distance dispersal is hypothesized to occur in two ways (Higgins et al., 2003). First, long-distance dispersal may occur when rare dispersal vectors act on a small proportion of propagules to disperse them to extreme distances. In these cases, dispersal is governed by two or more distinct dispersal vectors. The most common vectors act at relatively short distances and account for the majority of dispersal, while atypical vectors act at great distances. Such dispersal is said to be mixed (Nathan et al., 2008). Second, typical dispersal vectors, such as wind, which most often deposit propagules close to their source, may occasionally disperse much further (Bullock et al., 2006). Long-distance dispersal of this type may be attributed to fat- or heavy-tailed dispersal, both technical terms from probability relating to probability distributions with capacities to generate extreme events with low yet non-negligible probability (Cooke et al., 2014).

There are many examples of multiple reproduction and dispersal vectors in the dispersal of plants, many of which can reproduce vegetatively but also by seed, but also in the movements of ants (Suarez et al., 2001), beetles (Shigesada and Kawasaki, 1997), and birds (Kesler et al., 2010). Plants that reproduce by seed may have some proportion of their seeds transported long distances by birds and mammals (Janzen, 1984). Studies that have modeled the distribution on dispersal distances of seeds or pollen often resort to mixed models to achieve good fits to data (Bullock and Clarke, 2000; Streiff et al., 1999; Goto et al., 2006). Even within a movement vector, dispersal may be stratified. Horn et al. (2001) partition dispersal of tree seeds by wind according to whether the seed falls below or rises above the canopy, with the latter portion becoming candidates for long-distance dispersal; Higgins and Richardson (1999) hypothesize similarly.

"Fat-tailed" dispersal kernels have become popular for describing dispersal data (Nathan et al., 2012), and the tail of the dispersal kernel is often cited as a cause of long-distance

dispersal (Katul et al., 2005) or faster-than-expected spread (Clark, 1998; Caswell et al., 2003). Although the term has a formal definition in probability, it is often used beyond that scope in ecology to describe heavy-tailed or leptokurtic kernels. "Fat-tailed" kernels from ecology are often in fact heavy tailed. Fat- and heavy-tailed kernels have been found to accurately represent many sets of dispersal data, where thin-tailed kernels do not. A recent and comprehensive meta-analysis of plant dispersal data conducted by Bullock et al. (2017) compared popular thin- and heavy-tailed kernels, and found the best fitting ones to be heavy- and fat-tailed.

Dispersal is undoubtedly mixed, at least for some species, but fat-tailed kernels may still be useful models. Even if dispersal is better explained mechanistically by mixed-dispersal kernels, such kernels may be harder to deal with practically. Mixed kernels have, in general, more parameters than fat-tailed kernels, and so require more data or types of observations to properly fit (Higgins et al., 2003). Some researchers argue that, when taken together in combination, the sum total of dispersal by multiple vectors will yield a fat-tailed kernel (Nathan et al., 2008). Ultimately, the choice between mixed and fat-tailed kernels may in some cases be moderated by whether a mechanistic or phenomenological model is desired.

Integrodifference equation (IDE) models are one way by which many types of dispersal, including mixed dispersal and fat-tailed dispersal, can be incorporated into models of spread. IDE models are discrete-time, continuous-space models that describe populations whose growth and dispersal occur in distinct, non-overlapping stages. At each generation, reproduction occurs in-place, followed by dispersal according to a dispersal kernel, a probability density function that governs the likelihood of an offspring settling at any location relative to it parent.

In this chapter, I analyze IDE models with two classes of dispersal kernels: mixed thin-tailed dispersal kernels and fat-tailed dispersal kernels, a particular class of heavy-tailed kernels whose tails decay according to power laws. I use a combination of known approaches, as well as new analytic techniques to analyze point-release invasions. Whereas many analyses of invasions focus on asymptotic properties of spread, I focus on their transient dynamics. I

show how both mixed-dispersal and fat-tailed kernels can give rise to invasions with biphasic range expansions, which have two distinct phases of spread. For fat-tailed kernels, I introduce a way of quantifying how different parts of the kernel contribute to the rate of spread of an invasion, allowing me to more clearly define the "shoulders" of a dispersal kernel in the context of an invasion.

The remainder of this chapter is organized as follows. In *Model*, I introduce the nonlinear and linear IDE models that I study, their components, how to measure invasion, and the key assumptions I make when using these models. I next review the relevant types and characteristics of *Dispersal kernels*, focusing on mixed and fat-tailed kernels. I also review thin-tailed and regularly varying probability densities for the role that they play in my analyses. I begin by analyzing *Invasions with mixed thin-tailed dispersal*, and show that they produce biphasic range expansions. I relate their speeds of spread to short- and long-distance dispersal. I find that a diminishing probability of LDD may or may not eliminate the effects of LDD, depending on the form of long-distance dispersal. In *Fat tails: Long- and short-distance dispersal*, I show that fat-tailed dispersal can also generate biphasic range expansions. Fat-tailed invasions can invade at near-constant speeds for long times, so I review techniques for approximating this speed. I also introduce a technique for graphically delineating between the peak and tail of a dispersal kernel based on speed rarefaction curves. For both mixed-dispersal and fat-tailed kernels, I find the *Time of phase transition*, which corresponds to a transition between dynamics governed by short- and long-distance dispersal. In *Discussion*, I briefly summarize and interpret my results and their implications for the study of long-distance dispersal, range expansions, and invasions.

3.1 Model

Consider the discrete-time, nonlinear integrodifference equation (IDE) model

$$\begin{aligned} n_{t+1}(x) &= \int_{-\infty}^{\infty} f(n_t(y))k(x-y)\mathrm{d}y \\ &= \big(f(n_t) * k\big)(x). \end{aligned} \tag{3.1.1}$$

In this model, space is continuous and time is discrete, with t corresponding to the generation number. $n_t(x)$ is the population density at position x in generation t. Reproduction and dispersal occur in two distinct phases. First, the growth function $f(n)$ measures the recruitment of the next generation, during the sedentary stage, as a function of the population density n at a particular point. Dispersal then occurs according to the dispersal kernel $k(x-y)$, a probability density function that gives the probability of offspring from position y settling at location x.

I also study the linearized IDE model,

$$\begin{aligned} n_{t+1}(x) &= \int_{-\infty}^{\infty} R_0 n_t(y)k(x-y)\mathrm{d}y \\ &= R_0 \cdot \big(n_t * k\big)(x). \end{aligned} \tag{3.1.2}$$

Here, the nonlinear growth model $n_{t+1} = f(n_t)$ has been replaced with linear growth, $n_{t+1} = R_0 n_t$. The parameter $R_0 = f'(0)$ is the net reproductive rate, which governs recruitment at low densities. The linear model is often easier to analyze than the nonlinear model, but can have different dynamics. Under certain conditions on the growth function, the rate of spread of the linear model will match the nonlinear model. Further, for certain initial conditions, a formal solution exists.

3.1.1 Initial condition

The initial condition, $n_0(x)$, describes the spatial density or distribution of the population at time $t = 0$. In this chapter, I restrict my attention to point-release invasions, or invasions whose populations are initially highly localized.

The most idealized point-release condition corresponds to total concentration of the initial population at a single point. This condition is represented mathematically by the Dirac-delta distribution $\delta(x)$. This initial condition can only be used in conjunction with the linear model, for which the formal solution becomes,

$$\begin{aligned} n_t(x) &= R_0^t(\overbrace{k * k * \cdots * k}^{t\text{-many}})(x) \\ &= R_0^t k^{t*}(x). \end{aligned} \tag{3.1.3}$$

Here $k^{t*}(x)$ denotes the *convolution power*, or convolution of $k(x)$ with itself t-many times (Feller, 1971).

In simulations, and when using the nonlinear IDE model (3.1.1), a non-idealized initial condition must be used so that the population begins at a finite density. In this chapter, I use a uniform distribution as the initial condition,

$$n_0(x) = \begin{cases} 1 & |x| < \frac{1}{2} \\ \frac{1}{2} & |x| = \frac{1}{2} \\ 0 & \text{otherwise.} \end{cases} \tag{3.1.4}$$

I set $n_t(x) = 1/2$ at the discontinuities of the uniform distribution because $1/2$ is the average value across each discontinuity; I have found this to improve the convergence of numerical methods.

3.1.2 Growth function

The growth function $f(n)$ can take many forms, depending on how the population reproduces at various densities. Typically, zero and the population carrying capacity are fixed points of $f(n)$; it is possible that $f(n)$ may have other fixed points, but I will not be considering these cases in this chapter. Rescaling $n_t(x)$ so that the carrying capacity is 1, this means that $f(0) = 0$ and $f(1) = 1$, with $n = 0$ being an unstable and $n = 1$ a stable equilibrium of the non-spatial model, $n_{t+1} = f(n_t)$.

A key factor in growth, especially when considering long-distance dispersal, is whether the growth function has an *Allee effect*, or reduced recruitment at low densities compared with recruitment at higher densities (Allee, 1938). This occurs when $f(n^*)/n^* > R_0$ for some value $n^* > 0$. Under a weak Allee effect, $R_0 > 1$, so that the population will grow at low densities, but at a reduced rate. A strong Allee effect corresponds to the case where $R_0 < 1$, so that the population dies off at low densities (Wang et al., 2002). In this chapter, I will assume that there is no Allee effect, so that $f(n)/n \leq R_0$ for all $n > 0$. With no Allee effect, the speed of invasion of the linear model (3.1.2) matches that of the nonlinear model (3.1.1) (Lewis et al., 2002; Lutscher, 2019).

I further restrict my attention to growth functions with no overcompensation. Overcompensation occurs when the growth function is not monotonically increasing between zero and the population carrying capacity, typically at high densities (Li et al., 2009). These assumptions result in the discrete-time IDE model behaving qualitatively very similarly to a continuous-time reaction-diffusion model, such as the Fisher–KPP model.

Throughout this chapter, I will use the Beverton–Holt stock-recruitment curve (Beverton and Holt, 1957) as the growth function in all simulations of the nonlinear model,

$$f(n) = \frac{R_0 n}{(1 + (R_0 - 1)n)}. \tag{3.1.5}$$

This function has no Allee effect.

3.1.3 Measuring invasion extent

To measure the extent of an invasion at time t, I set a *detection threshold* $\overline{N} > 0$, and look for the position of the invasion front x_t such that

$$n_t(x_t) = \overline{N}. \tag{3.1.6}$$

In general, there may be many points satisfying equation (3.1.6). These points comprise the *level set* of $n_t(x)$ with level-set value $\overline{N}$. The number of points can even change in time, if for instance two spatially separated populations coalesce or the population goes extinct.

In a point-release invasion with conditions on the growth function as I have laid out, there will ultimately be two points satisfying (3.1.6), moving outward symmetrically from the point source. For values of $R_0 > 1$ that are close to 1, or if the kernel disperses very widely compared to the initial population distribution, the invasion front may recede, as the initially concentrated population is redistributed. In some cases, the population density may temporarily decrease below the detection threshold before ultimately increasing (Shigesada and Kawasaki, 1997).

3.2 Dispersal kernels

In this section, I briefly review thin-tailed, mixed, and fat-tailed dispersal kernels.

3.2.1 Thin-tailed kernels

The term "thin-tailed" comes from probability, and describes probability distributions that possess moment generating functions. For example, the Gaussian or Normal distribution, with variance σ^2 has kernel $k(x)$ given by

$$k(x) = \frac{1}{\sqrt{2\pi\sigma^2}} \exp\left(\frac{-x^2}{2\sigma^2}\right), \tag{3.2.1}$$

and corresponding moment generating function

$$M(s) = e^{\sigma^2 s^2/2}. \tag{3.2.2}$$

Another thin-tailed kernel commonly seen in modeling studies is the Laplace kernel,

$$k(x) = \frac{1}{2a} \exp\left(\frac{-|x|}{a}\right), \tag{3.2.3}$$

which has moment generating function

$$M(s) = \frac{1}{1 - a^2 s^2}, \quad |s| < \frac{1}{a}. \tag{3.2.4}$$

Note that the domain of the moment generating function is bounded for the Laplace kernel, but unbounded for the Gaussian kernel. The bounded support of the moment generating function is not unique to the Laplace kernel. The WALD kernel, used in ecology to model dispersal by wind, also has a moment generating function with bounded support (Thompson and Katul, 2008). We will see that the bounded support of the moment generating function has implications for long-distance dispersal in *Invasions with mixed thin-tailed dispersal*.

Invasions with thin-tailed kernels are known to approach constant speeds of invasion. An invasion starting from a point release, or any initial condition with bounded support, will approach an asymptotic speed c, known as the *spreading speed*. When the growth function has no Allee effect, this speed can be found in terms of the net reproductive rate R_0 and the moment generating function $M(s)$ of the kernel,

$$c = \inf_{s>0} \frac{\log\left(R_0 M(s)\right)}{s}. \tag{3.2.5}$$

For a derivation of this result, see Lewis et al. (2016). Alternatively, equation (3.2.5) can be

transformed into a system of parametric equations,

$$c = \frac{M'(s)}{M(s)}, \tag{3.2.6a}$$

$$R_0 = \frac{\exp\left[sM'(s)/M(s)\right]}{M(s)}. \tag{3.2.6b}$$

This latter representation was first derived by Kot et al. (1996).

Thin-tailed kernels, and in particular the Gaussian kernel, have largely fallen out of favor for representing dispersal data, as numerous studies have shown that dispersal is leptokurtic and potentially even heavy-tailed. One notable study by Bullock et al. (2017) found that thin-tailed kernels generally performed worse than heavy-tailed kernels when fit to dispersal data. In the study, eleven common kernel forms, both thin- and heavy-tailed, were fit to dispersal data from over one hundred plant species; the Gaussian kernel was said to perform "very poorly," and the two overall best-fitting kernels that they tested were both heavy-tailed.

Thin-tailed kernels are still popular as mechanistically derived models of dispersal. The Gaussian kernel corresponds to movement by a diffusive process for a fixed amount of time, and the Laplace kernel to diffusive movement for an exponentially distributed amount of time (Lewis et al., 2016). The thin-tailed WALD kernel was mechanistically derived to model the dispersal of seeds by wind with the goal of having parameters that can be estimated from characteristics of the environment and the dispersing species, rather than from dispersal data (Katul et al., 2005).

3.2.2 Mixed dispersal

A mixed-dispersal kernel is a dispersal kernel that represents dispersal through distinct vectors by combining multiple dispersal kernels. Mixed-dispersal kernels, functions, or models are also called mixtures (Higgins and Richardson, 1999) or composite (Shigesada and Kawasaki, 2002).

For each of m-many dispersal modes or vectors, there is a probability $p_i \geq 0$ of a propagule dispersing according to that vector, and an associated dispersal kernel $k_i(x)$ that governs the probability and distance of dispersal according to that vector. The probabilities sum to one, so that dispersal by one of the vectors is guaranteed. These distinct dispersal kernels are combined into a single dispersal kernel in a weighted sum,

$$k(x) = \sum_{j=1}^{m} p_i k_i(x). \tag{3.2.7}$$

In principle, mixed kernels can combine any number of dispersal vectors that may act at similar or dissimilar spatial scales.

In a mixed kernel, the heaviness of the tail is determined by the tail of the heaviest component kernel. This means that if any constituent kernel is heavy-tailed, the resulting mixed kernel will itself by heavy tailed. If all constituent kernels are thin-tailed, the resulting mix is thin-tailed.

3.2.3 Fat-tailed kernels

Despite their name, fat-tailed kernels are not "opposite" or complementary to thin-tailed kernels. While thin-tailed kernels possess moment generating functions, it is actually heavy-tailed kernels that are defined by their lack of moment generating functions; therefore, every symmetric dispersal kernel is either thin- or heavy-tailed. Fat-tailed kernels are a subclass of heavy-tailed kernels with a much more specific form. A kernel $k(x)$ is *fat-tailed* if it has tails that decay asymptotically like a power law,

$$k(x) \sim \widetilde{c} x^{-\alpha}, \qquad x \to \infty, \tag{3.2.8}$$

where $\widetilde{c}$ is a scaling constant and $\alpha > 1$ is the degree of tail fatness. A smaller value of α indicates more slowly decaying tails, and so increases the fatness of the tails. Because fat-tailed kernels are also heavy-tailed, they lack moment generating functions. In addition,

fat-tailed kernels have infinitely many divergent moments, with all moments of order $\alpha - 1$ and higher failing to converge.

Perhaps the most well-known fat-tailed kernel is the Cauchy distribution,

$$k(x) = \frac{1}{\pi b \left[1 + \left(\frac{x}{b}\right)^2\right]}. \tag{3.2.9}$$

Here b is a shape parameter that controls the width of the kernel. The Cauchy distribution has degree of tail fatness $\alpha = 2$; as such, it is so fat-tailed that none of its moments, including its mean, variance, and kurtosis, are defined.

Student's t-distribution is a family of fat-tailed distributions, indexed by a parameter ν that controls the degree of tail fatness. For $\nu \geq 1$, the density function is given by

$$k(x) = \frac{\Gamma\left(\frac{\nu+1}{2}\right)}{\Gamma\left(\frac{\nu}{2}\right)\sqrt{\nu\pi}} \left(1 + \frac{x^2}{\nu}\right)^{-\left(\frac{\nu+1}{2}\right)}. \tag{3.2.10}$$

Student's t-distribution has tail fatness of degree $\nu + 1$. For $\nu = 1$, the t-distribution reduces to the Cauchy distribution (3.2.9). In the limit as $\nu \to \infty$, the t-distribution converges to the Gaussian distribution.

I also introduce the following fat-tailed kernel, which I term the *fat-tailed Laplace* kernel,

$$k(x) = \frac{\alpha - 1}{2\alpha(1 + |x|/\alpha)^\alpha}. \tag{3.2.11}$$

This kernel has a peaked shape at the origin, and in the limit as $\alpha \to \infty$, $k(x)$ converges to the Laplace distribution.

3.2.4 Regular variation and tail additivity

A class of distributions that has not received much attention in ecology is that of *regularly varying* distributions. A kernel $k(x)$ is regularly varying with index β if, for all $t > 0$,

$$\lim_{x\to\infty} \frac{k(tx)}{k(x)} = t^{\beta}. \tag{3.2.12}$$

Regularly varying distributions can be thought of as a generalization of fat-tailed kernels. A fat-tailed kernel with degree of tail fatness α is also necessarily regularly varying with index $-\alpha$.

Regularly varying densities possess several useful *tail additivity properties*. For my purposes, the most useful theorems are those proven by Bingham et al (2006). First, if $k(x)$ is a regularly varying probability density, then

$$(k * k)(x) \sim 2k(x), \qquad x \to \infty. \tag{3.2.13}$$

This result says that the convolution, which in general has no simple closed-form expression, can be approximated in the tails as simply twice the original kernel density. A similar result holds for repeat convolutions, in which

$$(k^{t*})(x) \sim tk(x), \qquad x \to \infty. \tag{3.2.14}$$

This latter property is particularly useful in analyzing point-release invasions under the linear model, where the formal solution (3.1.3) involves the repeat convolution of the kernel $k(x)$.

3.2.5 Comparing mixed and fat-tailed dispersal

Shape In practice, a near surefire way of distinguishing thin- and fat-tailed kernels is by viewing log-scale plots of their tails. For a fat-tailed kernel, the log of $k(x)$ appears concave-up in the tail, rather than concave-down; see for example Figure 3.1. This behavior is in

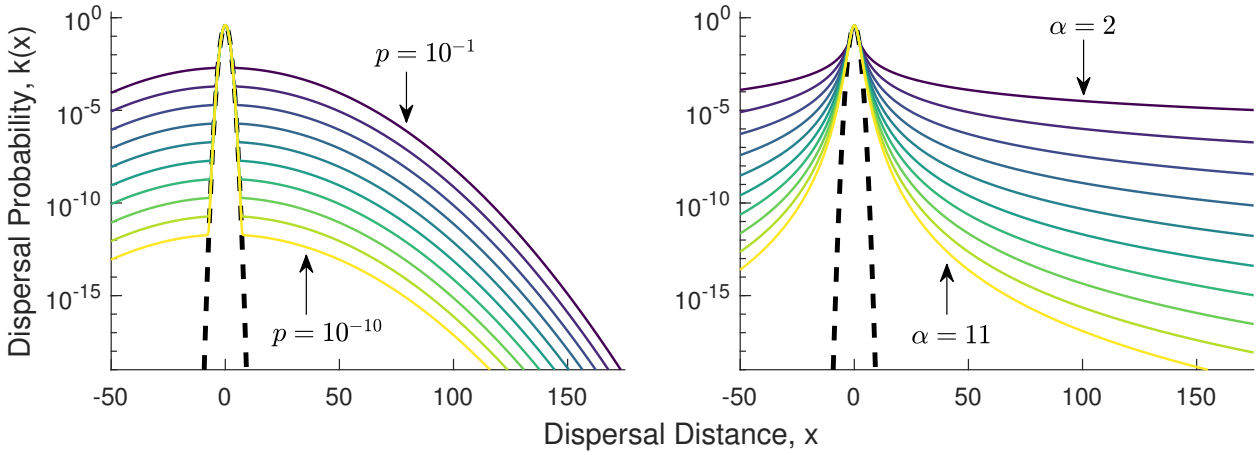

Figure 3.1: Mixed and fat-tailed dispersal kernels. **(Left)** Mixed thin-tailed dispersal kernels. The short-distance kernel $k_S(x)$ is the Gaussian kernel with $\sigma_S = 1$, and is shown as a black dashed curve. The long-distance kernel $k_L(x)$ is another Gaussian kernel, but with $\sigma_L = 20$. The plot shows the mixed kernel for $p = 10^{-1}, 10^{-2}, \ldots, 10^{-10}$, from top to bottom. **(Right)** Fat-tailed dispersal kernels. Each solid curve is a t-distribution (3.2.10), with $\alpha = 2, 3, \ldots, 11$, from top to bottom. The Gaussian kernel with $\sigma = 1$ is shown for comparison, as a black dashed curve.

direct contrast to that of the Gaussian kernel, whose tails decay rapidly to zero; its tails appear concave-down. Most heavy-tailed kernels that are used in practice have tails that are concave-up, although pathological examples can be constructed as exceptions. Near the source, a fat-tailed kernel can be either concave-up or concave-down (called convex by some authors, see for example Clark et al., 1999), examples include the fat-tailed Laplace kernel (3.2.11) and the t-distribution (3.2.10). A mixed thin-tailed kernel can be shaped similarly to a fat-tailed kernel on a limited domain; in Figure 3.1, the Gaussian–Gaussian mixed kernels flare outward where the long-distance kernel meets the short-distance kernel.

Short- and long-distance dispersal Mixed kernels clearly delineate between distinct dispersal vectors. Each vector may be clearly defined as short- or long-distance, and its corresponding component kernel can be tuned to disperse widely or narrowly. The probability of dispersal by each vector is set by a parameter, and so the total probability of dispersal by

LDD vectors can be considered the probability of long-distance dispersal.

Fat-tailed dispersal kernels naturally incorporate capacities for short- and long-distance dispersal in a continuum of dispersal distances. Although the degree of tail fatness can be controlled, fat-tailed kernels do not have a parameter that directly tunes the probability of long-distance dispersal. Although short- and long-distance dispersal can be attributed to the 'peak' and 'tail' of the kernel, there is no clear or obvious delineation between these parts of the kernel. In *Spreading speeds for truncated fat-tailed kernels*, I introduce a method of characterizing the "shoulder" of a fat-tailed kernel as a region lying between the peak and tail.

Capacity to generate LDD There are two commonly used criteria for classifying LDD. The first stipulates that LDD is defined proportionally, for example by the furthest 5% or even 1% of dispersing propagules. The second stipulates an absolute criterion, whereby a fixed distance, say 100 km, qualifies long-distance dispersal. Both mixed and fat-tailed kernels can generate LDD according to either of these criteria.

Heavy- and fat-tailed kernels have special capacities for generating extreme events. This capability is exemplified by the tail additivity property of regularly varying densities (also of the larger subexponential class) and can be interpreted as follows. Suppose that several random dispersal displacements are summed, and that the sum is very large. If the displacements are drawn from a thin-tailed distribution, such as the Gaussian or Laplace, then it is most likely that each individual displacement was larger than typical. If on the other hand, the displacements are from a fat-tailed distribution, then it is more likely that a single displacement was very large, or "extreme" (Cooke et al., 2014).

3.3 Invasions with mixed thin-tailed dispersal

In this section, I analyze thin-tailed mixed dispersal kernels of the form

$$k(x) = (1-p)k_S(x) + pk_L(x). \tag{3.3.1}$$

Here p is the probability of dispersal by the long-distance vector, with $0 < p < 1$. The kernels $k_S(x)$ and $k_L(x)$ are dispersal kernels associated with short- and long-distance dispersal vectors, respectively. In addition to assuming both kernels are thin-tailed, I also assume that $k_S(x)$ is thinner-tailed than $k_L(x)$, or that $k_L(x)$ dominates $k_S(x)$ in the tail. This assumption is important for guaranteeing that all long-distance dispersal is in fact due to $k_L(x)$.

I show that invasions with mixed dispersal can have biphasic range expansions that spread at an initially slow speed before transitioning to a higher speed. The invasion speed during the first phase is governed by short-distance dispersal, whereas long-distance dispersal boosts the speed in the second phase of spread. The parameter p, governing the probability of long-distance dispersal, controls the time of occurrence of the transition between phases of spread. A lower probability of LDD delays the onset of the second phase, and extends the initial phase of spread.

The probability of LDD also influences the speed of spread during the second phase of spread, but the nature of this influence depends heavily on the long-distance dispersal kernel $k_L(x)$. In some cases, long-distance dispersal elevates speeds of invasion even when p is made arbitrarily small, while in others, the speed smoothly reduces to that of short-distance dispersal. I explore this phenomenon in detail in *Persistent effects of infinitesimal LDD*.

3.3.1 Speeds of spread and biphasic range expansion

In a mixed kernel, the spreading speeds for both the mixed and unmixed kernels can be found.

For a mixed-dispersal kernel $k(x)$ of the form (3.3.1), the moment generating function $M(s)$ is given in terms of the moment generating functions of the constituent kernels. Denoting the moment generating functions of $k_S(x)$ and $k_L(x)$ as $M_S(s)$ and $M_L(s)$, respectively,

$$M(s) = (1-p)M_S(s) + pM_L(s). \tag{3.3.2}$$

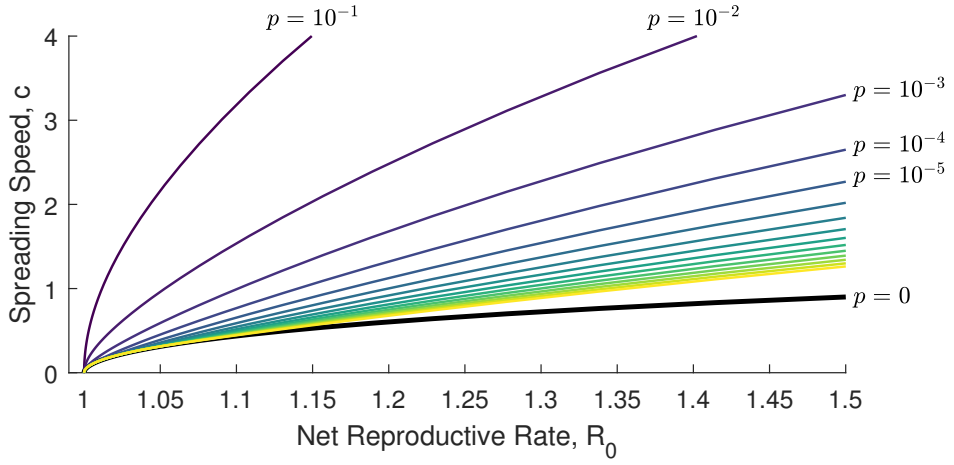

Figure 3.2: Spreading speed c as a function of net reproductive rate R_0 for mixed-dispersal kernels. For each mixed kernel, $k_S(x)$ and $k_L(x)$ are Gaussian kernels with $\sigma_S = 1$ and $\sigma_L = 20$. The probability p of long-distance dispersal varies from $p = 10^{-1}, 10^{-2}, \ldots, 10^{-15}$; the curves for the largest given values of p are labeled. The thick black curve corresponds to $p = 0$, or dispersal by the short-distance kernel $k_S(x)$ only.

Thus, if the moment generating functions of all of the constituent kernels are known, it is easy to find the moment generating function of a mixed kernel itself. The resulting moment generating function can be used in system (3.2.5) to find the spreading speed for a particular value of R_0. Alternatively, the parametric system (3.2.6) can be used to relate spreading speed c and net reproductive value R_0 as the parameter s is varied. Doing so yields a speed curve, which can be graphically interpreted to yield c as a function of R_0.

Figure 3.2 shows speed curves for mixed-dispersal kernels, along with the speed curve for an unmixed kernel representing short-distance dispersal only. In each mixed kernel, both $k_S(x)$ and $k_L(x)$ are Gaussian kernels, with variances $\sigma_S^2 = 1$ and $\sigma_L^2 = 100$. The thick black curve indicates the spreading speed c_S associated with short-distance dispersal only. For $p = 10^{-1}$, long-distance dispersal is less common than short-distance dispersal, but still disperses one tenth of propagules. The speed of invasion is significantly increased, relative to c_S, for all values of $R_0 > 1$. As p is reduced, the speed likewise reduces, and eventually converges to c_S. The speed curve for $p = 10^{-15}$, shown in yellow, is visually closest to the

short-distance speed curve, and shows that c essentially coincides with c_S for values of R_0 less than around 1.15. Smaller values of p are omitted for visual clarity, but further reducing p results in closer agreement for larger values of R_0. Note that this behavior does not occur with all mixed kernels; Lutscher (2019) has proven when the speed of the mixed kernel converges to that of the short-distance kernel, as well as when it does not. For further information on how this latter case affects range expansion, see *Persistent effects of infinitesimal LDD*.

3.3.2 Numerical simulations

I perform numerical simulations to complement my analytic results. While the spreading speed tells us how fast an invasion will spread as time becomes large, it does not inform us about any transient behaviors that may occur. Transient dynamics can last for short or long times, and can be difficult to predict or anticipate.

In my simulations, the domain is a large interval, centered about the origin, with half-width H. The domain is represented by an evenly spaced grid of points, with grid-spacing Δx. The population density $n_t(x)$ is represented on this domain. In each simulation, H is chosen sufficiently large so that the invasion front position does not tend too close to the boundary of the domain. I implement point-release initial conditions by setting $n_0(x_j) = 1$, for all gridpoints x_j where $x_j \in (-1/2, 1/2)$, and $n_0(x_j) = 1/2$ for $|x_j| = 1/2$.

I perform my simulations in MATLAB. To evaluate the convolution integrals in the nonlinear IDE (3.1.1), I use a midpoint-rule integration scheme. I implement this scheme with the numerical convolution function `conv` with the `'same'` option. To find the invasion extent x_t, I define a threshold value $\overline{N}$, typically $\overline{N} = 0.1$, and use the `find` command to select the last grid point x_j such that $n_t(x_j) > \overline{N}$. I then use the `interp1` command to perform cubic spline interpolation on the points $x_{j-1}, x_j, x_{j+1}, x_{j+2}$ to compute the position x_t satisfying $n_t(x_t) = \overline{N}$.

Figure 3.3 shows range expansion curves from four separate invasions, two with mixed dispersal and two with unmixed, short-distance dispersal only. Dispersal is as in Figure 3.2, with $k_S(x)$ Gaussian with $\sigma_S = 1$, and $k_L(x)$ Gaussian with $\sigma_L = 10$. The probability of

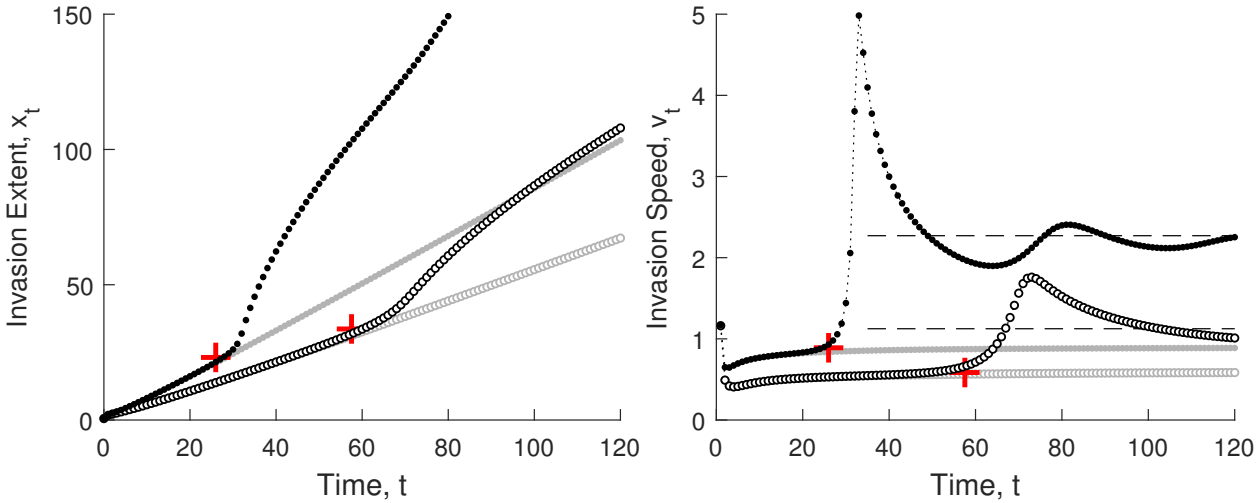

Figure 3.3: Invasions with short- and long-distance dispersal and R_0 varied. Plots show range expansion curves for four invasions, two with mixed dispersal and two with unmixed, short-distance dispersal only. In all cases, short- and long-distance dispersal are Gaussian with $\sigma_S = 1$ and $\sigma_L = 20$, respectively. Growth is Beverton–Holt with $R_0 = 1.2$ (open circles) and $R_0 = 1.5$ (dots). For invasions with mixed dispersal (black markers), the probability of LDD is $p = 10^{-5}$; invasions with unmixed, short-distance dispersal (gray markers) have $p = 0$. The dashed lines in the plots of invasion speed indicate the asymptotic spreading speed of the mixed-dispersal kernel for each value of R_0. Red cross symbols indicate the approximate time and position of the phase transition as determined by the procedure in *Time of phase transition*. In all simulations, the grid spacing is $\Delta x = 1/16$ and the domain half-width is $H = 1000$.

LDD is $p = 10^{-5}$. Only R_0 is varied, taking on the values $R_0 = 1.2, 1.5$. For each value of R_0, two invasions, one with mixed dispersal ($p = 10^{-5}$) and one with unmixed dispersal ($p = 0$), are shown.

Perhaps the most striking feature in Figure 3.3 is that each invasion with mixed dispersal has a biphasic range-expansion curve. These invasions initially spread at slow constant speeds, but later transition to faster speeds. In plots of invasion extent x_t versus time, the transition appears very rapid. Plots of the per-step invasion speed, $v_t = x_t - x_{t-1}$, show that the velocity can grow rapidly during this transition, and can temporarily spike to very high speeds before slowing.

The spreading speed c of the mixed-dispersal kernel determines the asymptotic speed of invasion during the second, ultimate phase of spread. This speed is calculated using the parametric system (3.2.6), and is shown in Figure 3.3 as black dashed lines for each mixed-dispersal invasion and associated value of R_0. At the start of the second phase of spread, the per-step invasion speed v_t jumps far above the spreading speed, but soon after decays and begins oscillating around the spreading speed. These oscillations continue to dampen as the per-step invasion speed converges to c.

During the initial phase of spread, the speed does not match or approach the spreading speed. Instead, each mixed-dispersal invasion initially advances at the spreading speed c_S associated with the short-distance dispersal kernel, $k_S(x)$. This can be seen by the close agreement of the invasions with mixed and unmixed dispersal for each value of R_0; the timeseries of x_t from the two invasions are indistinguishable, and the same is true for the timeseries of v_t. This indicates that the initial rate of spread of invasions with mixed dispersal is governed by short-distance dispersal. To calculate c_S, I again use system (3.2.6), this time with the moment generating function $M_S(s)$ of the short-distance kernel $k_S(x)$.

There are a number of ways to conceptualize why LDD only affects the latter phase of an invasion. First, if we consider the mixed kernel as a perturbation of the unmixed kernel, it makes sense that the timeseries of the two invasions would initially closely agree. A second perspective comes from how steepness and speed of the invasion front are related, and how thin-tailed invasions converge to a traveling-wave profiles. As a thin-tailed invasion progresses, the tail of its population density $n_t(x)$ converges to a decaying exponential, proportional to e^{-sx} for some $s > 0$. A smaller value of s corresponds to a shallower yet more rapidly traveling invasion front, whereas larger values of s describe steeper and more slowly moving fronts. On the other hand, after only one generation, $n_1(x)$ closely resembles the dispersal kernel, which can be seen from the formal solution (3.1.3). Initially, the invasion front is close to the origin, well away from the tails, and the shape of the kernel in this region is governed by the short-distance kernel. The invasion-front profile produced by the mixed-distance kernel is typically much shallower in shape than the short-distance dispersal kernel,

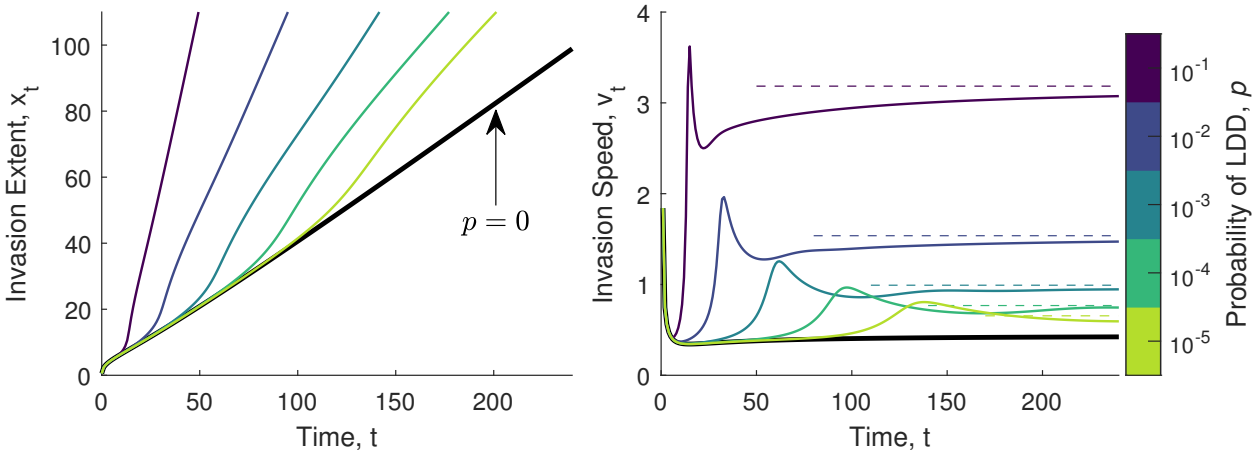

Figure 3.4: Invasions with mixed dispersal and the probability p of long-distance dispersal varied. Dispersal is as in Figure 3.3, growth is Beverton–Holt with $R_0 = 1.1$, and $p = 10^{-1}, 10^{-2}, \ldots, 10^{-5}$. Dashed lines in the plot of invasion speeds indicates the spreading speed of the mixed kernel for each value of R_0. The thick black curve corresponds to an invasion with short-distance dispersal only ($p = 0$). In all simulations, the grid spacing is $\Delta x = 1/16$; the domain half-width is $H = 1000$ for $p = 10^{-1}$, $H = 700$ for $p = 10^{-2}$, and $H = 500$ for $p = 10^{-3}, 10^{-4}, 10^{-5}$.

and takes time to develop; the invasion front is steep and moves slowly during this time, until the exponentially decaying tail develops and boosts the speed of invasion, after which point it is shallower and faster. For a relevant discussion of how the slope of a decaying exponential determines the speed of traveling waves in reaction-diffusion equations, see (Murray, 2002, p. 442).

The parameter R_0 affects mixed-dispersal range expansions in two ways. First, R_0 determines the speed of spread during both phases of the invasion. This conforms with the behavior of the speed curves in Figure 3.2, where all curves increase as R_0 grows. Second, as R_0 is increased, the duration of the initial phase of spread decreases. For $R_0 = 1.2$, the initial phase of spread lasts for around 60–65 generations. In contrast, for $R_0 = 1.6$, the initial phase lasts for a shorter time of around 30 generations.

To see how the probability p of LDD events affects range expansion, I perform additional simulations, this time keeping R_0 constant and varying p. Figure 3.4 shows range expansion

curves from six invasion simulations. Dispersal is as in Figure 3.2; both $k_S(x)$ and $k_L(x)$ are Gaussian kernels, with $\sigma_S^2 = 1$ and $\sigma_L^2 = 100$. The only parameter varied is $p = 10^{-1}, 10^{-2}, \ldots, 10^{-5}$; the case where $p = 0$, which corresponds to dispersal by the short-distance vector only, is also shown.

The range expansions in Figure 3.4 appear similar to those shown when R_0 was varied, but there is an important difference in the initial phase of spread. All of the mixed-dispersal invasions have linear–linear biphasic range expansions, but the speed of spread during the initial phase is identical across simulations. This is because the net reproductive rate R_0 and short-distance dispersal are kept constant, so the short-distance spreading speed c_S does not change.

The probability p of LDD affects the second phase of range expansion in two ways. First, as p is decreased, the spreading speed c of the mixed kernel decreases. We first saw this in Figure 3.2, and the range expansions in Figure 3.4 confirm this; the spreading speed for each value of p is shown as a dashed line, and the per-step invasion speed v_t converges to the spreading speed. Second, decreasing p delays the onset of the second phase of spread, or equivalently lengthens the initial phase of spread. The initial phase of spread lasts for around ten generations for $p = 10^{-1}$, fifty generations for $p = 10^{-3}$, and around one hundred generations for $p = 10^{-5}$.

In all of the mixed-dispersal invasions shown so far, the effects of long-distance dispersal vanished as p was reduced to zero. This is not always the case, and in fact even when p is decreased to zero, some kernels significantly impact range expansion when used as the long-distance kernel. The determining factor turns out to be the moment generating function. I next explore this phenomenon, when it happens, and how it affects range expansions.

3.3.3 Persistent effects of infinitesimal LDD

Vanishingly rare long-distance dispersal may or may not impact range expansions, depending on the nature of the long-distance kernel $k_L(x)$. In this section, I analyze how range expansions respond when the probability p of long-distance dispersal is reduced to zero, and

show that invasions may nevertheless invade faster and exhibit biphasic range expansions. Lutscher has previously found that the asymptotic spreading speed can be boosted in sedentary (Lutscher, 2007) and dispersing populations (Lutscher, 2019), and that the deciding factor is whether the moment generating function $M_L(s)$ of $k_L(x)$ diverges within the support of $M_S(s)$. Here, I examine this result in the context of range expansions.

The first case occurs if $M_L(s)$ converges on the entire support of $M_S(s)$, as in the case of the Gaussian–Gaussian mixed kernels in the preceding section. Here, the effects of LDD vanish as p goes to zero. In the second, the moment generating function $M_L(s)$ diverges within the support of $M_S(s)$. This can occur, for example, in a Gaussian–Laplace or Laplace–Laplace mixed kernel. In these cases, the effects of LDD do not disappear as p is reduced to zero, and I refer to the long-distance kernel $k_L(x)$ as *persistent*.

A persistent long-distance dispersal kernel affects the R_0-versus-c speed curve in the following way. Denote by C_0 the R_0-versus-c speed curve of the short-distance dispersal kernel $k_S(x)$, and by C_p the speed curve for the mixed kernel with parameter value p. As p is decreased, C_p does not converge to C_0, but rather to a curve I will denote by C_{0^+}. In a neighborhood of $R_0 = 1$, the curves C_0 and C_{0^+} coincide. At a transition point T, the curves C_0 and C_{0^+} diverge, with C_{0^+} taking on larger values than C_0 for increasing R_0 (Lutscher, 2019). Figure 3.5 shows how this behavior manifests in the speed curves for a Laplace–Laplace family of mixed kernels. Here, the transition point T occurs at roughly $R_0 = 1.0434$ and $c \approx 0.41667$.

Typically, the R_0-versus-c speed curve cannot be solved for in closed form; the parametric variable cannot in general be eliminated. In the case of a persistent LDD kernel, a portion of the C_{0^+} speed curve can be explicitly solved for. The portion of the curve lying between the point $(R_0, c) = (1, 0)$ and T exactly matches that of C_0, and so can be found parametrically; the point T lies on this curve, evaluated at the parametric value $s = a$, the point of divergence of $M_L(s)$. Beyond T, computing points on the curve C_{0^+} requires evaluating the parametric system (3.2.6) under the double limit as $s \to a$ and $p \to 0$. A proof for this latter case was

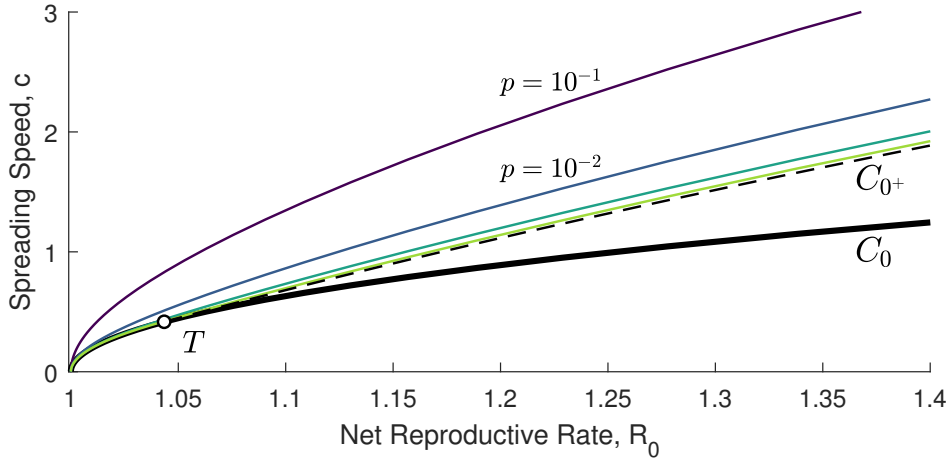

Figure 3.5: Speed curves for a family of mixed kernels with a persistent long-distance component. Here $k_S(x)$ is the Laplace kernel (3.2.3) with parameter $a = 1$ (variance $\sigma_S^2 = 2$), and $k_L(x)$ is also a Laplace kernel but with $a = 5$ (variance $\sigma_L^2 = 50$). Each curve indicates the spreading speed c as a function of R_0 for a mixed kernel with probability of LDD $p = 10^{-1}, 10^{-2}, \ldots, 10^{-4}$. The thick black curve (label C_0) corresponds to the case where $p = 0$, and the dashed black curve (label C_{0^+} corresponds to the limiting curve as p approaches zero from above. The curves C_0 and C_{0^+} meet in tangency at the point T, and overlap for smaller values of R_0.

given by Lutscher (2019), who gave the closed-form expression,

$$c = \frac{\log(R_0 M_S(a))}{a}, \quad R_0 \geq \frac{\exp\left[\frac{aM_S'(a)}{M_S(a)}\right]}{M_S(a)}. \tag{3.3.3}$$

Note that equation (3.3.3) is exact, and explicit rather than parametric. This function is shown in Figure 3.5 as a black dashed curve.

Figure 3.6 shows example range expansions with mixed dispersal where $k_L(x)$ is a persistent kernel. For nearly all values of p, the resulting range expansion is biphasic, with two distinct phases of spread. For $p = 10^{-1}$, the duration of the initial phase is shortened, but this also coincides with the LDD vector being quite common.

Although reducing the probability of occurrence of LDD has little effect on the ultimate spreading speed, it does affect when the transition between phases occurs. As we see in

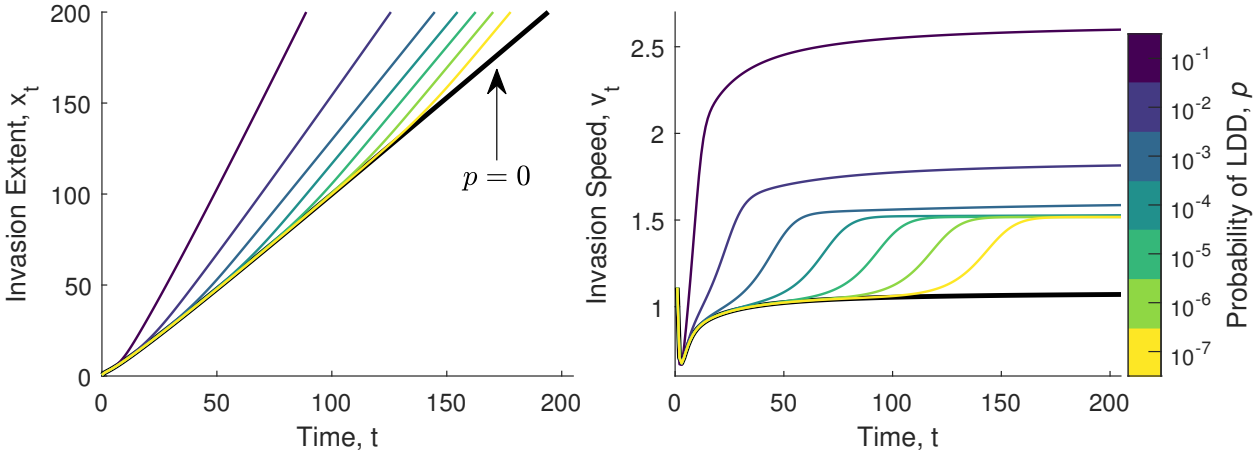

Figure 3.6: Mixed-dispersal invasions with persistent long-distance dispersal. Dispersal is as in Figure 3.5. Growth is Beverton–Holt with $R_0 = 1.3$. Seven mixed-dispersal invasions are shown, corresponding to $p = 10^{-1}, 10^{-2}, \ldots, 10^{-7}$, along with an unmixed invasion ($p = 0$). The ultimate speed of spread decreases as p is reduced, but for $p < 10^{-3}$, the reduction in speed is negligible. The duration of the first phase of spread increases as p decreases; rarer long-distance dispersal delays the onset of the phase of spread that is dominated by LDD. In all simulations, the grid spacing is $\Delta x = 1/16$, and the domain half-width is $H = 1000, 800, 600$ for $p = 10^{-1}, 10^{-2}, 10^{-3}$ respectively, and $H = 400$ for $p = 10^{-4}, \ldots, 10^{-7}$.

Figure 3.4, as p is decreased, the onset of the phase transition is delayed; thus, p plays a role similar to R_0 in determining when the phase transition occurs. Further, as p decreases in orders of magnitude, this delay grows roughly linearly.

3.4 Fat tails: Long- and short-distance dispersal

I now turn to invasions with true fat-tailed dispersal. In contrast with the mixed-dispersal models described in the previous section, where two distinct modes of dispersal were incorporated into a single dispersal kernel, there is no such distinction with fat-tailed dispersal. As such, there is no clear way to separate the effects of short- and long-distance dispersal. Furthermore, an invasion with true fat-tailed dispersal will continuously accelerate, and so has no asymptotic spreading speed (Kot et al., 1996).

Despite these differences, fat-tailed invasions behave qualitatively very similarly to mixed-

dispersal invasions: they can express biphasic range expansions, and can initially progress at near-constant speeds for long times before ultimately accelerating. To find this speed, I review approaches for approximating the speed of spread and introduce a new method based on speed rarefaction curves (Kot and Neubert, 2008). This method also enables us to measure the contribution of different parts of the dispersal kernel to the invasion speed, which defines a notion of kernel "shoulders" in the context of invasion.

3.4.1 Range expansions with fat-tailed dispersal

The previous chapter detailed how the tail-additivity properties of regularly varying probability density functions can be used to approximate the tail of a point-release invasion with fat-tailed dispersal. We used these tail approximations to find that the invasion front position, x_t, advances geometrically fast, with the base of geometric growth a function of net reproductive rate R_0 and the degree of tail fatness α,

$$x_{t+1} \approx R_0^{1/\alpha} x_t, \qquad t \to \infty. \tag{3.4.1}$$

Consequently, the per-step invasion speed $v_t = x_t - x_{t-1}$ itself grows geometrically quickly,

$$v_{t+1} \approx R_0^{1/\alpha} v_t, \qquad t \to \infty. \tag{3.4.2}$$

Despite asymptotically accelerating without bound, fat-tailed invasions initially spread slowly. How long an invasion spreads at a slow speed depends in part on the rate of acceleration of the invasion, but there can also be a delay before the onset of acceleration. Figure 3.7 shows plots of range expansions for invasions with fat-tailed dispersal. In each case, dispersal is governed by the fat-tailed Laplace kernel (3.2.11). Growth is according to the Beverton–Holt stock-recruitment function (3.1.5) with $R_0 = 1.3, 1.5, 2.0$. These invasions have linear–accelerating biphasic range expansions: in the first phase spread is linear at a constant speed, and in the second phase they continuously accelerate.

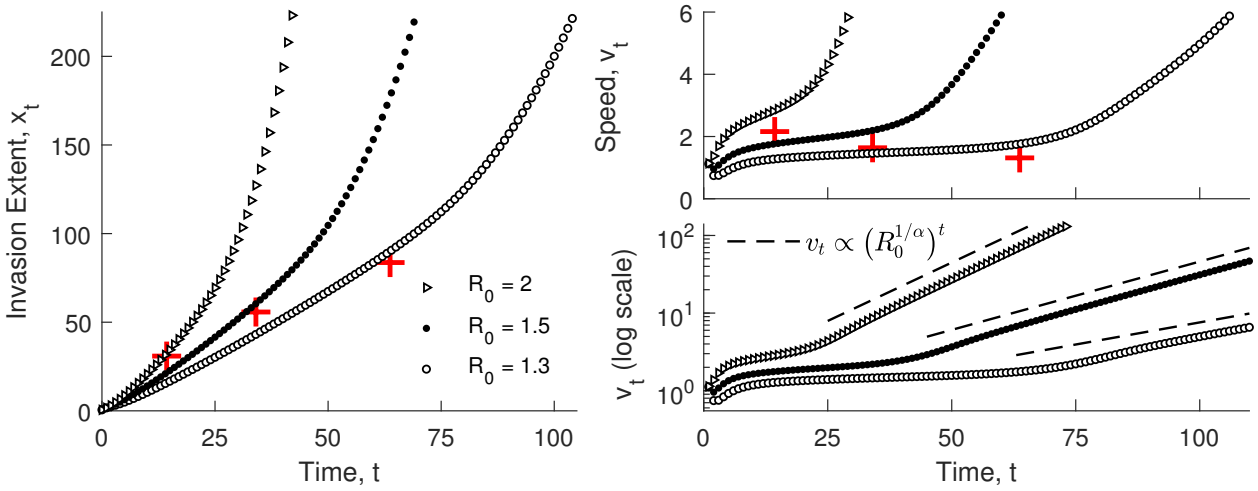

Figure 3.7: Range-expansion curves of fat-tailed invasions. Each invasion follows from a point-release, with dispersal given by the fat-tailed Laplace kernel (3.2.11) with $\alpha = 8$, and Beverton–Holt growth with $R_0 = 1.3, 1.5, 2.0$. Range expansion can be biphasic linear–accelerating or continuously accelerating; for small values of R_0, the initial phase of spread is at a constant speed, but for larger values this phase disappears. Each invasion eventually enters into an accelerating regime, where its rate of advance is geometric with base $R_0^{1/\alpha}$; this can be seen in logarithmic scale (bottom right), when the per-step invasion speed v_t tends to follow straight lines, indicating geometric growth at the expected rate (3.4.2). Red crosses in the plots of x_t indicate the approximate time $\bar{t}$ and position $\overline{x}$ of the phase transition between constant and accelerating phases, as determined by the procedure in *Time of phase transition*. In the plots of v_t, red crosses are plotted on the vertical axis at the value $\overline{x}/\bar{t}$. In all simulations, the grid spacing is $\Delta x = 1/16$ and the domain half-width is $H = 2000$.

Raising and lowering the net reproductive rate R_0 affects fat-tailed invasions similarly to mixed-dispersal invasions. As R_0 is increased, the speed of range expansion increases, both during the initial rate of constant-speed expansion as well as during the accelerating phase. Lowering R_0 delays the onset of the accelerating phase, or extends the duration of the initial phase.

Unlike mixed dispersal kernels, fat-tailed kernels do not comprise distinct short- and long-distance dispersal vectors. As such, there is no obvious speed that can be associated to short-distance dispersal only. In the following section, I review ways of approximating this speed.

3.4.2 Spreading speeds for truncated fat-tailed kernels

Fat-tailed invasions have no finite spreading speed (Kot et al., 1996), but some techniques for finding or approximating the spreading speed can be applied or adapted. Techniques for calculating the spreading speed of thin-tailed kernels depend on the moment generating function — something that fat-tailed kernels lack — but there are approximations for the speed with milder requirements. Here I review two such approximations: the Gaussian and kurtosis approximations. I then introduce a technique based on truncation of tails of the kernel.

To apply the Gaussian approximation, it is necessary that $k(x)$ have finite variance. Many fat-tailed kernels have finite variance, with notable exceptions being the Cauchy distribution or any fat-tailed kernel with tail fatness $\alpha \leq 3$. Denoting σ^2 as the variance of $k(x)$, the Gaussian approximation gives the approximate speed

$$c_G = \sqrt{2\sigma^2 \log R_0}. \tag{3.4.3}$$

The Gaussian approximation comes from replacing the kernel $k(x)$ with a Gaussian kernel of equal variance, and in practice under-predicts the speed of invasion. Alternatively, the Gaussian approximation can be derived from a truncation of the Taylor series expansion of the moment generating function (Lutscher, 2007).

The kurtosis approximation comes from a higher-order truncation of the moment generating function (Lutscher, 2007), and is given by

$$c_{\gamma_2} = c_G \left(1 + \frac{\gamma_2}{12} \log R_0\right). \tag{3.4.4}$$

Whereas the variance σ^2 is the second-order moment of $k(x)$, the excess kurtosis γ_2 is derived from the fourth-order moment. In order for the excess kurtosis to be defined, $k(x)$ must have tail decay of order $\alpha > 5$; the kurtosis is undefined for $\alpha \leq 5$. Therefore, despite being more accurate, the kurtosis approximation is more restrictive in that it cannot be applied to as

many kernels as can the Gaussian approximation.

To find a better approximation for the initial constant speed of spread of a fat-tailed invasion, I return to the moment generating function, formally defined as

$$M(s) = \int_{-\infty}^{\infty} e^{sx} k(x) \mathrm{d}x. \tag{3.4.5}$$

The key feature of heavy- and fat-tailed kernels that distinguishes them from thin-tailed kernels is their lack of moment generating functions. This means that analytic methods for characterizing thin-tailed dispersal that use the moment generating function cannot be simply extended for use with fat-tailed kernels.

The moment generating function fails to exist for fat-tailed dispersal kernels precisely because of their tails, which do not decay to zero fast enough for the integral in equation (3.4.5) to converge. Truncating these tails, even at a great distance from their peak, will cause the integral to converge. This is because a dispersal kernel with compact support, where the kernel is nonzero only over a closed and bounded interval, must be thin tailed.

I define the moment generating function of the normalized dispersal kernel with truncated support $-H \leq x \leq H$, denoted $M_H(s)$, as

$$M_H(s) = \frac{\int_{-H}^{H} e^{sx} k(x) \mathrm{d}x}{\int_{-H}^{H} k(x) \mathrm{d}x}. \tag{3.4.6}$$

In this definition, the integral in the numerator is modified from the moment generating function, and the integral in the denominator is a normalization constant. This normalization constant accounts for the fact that truncating the tails of the dispersal kernel results in its integral being less than one.

The truncated moment generating function (3.4.6) can be used in the parametric relations (3.2.6). Doing so yields the spreading speed of the thin-tailed kernel that is obtained from truncating and re-normalizing the fat-tailed kernel $k(x)$ at a fixed half-width H. I denote this speed as c_H, with H indicating the truncation half-width. Holding H constant and finding

the spreading speed as a function of R_0 yields a speed curve like those shown in Figure 3.2 or Figure 3.5. Alternatively, fixing R_0 and varying H allows us to find the spreading speed of a truncated fat-tailed kernel as a function of the H, yielding a "speed rarefaction curve".

Speed rarefaction curves were first introduced by Kot and Neubert (2008) in the study of range-limited or censored dispersal data. They studied thin- rather than fat-tailed kernels, for which the speed rarefaction curve approaches a finite limit: the spreading speed of the non-truncated thin-tailed kernel. They used speed rarefaction curves to determine the sampling radius required for accurate estimates of the spreading speed.

For fat-tailed kernels, the speed rarefaction curve does not approach a finite limit. Instead, as the truncation half-width increases, the speed of spread of the truncated kernel approaches infinity. Despite having no finite limit, the shape of the speed rarefaction curve is useful in indicating the importance of different parts of the kernel.

Rarefaction curves for the fat-tailed t-distribution for a variety of values of R_0 are shown in Figure 3.8. For each curve, the spreading speed increases as truncation length increases, but the rate of increase is not steady. The behavior of these rarefaction curves is most easily understood for very large and very small values of H. The spreading speed first increases rapidly near $H = 0$; for a zero-width kernel, spread does not occur. As the truncation width H approaches infinity, so does the spreading speed; this is consistent with the fact that full, non-truncated fat-tailed kernel produces continuously accelerating invasions, for which the invasion speed is unbounded and approaches infinity.

For some range of intermediate truncation widths, the rarefaction curve of a fat-tailed kernel can plateau or become nearly flat. For the curves in Figure 3.8, this occurs in a range of values of approximately $8 \leq H \leq 50$ for $R_0 = 1.2$. For $R_0 = 1.4$ the interval is shorter, around $8 \leq H \leq 30$. As R_0 increases, the length the interval decreases; for $R_0 = 2.0$, the rate of increase of the curve slows near $H \approx 12$, but does not flatten to the degree seen in the curves for lower values of R_0. When the plateau is present, I denote by H^* the truncation half-width at which c_H changes most slowly, or the derivative $\mathrm{d}c_H/\mathrm{d}H$ is minimal. The corresponding speed c_{H^*} is the speed at which the rarefaction curve plateaus.

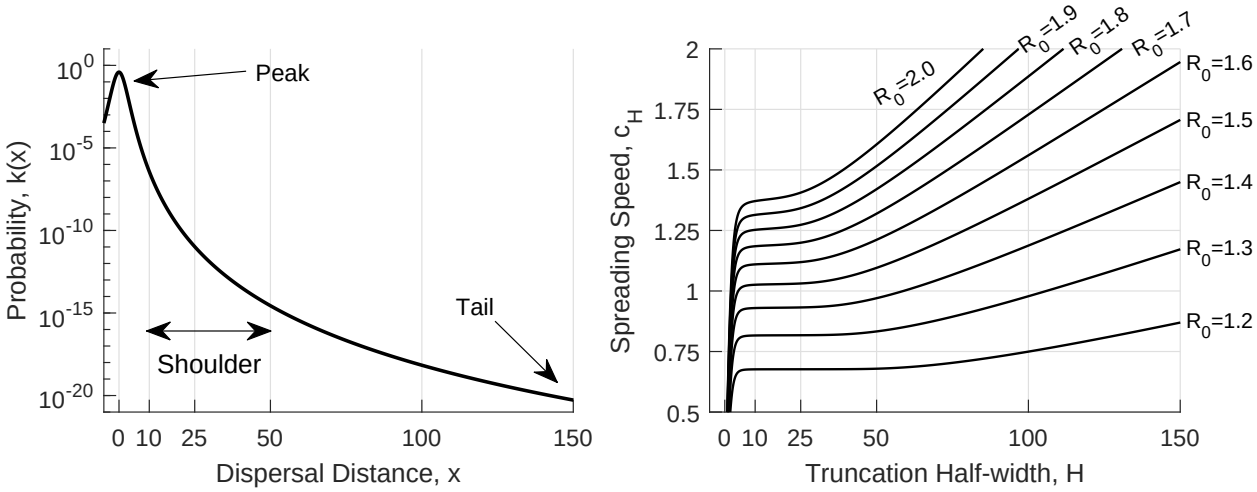

Figure 3.8: Rarefaction curves for a fat-tailed kernel. Horizontal axes on each plot both correspond to distance at the same scale. **(Left)** A fat-tailed dispersal kernel. The peak corresponds to the bulk of dispersal that occurs at a short scale, and the tail corresponds to rare long-distance dispersal. The term "shoulder" describes a part of the kernel that lies between the peak and the tail. **(Right)** The spreading speed associated with truncating and re-normalizing the fat-tailed kernel at various lengths. As the truncation half-width increases, the spreading speed increases. A flat part of the curve indicates a part of the kernel that contributes minimally to the spreading speed. This plateau defines the shoulder of the kernel in the context of invasion.

It is not immediately obvious that c_{H^*} should be relevant to a true fat-tailed invasion, but I have found c_{H^*} to be a good predictor of the near-constant speed of spread during fat-tailed invasions. I give the following heuristic argument for why this may be the case. Denote by v_t the per-step invasion speed of the invasion with the non-truncated, true fat-tailed dispersal kernel $k(x)$. Consider the family of invasions by the truncated kernels $k_H(x)$ for all H, and denote the per-step invasion speed for these invasions by v_t^H. As the truncation half-width H is taken to infinity, $v_t^H \to v_t$ for each fixed t. Furthermore, for each invasion with truncated dispersal, the per-step invasion speed will approach the spreading speed, so $v_t^H \to c_H$ as time increases. These two facts mean that $|v_t^H - v_t|$ becomes small as H becomes large, while

$|v_t^H - c_H|$ becomes small as t becomes large. Applying the triangle inequality gives

$$|v_t - c_H| \leq |v_t - v_t^H| + |v_t^H - c_H|. \tag{3.4.7}$$

At certain times and for certain truncation widths, the two positive quantities on the right are simultaneously small, and consequently so is the difference on the left. I have observed that this occurs for values of $H \approx H^*$. Under these circumstances, the per-step speed v_t approaches or becomes very close to the spreading speed of the truncated kernel. Formalizing this heuristic argument is difficult because these limits do not concurrently hold as both t and H become infinite, and indeed the per-step speed cannot be said to converge in a typical limiting sense. I hope to expand on this argument in future work.

Figure 3.9 shows how the Gaussian, kurtosis, and rarefaction approaches compare with the speed of spread of a fat-tailed invasion. The invasion has Beverton–Holt growth with $R_0 = 1.8$ and fat-tailed Laplace dispersal (3.2.11) with tail fatness $\alpha = 100$. These values were chosen to increase the differences between the three quantities c_G, c_{γ_2}, and c_{H^*} in order to make comparison with data clearer and to delay the onset of the accelerating regime of spread. The plots show that the per-step invasion speed v_t appears to asymptotically approach a constant value up until a time around $t = 225$, after which the speed rapidly grows, corresponding to the transition between the constant-speed and accelerating phases of range expansion. The Gaussian approximation under-predicts this speed, the kurtosis approximation over-predicts but is closer, and the speed c_{H^*} from the rarefaction curve closely matches the apparent limit of v_t before the phase transition.

3.5 Time of phase transition

In this section, I find an approximation for the time at which a phase transition will occur in a biphasic range expansion of a fat-tailed invasion. To do this, I develop an approximation for the central, established portion of the invading population, and another for the tail of the population under the linear model. I then look for the time at which these approximations

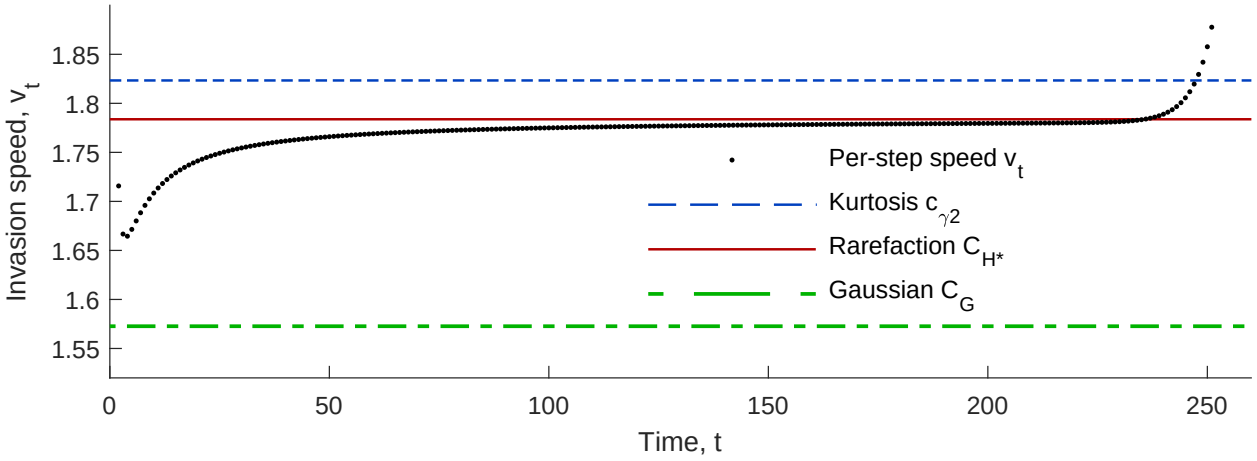

Figure 3.9: Speed of spread of a fat-tailed invasion. Data (black points) indicate the per-step invasion speed v_t of a simulated fat-tailed invasion; the grid spacing is $\Delta x = 1/16$ and the domain half-width is $H = 1000$. Dispersal is governed by the fat-tailed Laplace kernel with tail fatness $\alpha = 100$. Growth is Beverton–Holt with $R_0 = 1.8$. The invasion progresses at a steady pace for over 200 generations, and appears to approach a finite spreading speed before rapidly accelerating. The solid, dashed, and dash-dotted lines indicate estimates of the transient speed from the rarefaction curve (C_{H^*}), the kurtosis approximation (c_{γ_2}), and the Gaussian approximation C_G, respectively.

are simultaneously equal and match a detection threshold. At this time, the invasion front transitions from being governed by short-distance dispersal to long-distance dispersal.

I begin by developing an approximation for the central portion of the population density, $n_t(x)$. Assume that $k(x)$ has finite variance, denoted by σ_S^2. All thin-tailed kernels possess a finite variance, as do fat-tailed kernels with tail fatness $\alpha > 3$. As long as the dispersal kernel $k(x)$ has finite variance, the central limit theorem applies.

The central limit theorem deals with sums of independent random variables, and states conditions under which such the sums tend to Gaussian or normal distributions. Lutscher (2007) previously detailed how local limit theorems can be used to analyze integrodifference equations, and I follow his approach here. Let X_j represent independent and identically

distributed random variables, and Z_t denote the normalized sum,

$$Z_t = \frac{1}{\sigma\sqrt{t}} \sum_{j=1}^{t} X_j.$$

Assuming that all X_j have finite variance, then the central limit theorem applies and states that the cumulative distribution function of Z_t will tend to a standard normal distribution. For my purposes, the related local limit theorems are more useful, as they deal with probability densities rather than distribution functions. Petrov (1975) details that

$$\sup_x \left| p_t(x) - \frac{1}{\sqrt{2\pi}} e^{-x^2/2} \right| \to 0$$

where $p_t(z)$ is the density function of the normalized sum Z_t. If the random variables X_j themselves have density function $k(x)$, then $p_t(x)$ is simply

$$p_t(x) = k^{t*}(x).$$

By performing the change of variables $x \mapsto x/\sqrt{t\sigma_S^2}$, we obtain

$$k^{t*}(x) \to \frac{1}{\sqrt{2\pi t\sigma_S^2}} \exp\left(\frac{-x^2}{2t\sigma_S^2}\right), \quad t \to \infty. \tag{3.5.1}$$

Equation (3.5.1) can be combined with the formal solution for a point-release invasion under linear IDE model (3.1.3),

$$n_t(x) \approx \frac{R_0^t}{\sqrt{2\pi t\sigma_S^2}} \exp\left(\frac{-x^2}{2t\sigma_S^2}\right). \tag{3.5.2}$$

Unfortunately, this approximation converges too slowly to provide a good approximation in the tails of $n_t(x)$ at large times; this is because approximation (3.5.1) converges more slowly than the growing factor of R_0^t due to repeated growth of the population. Fortunately, I will use this approximation at the edge of the central bulk of the invasion, rather than in the

tails, and restrict my attention to finite and relatively small, rather than large, times.

To approximate $n_t(x)$ in the tails, I use the tail additivity properties of fat-tailed kernels. Assuming that $k(x)$ is fat-tailed, it is also a regularly varying density. Due to tail additivity of the kernel (3.2.14), $n_t(x)$ is asymptotically equal to a scaled copy of the dispersal kernel,

$$n_t(x) \sim R_0^t t k(x), \qquad x \to \infty. \tag{3.5.3}$$

To predict when the behavior of the invasion front transitions from being dominated by short- to long-distance dispersal, I look for when these two terms are equal and match a detection threshold $\overline{N}$. This occurs when all three quantities are equal,

$$\frac{R_0^{\bar{t}}}{\sqrt{2\pi \bar{t} \sigma_S^2}} e^{-\bar{x}^2/(2\bar{t}\sigma_S^2)} = \overline{N}, \tag{3.5.4a}$$

$$R_0^{\bar{t}} \bar{t} k(\overline{x}) = \overline{N}. \tag{3.5.4b}$$

Here $\overline{x}$ and $\bar{t}$ indicate the spatial position and time at which the regime shift occurs. Figure 3.10 shows how the equations are satisfied by the two approximations and the detection threshold in a fat-tailed invasion.

In general, solving for $\overline{x}$ and $\bar{t}$ in system (3.5.4) is not possible analytically, but can be done numerically. $\bar{t}$ may be non-integer, in which case the largest integer that is smaller than $\bar{t}$ will provide a more conservative estimate for the time at which the regime shift occurs. Furthermore, approximation (3.5.5) was derived under the linear integrodifference model (3.1.2). Assuming that the growth function $f(n)$ has no Allee effect, the linear and nonlinear models will have the same asymptotic spreading speeds, but the two models generally have different transient dynamics. The nonlinear model typically lags behind the linear model.

I have applied this approximation to the simulations in Figure 3.7, which shows invasions extent and speed versus time for multiple fat-tailed invasions. Red crosses indicate the time $\bar{t}$ and position $\overline{x}$ of the phase transition as predicted by the solution of system (3.5.4). While the transition between phases of spread is not sharp, $\bar{t}$ precedes the onset of acceleration in

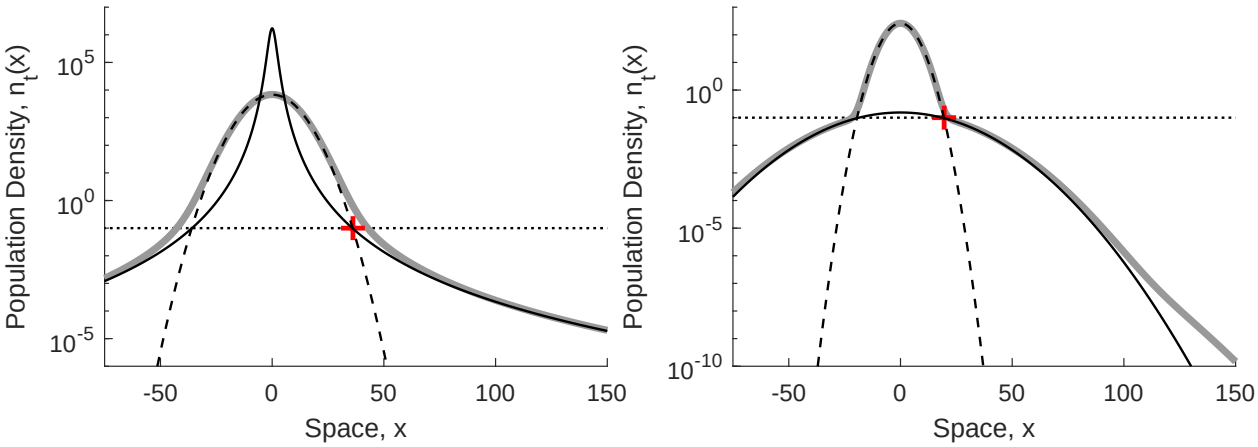

Figure 3.10: Population densities at phase transition. The population density $n_t(x)$ (thick gray curves) according to the linear model (3.1.2) follows a Gaussian-like profile (black dashed curves) in a central region. **(Left)** A fat-tailed invasion transitions between being dominated by short- to long-distance dispersal at time $t = 35$. The tails are approximated by equation (3.5.3) using tail additivity (solid black curve). The central and tail approximations intersect and both equal a detection threshold $\overline{N} = 0.1$ (black dotted curve) at the position indicated by the cross. Dispersal is governed by the t-distribution with $\nu = 5$. Growth is linear with $R_0 = 1.4$. **(Right)** The phase transition of a mixed-dispersal invasion. Similar to the fat-tailed invasion, approximations for the central bulk (black dashed curve) and tail (solid black curve) of the invasion meet at the detection threshold. Both short- and long-distance dispersal are Gaussian, with $\sigma_S = 1$ and $\sigma_L = 20$. Figure shows $n_t(x)$ at time $t = 24$.

all cases where a demarcation is evident.

Although the system (3.5.4) cannot be solved for in general, we can make some broad inferences. First, the time $\bar{t}$ of the phase transition increases as R_0 is decreased. This is because in (3.5.4b), R_0 must be raised to the power of $\bar{t}$ for the left-hand side to be of sufficient magnitude; that is, the compounding geometric growth at rate R_0 must counteract the small probability $k(\overline{x}) \ll 1$ in order to reach the threshold of detection. Second, all things being equal, larger values of α indicate more rapidly decaying tails; $\bar{t}$ correspondingly increases as α is increased, at least within a parameterized family of kernels such as the t-distribution.

3.5.1 Mixed dispersal

Thin-tailed mixed-dispersal kernels do not possess the asymptotic tail additivity properties of fat-tailed kernels that I used in tail approximation (3.5.3). Instead, for a mixed kernel with $k(x) = (1-p)k_S(x) + pk_L(x)$, I derive the approximation

$$n_t(x) \approx \frac{R_0^t}{\sqrt{2\pi t\sigma_S^2}} \exp\left(\frac{-x^2}{2t\sigma_S^2}\right) + R_0^t tpk_L(x). \tag{3.5.5}$$

Details of this derivation are in appendix *Approximation of point-release invasions with mixed dispersal*. The key assumptions are (1) that long-distance dispersal events are rare, so $p \ll 1$, (2) that $k_S(x)$ has finite variance σ_S^2, so that the self-convolution $k_S^{t*}(x)$ can be approximated with a Gaussian distribution, and (3) that $k_S(x)$ disperses very narrowly compared to $k_L(x)$, with $\sigma_S^2 \ll \sigma_L^2$. Under these assumptions, equation (3.5.5) provides a good approximation for $n_t(x)$ in a spatial domain that encompasses the transition point between spread governed by short- and long-distance dispersal.

I now proceed similarly to how I found the transition time for fat-tailed kernels. The first term in (3.5.5) approximates the central bulk of $n_t(x)$, while the second term is a first-order approximation of the tails of $n_t(x)$. I equate these terms to $\overline{N}$, and look for the time $\bar{t}$ and position $\overline{x}$ that solve this system,

$$\frac{R_0^{\bar{t}}}{\sqrt{2\pi\bar{t}\sigma_S^2}} \exp\left(\frac{-\overline{x}^2}{2\bar{t}\sigma_S^2}\right) = \overline{N}, \tag{3.5.6a}$$

$$R_0^{\bar{t}}\bar{t}pk_L(\overline{x}) = \overline{N}. \tag{3.5.6b}$$

This system is nearly identical to system (3.5.4), with the major difference that $pk_L(\overline{x})$ replaces $k(\overline{x})$ in the second equation. Figure 3.10 shows how these two terms relate to and approximate the population density in a mixed-dispersal invasion.

Figure 3.3 shows how this approximation applies to mixed-dispersal invasions. In these invasions, dispersal is Gaussian–Gaussian mixed, with $k_S(x)$ having variance $\sigma_S^2 = 1$ and

$k_L(x)$ with variance $\sigma_L^2 = 400$. Each red cross in the figure marks the time $\overline{t}$ and position $\overline{x}$ of the phase transition, as calculated by system (3.5.6).

System (3.5.6) is very similar to (3.5.4), with the difference that $k_L(x)$ is thin-tailed. This important distinction can, in some cases, result in the system having no solution. This can happen if, for example, $k_L(x)$ is a Gaussian kernel; in this case, the approximation for the central bulk (3.5.6a) will eventually become heavier-tailed than $k_L(x)$, and the two approximations may never intersect at a value matching the detection threshold $\overline{N}$. This only occurs when $k_L(x)$ is as thin-tailed or thinner tailed than a Gaussian kernel. If $k_L(x)$ is heavier-tailed than any Gaussian distribution (e.g. a Laplace kernel) then a solution is guaranteed.

3.6 Discussion

In this chapter, I analyzed two approaches for modeling spread with long-distance dispersal: mixed-dispersal kernels and fat-tailed dispersal kernels. Both approaches are commonly used in the modeling and study of dispersal data, and can be incorporated into integrodifference-equation models of spread. My results contribute to our developing understanding of two aspects of spread and invasions: long-distance dispersal and transient phenomena.

There are several common patterns that emerge from both approaches. First and foremost, range expansion with LDD can be biphasic; invasions with short- and long-distance dispersal may progress at slow constant speeds before accelerating or switching to faster speeds. For both mixed and fat-tailed dispersal, short-distance dispersal determines the speed during the initial phase, while long-distance dispersal boosts the ultimate speed. Rarity of long-distance dispersal and the net reproductive rate control the time of transition between phases of spread; rarer long-distance dispersal and a lower value of R_0 increases the delay.

For mixed-dispersal invasions, both phases of spread are at constant speeds. The speed during the second phase of spread is boosted by long-distance dispersal, and the speedup can

be significant. For some combinations of kernels, I found that even exceedingly rare LDD (of arbitrarily small probability) can boost the speed significantly. In these cases, reducing the probability of LDD delays the onset of the second phase of spread, and has an essentially fixed effect on the ultimate spreading speed. For this to occur, the net reproductive rate must be sufficiently large; if R_0 is close to one, long-distance dispersal no longer overshadows short-distance dispersal.

Mixed dispersal has been studied as a means of producing biphasic range expansions by Ramanantoanina et al. (2014) in a similar model. In their study, dispersal ability is heritable, and the population consists of two or more distinct types of individuals with different dispersal abilities. Short-dispersing individuals disperse according to a dispersal kernel with variance smaller than that of long-dispersing individuals. With suitable initial conditions, the resulting range expansion is biphasic with two linear phases. Although these results are similar to those I have presented in *Invasions with mixed thin-tailed dispersal*, there are some key differences. First, in my model, every propagule is equally likely to disperse according to the long-distance dispersal kernel. Long-distance dispersal is rare, and occurs with probability p for each dispersing propagule. In contrast, the longer dispersal ability of individuals in the model of Ramanantoanina et al. (2014) is a genetic trait, and is only initially rare due to their initially small number; after a number of generations, the longer dispersing individuals are in the majority. Second, Ramanantoanina et al. (2014) found that long-dispersing individuals eventually dominate the invasion front, with short-dispersing individuals persisting only in the initial core of invaded territory. In my model, there is a single combined population, demonstrating that a bias in the spatial distribution of short- and long-distance dispersers is not necessary to produce biphasic range expansions.

Fat-tailed kernels are popular for modeling dispersal data, but are less often used in conjunction with IDE models. With new analytic techniques, a focus on their behavior over ecologically relevant timescales rather than their asymptotic dynamics, and an improved understanding of their effect on range expansion, it is possible to incorporate them in models of spread.

Invasions with fat-tailed dispersal can have biphasic range expansions similar to those of mixed-dispersal invasions; however their ultimate phase of spread consists of continuous acceleration. During the initial phase of spread, the invasion speed is nearly constant. Fat-tailed kernels have no separate mechanisms for short- and long-distance dispersal, making estimation of this initial speed difficult. I reviewed two known approaches for approximating the speed of invasion and introduced a new approach based on speed rarefaction curves (Kot and Neubert, 2008) for finding the speed of spread of truncated fat-tailed kernels; I found this method best predicted the speed of spread.

Speed rarefaction curves also provide a way of delineating short- and long-distance dispersal for fat-tailed kernels. By truncating the tails of a fat-tailed kernel, it becomes thin-tailed and gains a finite spreading speed. Plotting spreading speed versus truncation distance generates an increasing curve of speed versus distance that indicates how different parts of the kernel contribute to the spreading speed. Speed rarefaction curves enable us to define a "shoulder" of a dispersal kernel as a part of the kernel between the peak and the tail that contributes minimally to the speed of spread.

Many types of range-expansion curves are now known to be possible under IDE model (3.1.1). Following the classification scheme of Shigesada et al. (1995), type 1 or linear expansion occurs under many common thin-tailed kernels, type 2 or linear biphasic emerges under certain mixed-dispersal kernels, and type 3 or continuously accelerating range-expansions can be generated from fat-tailed kernels (Liu and Kot, 2019). In addition to these types, fat-tailed kernels can generate a biphasic linear–accelerating range expansion absent in the original classification; we might think of this as a type 2.5 range expansion, with behavior somewhere between the classic linear biphasic and continuously accelerating types. These results demonstrate the capability of a simple, single-population model to produce a great variety of types of range expansion, driven purely by different forms of dispersal kernel.

All of the biphasic range expansions I have shown, where spread initially follows a regime that differs from its ultimate or asymptotic dynamics, are ultimately transient phenomena. It is important to remember that these rapid shifts in speed and dynamics arise solely as a

result of the dispersal kernel, rather than through a change in a parameter value or transition across a heterogeneous landscape. No outside influence or environmental change is necessary for a regime shift to occur in the case of transient dynamics (Hastings et al., 2018). An invasion that has progressed at a slow pace may accelerate with little warning; its apparent steady progress may in actuality be a long, transient phase of spread. Depending on the rarity and form of long-distance dispersal, the ultimate rate of spread of an invasion may be vastly different than its initial speed.

Researchers should note the causal connection between long-distance dispersal and transient dynamics in range expansion. Specifically, the study of LDD necessitates consideration of transient timescales and use of non-asymptotic analytic techniques. As long-distance dispersal is incorporated into models of spread, transient behavior will necessarily arise. A focus on spreading speed, for instance, may be misleading, if the effects of long-distance dispersal are not felt for many generations or only beyond ecologically relevant timescales.

Appendix

3.A Approximation of point-release invasions with mixed dispersal

Since $k(x) = (1-p)k_S(x)+pk_L(x)$, I will first establish the form of the convolution power of a sum of functions. Because convolution is a linear operation, the form of the convolution power closely follows that of a binomial expansion,

$$\begin{aligned}(g+h)*(g+h) &= g*g+g*h+h*g+h*h \\ &= g*g+2g*h+h*h,\end{aligned} \tag{3.A.1}$$

where the last equality comes from the fact that convolution is commutative. Similarly,

$$(g+h)^{t*} = \binom{t}{0}g^{t*} + \binom{t}{1}g^{(t-1)*}*h + \cdots + \binom{t}{t}h^{t*}. \tag{3.A.2}$$

Hence, for the mixture model,

$$k(x) = (1-p)k_S(x) + pk_L(x), \tag{3.A.3}$$

the convolution power becomes

$$k^{t*}(x) = (1-p)^t k_S^{t*}(x) + t(1-p)^{t-1}p\left(k_S^{(t-1)*} * k_L\right)(x) + \cdots + p^t k_L^{t*}(x). \tag{3.A.4}$$

Since we are considering $0 < p \ll 1$, we have $1 - p \approx 1$, and replace $(1-p)$ by unity.

I am ultimately interested in using this approximation to determine the time of phase transition in mixed-dispersal invasions. This transition occurs when the first and second terms in the sum are of equal magnitude. I therefore truncate the sum to two terms, giving

$$k^{t*}(x) = k_S^{t*}(x) + pt\left(k_S^{(t-1)*} * k_L\right)(x) + \mathcal{O}(p^2). \tag{3.A.5}$$

This approximation holds in an interval containing the origin and the intersection of the first and second terms. For larger values of x, the third and higher terms can become significant if $k_L(x)$ decays rapidly in space (e.g. the Gaussian kernel).

Assuming that $k_S(x)$ has finite variance and zero mean, then a local limit theorem gives the approximation

$$k_S^{t*}(x) \approx \frac{1}{\sqrt{2\pi t\sigma_S^2}} \exp\left(\frac{-x^2}{2t\sigma_S^2}\right). \tag{3.A.6}$$

To approximate beyond this central region, further into the tail, I turn to the second term in (3.5.5). Assuming that $k_S(x)$ disperses much more narrowly than $k_L(x)$, we may approximate it with the Dirac delta function, $\delta(x)$. The Dirac delta function can be thought of as the limit of increasingly narrow Gaussian distributions, and satisfies the sifting property, that

$(\delta * g)(x) = g(x)$ for any function $g(x)$ (Bracewell, 1986). Thus,

$$pt\left(k_S^{(t-1)*} * k_L\right)(x) \approx tpk_L(x). \tag{3.A.7}$$

Inserting (3.A.6) and (3.A.7) into the expansion of the convolution of a mixed kernel (3.A.5), we multiply by R_0^t and obtain an approximation for the formal solution (3.1.3),

$$n_t(x) \approx R_0^t\left[\frac{1}{\sqrt{2\pi t\sigma_S^2}}\exp\left(\frac{-x^2}{2t\sigma_S^2}\right) + tpk_L(x)\right]. \tag{3.A.8}$$

Chapter 4

DISCUSSION

Furthering the characterization of integrodifference equations Perhaps the most basic description of my work is that it is a continuation of the characterization of integrodifference-equation models of population spread. Heavy- and fat-tailed kernels, in particular, represent a conspicuous gap in our understanding of IDE models; for these kernels, there has been little development of analytical techniques for over 20 years (Kot et al., 1996; Lewis et al., 2016). Researchers have extensively studied thin-tailed spread, and have developed a rich vocabulary and theoretical framework to analyze, measure, and describe thin-tailed invasions. They have not yet developed similar items for fat-tailed invasions.

In my work, I showed that fat-tailed invasions asymptotically accelerate at geometric rates, but in truth this is an answer to a question we are just beginning to understand how to ask. Where we have the spreading speed for thin-tailed invasions, there is not yet any rigorously defined analogue for geometrically accelerating invasions, or for accelerating invasions in general. Without a definition or metric, it is not immediately evident how we should measure the progress of such invasions. Indeed, I have shown that the rate of geometric spread depends on the measurement used, a feature foreign to thin-tailed invasions. Other landmark properties of thin-tailed invasions are also lost, such as the connection between the minimum traveling-wave speed of a front-release invasion and the spreading speed of a compactly supported invasion.

Although fat-tailed invasions do not converge in a conventional sense, a promising avenue for further study is their apparent convergence in logarithmic coordinates. When a fat-tailed invasion is plotted with the domain in a logarithmic scale, the population density profile appears to converge in shape and speed. This is consistent with the invasion front moving at a geometrically accelerating rate, and also suggests that the invasion front has, in some

sense, a characteristic width that grows geometrically as the invasion progresses.

Regular variation and tail additivity The tail-additivity properties of regularly varying probability densities are central to many of my analyses. These properties allow the tails of the convolution of distributions to be found asymptotically as a sum of the original distributions. Tail additivity generalizes to convolutions of arbitrarily many kernels, allowing expressions involving repeat convolutions to be similarly simplified in the tails. The work of Bingham et al. (2006), where the authors prove these results for probability densities rather than distribution functions, is particularly useful.

Fat-tailed kernels are a subset of the regularly varying class, and so inherit their tail-additivity properties. These properties have proven to be powerful, enabling analyses of several types of invasions. Under the linear model, with point-release initial conditions, a formal solution involving repeat convolutions is known; tail additivity immediately simplifies this expression. Under the nonlinear model, a more circuitous approach enables analysis of invasions with front-release initial conditions.

Tail additivity enables analysis of some invasions with fat-tailed dispersal that would be challenging or impossible with thin-tailed dispersal. Allee effects, where a population experiences reduced reproductivity at low densities, are difficult to analyze except in special cases or constructed examples (Hadeler and Rothe, 1975; Lewis et al., 2016; Lutscher, 2019). For these invasions, the speed of invasion is typically not linearly determined, or does not match that of the linearized model, because dispersal coupled with greater reproduction behind the invasion front pushes the invasion forward faster than pioneers beyond the front can pull it forward Lewis and Kareiva (1993). With tail additivity, I characterized fat-tailed invasions with weak Allee effects. In these cases, the invasion is essentially linearly determined; the effects of long-distance dispersal induced by fat-tailed kernels are so strong that they pull invasions even in the presence of weak Allee effects.

Non-asymptotic analyses My results on fat-tailed invasions establish important analogues to asymptotic analyses and properties of thin-tailed invasions, but also highlight their limitations. Concepts such as the asymptotic spreading speed or convergence to a stable wavefront may be irrelevant over timescales of interest. While a fat-tailed invasion may be seen as problematic for having an asymptotically infinite rate of spread, its speed is finite for all finite times. Furthermore, the transient phenomena that I have showcased occur not just for fat-tailed spread, but also for thin-tailed spread; for thin-tailed kernels, classical analyses apply but clearly overlook these important dynamics.

Transient and short-to-intermediate timescales are especially important in ecology. The field has a long history of modeling and conceptualizing of systems as approaching or having reached asymptotically stable equilibria, but in recent times the importance of transient phenomena has been recognized (Hastings et al., 2018). This is particularly the case with invasions, which often occur rapidly and are studied as they are developing; it does not make sense to think of these scenarios as stable or approaching equilibria.

Demystifying fat-tailed kernels Fat-tailed kernels have become popular for modeling dispersal data, but have not yet been widely adopted in the modeling of invasions. This is likely because fat-tailed kernels can lead to accelerating invasions; indeed, there have been efforts to assign finite spreading speeds to fat-tailed kernels (Clark et al., 2001), and some studies outright dismiss fat-tailed kernels from consideration because they lead to asymptotically infinite speeds (Gharouni et al., 2015). This characteristic makes fat-tailed kernels hard to reconcile with established theory and practices, but may pose less of a problem for modern studies.

Growing recognition of the importance of transient phenomena will likely make these phenomena a focus and diminish the importance of asymptotic properties (Hastings, 2004), including the spreading speed. In a finite period of time, fat-tailed invasions have finite speeds of spread. The speed will increase with time, but this is not unheard of in invasions (Hengeveld, 1989; Shigesada et al., 1995). Preceding acceleration, the speed of a fat-tailed

invasion may be constant for many generations, just as in the case of a thin-tailed invasion.

Biphasic range expansions Long-distance dispersal can be studied in spatially explicit models of spread in several ways. In my work, I have shown that two of the most popular modeling approaches for LDD can lead to biphasic range expansions. Short-distance dispersal determines the rate of advance at early times, before long-distance dispersal eventually dominates and accelerates spread.

Mixed dispersal, in the form of stratified diffusion, is known to be a possible mechanism for biphasic range expansions. With distinct underlying dispersal mechanisms linked to short- and long-distance dispersal, the association and emergence of two distinct phases of spread is plausible and intuitive. Mixed dispersal vectors also have a prominent effect on the geometries of dispersal kernels; the point at which the long-distance vector dominates the short-distance vector is often marked by a change in shape of the kernel. With the very geometry of the kernel showing a sharp transition, it is tempting to attribute the sharp phase transition to multiple dispersal vectors.

Fat-tailed kernels lack distinct short- and long-distance dispersal vectors, and are not well-known for producing biphasic range expansions; fat-tailed dispersal is probably most often associated with accelerating spread. Nevertheless, in my work I have shown that fat-tailed dispersal can produce biphasic range expansions. Rather than a smooth transition, linear–accelerating biphasic range expansions exhibit a sharp transition between their phases. Here, the sharp transition cannot be justified by any obvious delineation in dispersal abilities or by a lack of regularity in the dispersal kernel. As such, biphasic range expansion may occur not only through mixed dispersal, but rather through the broader mechanism of long-distance dispersal.

Classes of range expansion The pioneering work of Shigesada et al. (1995) in stratified diffusion established that long-distance dispersal could give rise to several qualitatively different classes of range expansion. Linear range expansion, or Type 1, is the simplest case

and describes invasions in reaction-diffusion models. Type 2 and Type 3 are more complex, representing linear–linear biphasic and continuously accelerating range expansions, respectively.

The scattered colony and coalescing colony models (Shigesada et al., 1995) are two models capable of generating these classes of range expansions. Although in one sense these models explain how dispersal can lead to different types of range expansion, in another sense they do not explain how the dispersal itself occurs. These models are spatially implicit and do not track population densities or the location of individuals; instead, they track a distribution on the sizes of isolated colonies that are assumed to arise due to LDD relative to the initial point of invasion. The models are also limited by the assumption that local dispersal is governed by diffusion. Ultimately, these approaches are incompatible and somewhat disconnected from spatially explicit models of spread such as IDE models.

We now know that the three broad and established classes of range expansion can be achieved in spatially explicit IDE models with the dispersal kernel as the sole mechanism. Linear–linear biphasic range expansions arising from Laplace–Laplace dispersal are Type 2 range expansions. Continuously geometrically accelerating invasions arising from fat-tailed dispersal are examples of Type 3. Further, the linear–accelerating biphasic range expansions generated in some fat-tailed invasions represent a possible new type between Type 2 and Type 3. More complex mechanisms, such as models with structured populations (Ramanantoanina et al., 2014) or which incorporate LDD separately from the kernel, may also produce these range expansions, but are not required. Contrary to some studies (Shigesada et al., 1995; Ramanantoanina et al., 2014), a spatial bias in the distribution of short- and long-distance dispersers, where long-distance dispersers are at the forefront of an invasion, is not required to generate Type 2 spread.

Mixed-dispersal kernels Mixed-dispersal kernels have many characteristics that make them attractive for studying long-distance dispersal. Mixed kernels cleanly fit within the paradigm whereby long-distance dispersal occurs by mechanisms separate to conventional

spread, and clearly demarcate between short- and long-distance dispersal with distinct component kernels. Mixed kernels also possess an explicit parameter governing the chance of long-distance dispersal. When all of the components of a mixed-dispersal kernel are thin-tailed, the mixed kernel is itself thin-tailed. These traits make mixed kernels compatible with established techniques and useful for isolating effects when studying LDD, but also open the door for the study of transient phenomena and the roles of short- and long-distance dispersal in driving range expansions.

Mixed-dispersal kernels can also help bridge our understanding of long-distance dispersal to fat-tailed kernels. Fat-tailed kernels lack distinct mechanisms for short- and long-distance spread, and have no explicit parameter to control the probability of long-distance dispersal. Nevertheless, fat-tailed invasions are qualitatively very similar to those generated by mixed-dispersal kernels. We may therefore make valuable inferences and analogies to fat-tailed dispersal, which provide hints for new analyses and techniques for understanding these counter-intuitive kernels.

Connecting long-distance dispersal to transient dynamics Long-distance dispersal has been a longstanding topic of interest in the study of dispersal and population spread. In the greater field of ecology, transient phenomena have been of interest for just as long. While these topics do not at first seem closely related, we can now say there is a strong connection: long-distance dispersal induces transient dynamics in invasions.

Researchers studying long-distance dispersal must be mindful of transients. Long-distance dispersal can boost invasion speeds, but these increases may not immediately be realized, and can be delayed for long times; the impact of LDD may not be felt for many generations after the start of an invasion. At the same time, my results show that the consequences of LDD can manifest rapidly and dramatically; invasions that have progressed at slow, consistent rates for many years may rapidly accelerate due to even exceedingly rare LDD.

It is clear that long-distance dispersal must be included in studies of dispersal and spread when its presence is suspected. We must now also contend with the fact that transients must

be considered when long-distance dispersal is present. Studies of long-distance dispersal that focus on long-term behaviors are necessarily limited, and depending on the timescale of interest, they may even be irrelevant.

BIBLIOGRAPHY

Alfaro, M. Slowing Allee effect versus accelerating heavy tails in monostable reaction diffusion equations. *Nonlinearity*, 30:687–702, 2017.

Alfaro, M. and Coville, J. Propagation phenomena in monostable integro-differential equations: acceleration or not? *Journal of Differential Equations*, 263:5727–5758, 2017.

Allee, W. C. *The Social Life of Animals*. W.W. Norton & Company, New York, 1938.

Austerlitz, F., Dick, C. W., Dutech, C., Klein, E. K., Oddou-Muratorio, S., Smouse, P. E., and Sork, V. L. Using genetic markers to estimate the pollen dispersal curve. *Molecular Ecology*, 13:937–954, 2004.

Baeumer, B., Kovács, M., and Meerschaert, M. M. Fractional reproduction-dispersal equations and heavy tail dispersal kernels. *Bulletin of Mathematical Biology*, 69:2281–2297, 2007.

Bateman, A. J. Is gene dispersion normal? *Heredity*, 4:353–363, 1950.

Beverton, R. J. H. and Holt, S. J. *On the Dynamics of Exploited Fish Populations*. Her Majesty's Stationary Office, London, 1957.

Bingham, N. H., Goldie, C. M., and Teugels, J. L. *Regular Variation*. Cambridge University Press, Cambridge, 1987.

Bingham, N. H., Goldie, C. M., and Omey, E. Regularly varying probability densities. *Publications de l'Institut Mathématique. Nouvelle Série*, 80:47–57, 2006.

Borovkov, A. A. *Asymptotic Analysis of Random Walks*. Cambridge University Press, Cambridge, 2008.

Bracewell, R. N. *The Fourier Transform and Its Applications.* McGraw Hill, New York, 1986.

Britton, N. F. *Reaction-Diffusion Equations and Their Applications to Biology.* Academic Press, London, 1986.

Buckley, Y. M., Brockerhoff, E., Langer, L., Ledgard, N., North, H., and Rees, M. Slowing down a pine invasion despite uncertainty in demography and dispersal. *Journal of Applied Ecology*, 42:1020–1030, 2005.

Bullock, J. M. and Clarke, R. T. Long distance seed dispersal by wind: measuring and modelling the tail of the curve. *Oecologia*, 124:506–521, 2000.

Bullock, J. M., Kenward, R. E., and Hails, R. S. *Dispersal Ecology: 42nd Symposium of the British Ecological Society held at the University of Reading, 2-5 April 2001.* Blackwell Publishing, Malden, 2002.

Bullock, J. M., Shea, K., and Skarpaas, O. Measuring plant dispersal: an introduction to field methods and experimental design. *Plant Ecology*, 186:217–234, 2006.

Bullock, J. M., González, L. M., Tamme, R., Götzenberger, L., White, S. M., Pärtel, M., and Hooftman, D. A. P. A synthesis of empirical plant dispersal kernels. *Journal of Ecology*, 105:6–19, 2017.

Cain, M. L., Milligan, B. G., and Strand, A. E. Long-distance seed dispersal in plant populations. *American Journal of Botany*, 87:1217–1227, 2000.

Caswell, H., Lensink, R., and Neubert, M. G. Demography and dispersal: life table response experiments for invasion speed. *Ecology*, 84:1968–1978, 2003.

Clark, J. S. Why trees migrate so fast: Confronting theory with dispersal biology and the paleorecord. *The American Naturalist*, 152:204–224, 1998.

Clark, J. S., Fastie, C., Hurtt, G., Jackson, S. T., Johnson, C., King, G. A., Lewis, M., Lynch, J., Pacala, S., Prentice, C., Schupp, E. W., Webb, T., and Wyckoff, P. Reid's paradox of rapid plant migration: Dispersal theory and interpretation of paleoecological records. *BioScience*, 48:13–24, 1998.

Clark, J. S., Silman, M., Kern, R., Macklin, E., and HilleRisLambers, J. Seed dispersal near and far: Patterns across temperate and tropical forests. *Ecology*, 80:1475–1494, 1999.

Clark, J. S., Lewis, M., and Horvath, L. Invasion by extremes: Population spread with variation in dispersal and reproduction. *The American Naturalist*, 157:537–554, 2001.

Cooke, R. M., Nieboer, D., and Misiewicz, J. *Fat-Tailed Distributions: Data, Diagnostics and Dependence*. ISTE Ltd/John Wiley & Sons, Hoboken, 2014.

Crooks, J. A. Lag times and exotic species: The ecology and management of biological invasions in slow-motion. *Ecoscience*, 12:316–329, 2005.

Darwin, C. *On the Origin of Species by Means of Natural Selection*. John Murray, London, 1859.

Devaux, C., Lavigne, C., Falentin-Guyomarc'h, H., Vautrin, S., Lecomte, J., and Klein, E. K. High diversity of oilseed rape pollen clouds over an agro-ecosystem indicates long-distance dispersal. *Molecular Ecology*, 14:2269–2280, 2005.

Embrechts, P., Klüppelberg, C., and Mikosch, T. *Modelling Extremal Events: For Insurance and Finance*. Springer-Verlag, Berlin, 1997.

Feller, W. *An Introduction to Probability Theory and its Applications*, volume 2. John Wiley & Sons, New York, 1971.

Fisher, R. A. The wave of advance of advantageous genes. *Annals of Eugenics*, 7:355–369, 1937.

Foss, S., Korshunov, D., and Zachary, S. *An Introduction to Heavy-Tailed and Subexponential Distributions*. Springer, New York, 2011.

Garnier, J. Accelerating solutions in integro-differential equations. *SIAM Journal on Mathematical Analysis*, 43:1955–1974, 2011.

Gharouni, A., Barbeau, M., Locke, A., Wang, L., and Watmough, J. Sensitivity of invasion speed to dispersal and demography: an application of spreading speed theory to the green crab invasion on the northwest Atlantic coast. *Marine Ecology Progress Series*, 541:135–150, 2015.

Gilbert, M., Grégoire, J.-C., Freise, J. F., and Heitland, W. Long-distance dispersal and human population density allow the prediction of invasive patterns in the horse chestnut leafminer Cameraria ohridella. *Journal of Animal Ecology*, 73:459–468, 2004.

Goto, S., Shimatani, K., Yoshimaru, H., and Takahashi, Y. Fat-tailed gene flow in the dioecious canopy tree species Fraxinus mandshurica var. japonica revealed by microsatellites. *Molecular Ecology*, 15:2985–2996, 2006.

Greenberg, M. D. *Applications of Green's Functions in Science and Engineering*. Dover Publications, Mineola, 2015.

Hadeler, K. P. and Rothe, F. Travelling fronts in nonlinear diffusion equations. *Journal of Mathematical Biology*, 2:251–263, 1975.

Hamel, F. and Roques, L. Fast propagation for KPP equations with slowly decaying initial conditions. *Journal of Differential Equations*, 249:1726–1745, 2010.

Hastings, A. Transients: the key to long-term ecological understanding? *Trends in Ecology & Evolution*, 19:39–45, 2004.

Hastings, A., Cuddington, K., Davies, K. F., Dugaw, C. J., Elmendorf, S., Freestone, A., Harrison, S., Holland, M., Lambrinos, J., Malvadkar, U., Melbourne, B. A., Moore, K.,

Taylor, C., and Thomson, D. The spatial spread of invasions: new developments in theory and evidence. *Ecology Letters*, 8:91–101, 2005.

Hastings, A., Abbott, K. C., Cuddington, K., Francis, T., Gellner, G., Lai, Y.-C., Morozov, A., Petrovskii, S., Scranton, K., and Zeeman, M. L. Transient phenomena in ecology. *Science*, 361, 2018.

Hengeveld, R. *Dynamics of Biological Invasions*. Chapman and Hall, London, 1989.

Higgins, S. I., Nathan, R., and Cain, M. L. Are long-distance dispersal events in plants usually caused by nonstandard means of dispersal? *Ecology*, 84:1945–1956, 2003.

Higgins, S. I. and Richardson, D. M. Predicting plant migration rates in a changing world: The role of long-distance dispersal. *The American Naturalist*, 153:464–475, 1999.

Horn, H. S., Nathan, R., and Kaplan, S. R. Long-distance dispersal of tree seeds by wind. *Ecological Research*, 16:877–885, 2001.

Hovestadt, T., Binzenhöfer, B., Nowicki, P., and Settele, J. Do all inter-patch movements represent dispersal? A mixed kernel study of butterfly mobility in fragmented landscapes. *Journal of Animal Ecology*, 80:1070–1077, 2011.

Hsu, S. and Zhao, X. Spreading speeds and traveling waves for nonmonotone integrodifference equations. *SIAM Journal on Mathematical Analysis*, 40:776–789, 2008.

Janzen, D. H. Dispersal of small seeds by big herbivores: Foliage is the fruit. *The American Naturalist*, 123:338–353, 1984.

Jordano, P. What is long-distance dispersal? And a taxonomy of dispersal events. *Journal of Ecology*, 105:75–84, 2017.

Katul, G. G., Porporato, A., Nathan, R., Siqueira, M., Soons, M. B., Poggi, D., Horn, H. S., and Levin, S. A. Mechanistic analytical models for long-distance seed dispersal by wind. *The American Naturalist*, 166:368–381, 2005.

Kawasaki, K., Takasu, F., Caswell, H., and Shigesada, N. How does stochasticity in colonization accelerate the speed of invasion in a cellular automaton model? *Ecological Research*, 21:334, 2006.

Kesler, D. C., Walters, J. R., and Kappes, J. J. Social influences on dispersal and the fat-tailed dispersal distribution in red-cockaded woodpeckers. *Behavioral Ecology*, 21: 1337–1343, 2010.

Klein, E. K., Lavigne, C., and Gouyon, P.-H. Mixing of propagules from discrete sources at long distance: comparing a dispersal tail to an exponential. *BMC Ecology*, 6:3, 2006.

Kot, M., Lewis, M. A., and Neubert, M. G. Integrodifference equations. In Hastings, A. and Gross, L., editors, *Encyclopedia of Theoretical Ecology*, pages 381–384. University of California Press, Berkeley, 2012.

Kot, M. Discrete-time travelling waves: ecological examples. *Journal of Mathematical Biology*, 30:413–436, 1992.

Kot, M. and Neubert, M. G. Saddle-point approximations, integrodifference equations, and invasions. *Bulletin of Mathematical Biology*, 70:1790–1826, 2008.

Kot, M. and Schaffer, W. M. Discrete-time growth-dispersal models. *Math. Biosci*, 80: 109–136, 1986.

Kot, M., Lewis, M. A., and van den Driessche, P. Dispersal data and the spread of invading organisms. *Ecology*, 77:2027–2042, 1996.

Kotz, S., Kozubowski, T., and Podgorski, K. *The Laplace Distribution and Generalizations: A Revisit with Applications to Communications, Economics, Engineering, and Finance.* Birkhäuser, Boston, 2001.

Lewis, M. A. and Kareiva, P. Allee dynamics and the spread of invading organisms. *Theoretical Population Biology*, 43:141–158, 1993.

Lewis, M. and Schmitz, G. Biological invasion of an organism with separate mobile and stationary states: Modeling and analysis. *Forma*, 11, 1996.

Lewis, M. A. Variability, patchiness, and jump dispersal in the spread of an invading population. In Tilman, D. and Kareiva, P. M., editors, *Spatial Ecology: The Role of Space in Population Dynamics and Interspecific Interactions*, pages 46–69. Princeton University Press, Princeton, 1997.

Lewis, M. A., Li, B., and Weinberger, H. F. Spreading speed and linear determinacy for two-species competition models. *Journal of Mathematical Biology*, 45:219–233, 2002.

Lewis, M. A., Neubert, M. G., Caswell, H., Clark, J. S., and Shea, K. A guide to calculating discrete-time invasion rates from data. In Cadotte, M. W., McMahon, S. M., and Fukami, T., editors, *Conceptual Ecology and Invasion Biology: Reciprocal Approaches to Nature*, pages 169–192. Springer, Dordrecht, 2006.

Lewis, M. A., Petrovskii, S. V., and Potts, J. R. *The Mathematics Behind Biological Invasions*. Springer, Cham, 2016.

Li, B., Lewis, M. A., and Weinberger, H. F. Existence of traveling waves for integral recursions with nonmonotone growth functions. *Journal of Mathematical Biology*, 58:323–338, 2009.

Liebhold, A. M. and Tobin, P. C. Exploiting the Achilles heels of pest invasions: Allee effects, stratified dispersal and management of forest insect establishment and spread. *New Zealand Journal of Forestry Science*, 40(Suppl.):S25–S33, 2010.

Liu, B. R. Biphasic range expansions with short- and long-distance dispersal. *Theoretical Ecology*, (in press), 2021.

Liu, B. R. and Kot, M. Accelerating invasions and the asymptotics of fat-tailed dispersal. *Journal of Theoretical Biology*, 471:22–41, 2019.

Lutscher, F. A short note on short dispersal events. *Bulletin of Mathematical Biology*, 69: 1615–1630, 2007.

Lutscher, F. Density-dependent dispersal in integrodifference equations. *Journal of Mathematical Biology*, 56:499–524, 2008.

Lutscher, F. *Integrodifference Equations in Spatial Ecology*. Springer, Cham, 2019.

Lutscher, F. and Seo, G. The effect of temporal variability on persistence conditions in rivers. *Journal of Theoretical Biology*, 283:53–59, 2011.

Miller, J. and Thomas, J. Detectors for discrete-time signals in non-Gaussian noise. *IEEE Transactions on Information Theory*, 18:241–250, 1972.

Mollison, D. Dependence of epidemic and population velocities on basic parameters. *Mathematical Biosciences*, 107:255–287, 1991.

Mundt, C. C., Sackett, K. E., Wallace, L. D., Cowger, C., and Dudley, J. P. Long-distance dispersal and accelerating waves of disease: empirical relationships. *American Naturalist*, 173:456–466, 2009.

Murray, J. D. *Mathematical Biology*. Springer-Verlag, Berlin, 1989.

Murray, J. D. *Mathematical Biology: I. An Introduction*. Springer, New York, 2002.

Nathan, R. Long-distance dispersal research: building a network of yellow brick roads. *Diversity and Distributions*, 11:125–130, 2005.

Nathan, R. Long-distance dispersal of plants. *Science*, 313:786–788, 2006.

Nathan, R., Katul, G. G., Horn, H. S., Thomas, S. M., Oren, R., Avissar, R., Pacala, S. W., and Levin, S. A. Mechanisms of long-distance dispersal of seeds by wind. *Nature*, 418: 409–413, 2002.

Nathan, R., Perry, G., Cronin, J. T., Strand, A. E., and Cain, M. L. Methods for estimating long-distance dispersal. *Oikos*, 103:261–273, 2003.

Nathan, R., Schurr, F. M., Spiegel, O., Steinitz, O., Trakhtenbrot, A., and Tsoar, A. Mechanisms of long-distance seed dispersal. *Trends in Ecology & Evolution*, 23:638–647, 2008.

Nathan, R., Klein, E., Robledo-Arnuncio, J. J., and Revilla, E. Dispersal kernels: Review. In Clobert, J., Baguette, M., Benton, T., and Bullock, J., editors, *Dispersal Ecology and Evolution*, pages 187–210. Oxford University Press, Oxford, 2012.

Okubo, A. *Diffusion and Ecological Problems: Mathematical Models*. Springer-Verlag, Berlin, 1980.

Paradis, E., Baillie, S. R., and Sutherland, W. J. Modeling large-scale dispersal distances. *Ecological Modelling*, 151:279–292, 2002.

Parker, I. M. Mating patterns and rates of biological invasion. *Proceedings of the National Academy of Sciences of the United States of America*, 101:13695–13696, 2004.

Petrov, V. *Sums of Independent Random Variables*. Springer, Berlin, 1975.

Phillips, A. and Kot, M. Persistence in a two-dimensional moving-habitat model. *Bulletin of Mathematical Biology*, 77:2125–2159, 2015.

Ramanantoanina, A., Ouhinou, A., and Hui, C. Spatial assortment of mixed propagules explains the acceleration of range expansion. *PLOS ONE*, 9, 2014.

Reid, C. *The Origin of the British Flora*. Dulau and Company, London, 1899.

Schurr, F. M., Spiegel, O., Steinitz, O., Trakhtenbrot, A., Tsoar, A., and Nathan, R. Long-Distance Seed Dispersal. In Østergaard, L., editor, *Fruit Development and Seed Dispersal*, pages 204–237. Wiley-Blackwell, Chichester, 2009.

Shigesada, N. and Kawasaki, K. Invasion and the range expansion of species: Effects of long-distance dispersal. In Bullock, J. M., Kenward, R. E., and Hails, R. S., editors, *Dispersal Ecology: 42nd Symposium of the British Ecological Society held at the University of Reading, 2-5 April 2001*, pages 350–73. Blackwell Publishing, Malden, 2002.

Shigesada, N. and Kawasaki, K. *Biological Invasions: Theory and Practice*. Oxford University Press, Oxford, 1997.

Shigesada, N., Kawasaki, K., and Takeda, Y. Modeling stratified diffusion in biological invasions. *The American Naturalist*, 146:229–251, 1995.

Skellam, J. G. Random dispersal in theoretical populations. *Biometrika*, 38:196–218, 1951.

Slavov, G. T., Leonardi, S., Burczyk, J., Adams, W. T., Strauss, S. H., and Difazio, S. P. Extensive pollen flow in two ecologically contrasting populations of Populus trichocarpa. *Molecular Ecology*, 18:357–373, 2009.

Streiff, R., Ducousso, A., Lexer, C., Steinkellner, H., Glossel, J., and Kremer, A. Pollen dispersal inferred from paternity analysis in a mixed oak stand of Quercus robur L. and Q. petraea (Matt.) Liebl. *Molecular Ecology*, 8:831–841, 1999.

Student. The probable error of a mean. *Biometrika*, 6:1–25, 1908.

Suarez, A. V., Holway, D. A., and Case, T. J. Patterns of spread in biological invasions dominated by long-distance jump dispersal: Insights from Argentine ants. *Proceedings of the National Academy of Sciences of the United States of America*, 98:1095–1100, 2001.

Sullivan, L. L., Li, B., Miller, T. E. X., Neubert, M. G., and Shaw, A. K. Density dependence in demography and dispersal generates fluctuating invasion speeds. *Proceedings of the National Academy of Sciences of the United States of America*, 114:5053–5058, 2017.

Thompson, S. and Katul, G. Plant propagation fronts and wind dispersal: An analytical

model to upscale from seconds to decades using superstatistics. *The American Naturalist*, 171:468–479, 2008.

Trakhtenbrot, A., Nathan, R., Perry, G., and Richardson, D. M. The importance of long-distance dispersal in biodiversity conservation. *Diversity and Distributions*, 11:173–181, 2005.

van den Bosch, F., Metz, J. A. J., and Diekmann, O. The velocity of spatial population expansion. *Journal of Mathematical Biology*, 28:529–565, 1990.

Van Houtan, K. S., Pimm, S. L., Halley, J. M., Bierregaard, R. O., and Lovejoy, T. E. Dispersal of Amazonian birds in continuous and fragmented forest. *Ecology Letters*, 10: 219–229, 2007.

Vasilyeva, O. and Lutscher, F. How flow speed alters competitive outcome in advective environments. *Bulletin of Mathematical Biology*, 74:2935–2958, 2012.

Wang, M.-H., Kot, M., and Neubert, M. G. Integrodifference equations, Allee effects, and invasions. *Journal of Mathematical Biology*, 44:150–168, 2002.

Weinberger, H. Long-time behavior of a class of biological models. *SIAM Journal on Mathematical Analysis*, 13:353–396, 1982.

Weinberger, H. F., Lewis, M. A., and Li, B. Analysis of linear determinacy for spread in cooperative models. *Journal of Mathematical Biology*, 45:183–218, 2002.